Université de Montréal

Understanding and Treating Herpes Simplex Virus Type 1 Corneal Infections

Par

Marc Groleau

Unité académique de microbiologie, infectiologie et immunologie, Université de Montréal, Faculté de médecine

Mémoire présenté(e) en vue de l'obtention du grade de maîtrise

en microbiologie et immunologie, option (nom de l'option s'il y a lieu)

Août 2022

Université de Montréal

Unité académique : microbiologie, infectiologie et immunologie, Université de Montréal

---

Ce mémoire intitulé

Understanding and Treating Herpes Simplex Virus Type 1 Corneal Infections

Présenté par

Marc Groleau

A été évalué par un jury composé des personnes suivantes

Dr Soren Gantt
Président-rapporteur

Dre May Griffith
Directeur de recherche

Dr Rongtuan Lin
Membre du jury

Résumé

Le virus de l'herpès simplex de sérotype 1 (HSV-1) est la plus grande cause de l'aveuglement infectieuse dans les pays développés. Les infections cornéennes à HSV-1 ont plusieurs conséquences, comme la difficulté à éliminer l'infection virale et l'inflammation provoquant une plus grande opacité de la cornée. Une infection cornéenne a montré qu'il y a colocalisation des cellules souches et les cellules amplificatrices transitoires avec le virus, mais le HSV-1 était toujours abondant dans le limbe de l'œil. Pour combattre le virus, anciennes publications ont montré que LL37, une cathélicidine humaine, peut réduire la charge virale. Le GF19, un fragment de LL37 modifié pour favoriser la perméabilité, a été capable de réduire la charge virale *in vitro* et *ex vivo*, avec la possibilité d'avoir des effets thérapeutique et préventif. Pour combattre les conséquences inflammatoires, un agoniste cannabinoïde CB2r impliqué dans la modulation de la neuroinflammation, TA-A001, a été testé. Des souris ayant reçu des brûlures alcalines pour induire l'inflammation et ils ont montré de meilleurs résultats cliniques avec le TA-A001 qu'avec le véhicule du médicament seul ou un corticostéroïde, la prednisolone. En conclusion, il apparaît que l'HSV-1 infecte rapidement le limbe, que le GF19 a pu réduire la charge virale, et que le TA-A001 a pu réduire l'inflammation en ayant peu d'effets secondaires. Une combinaison des traitements antiviraux et immunosuppresseurs administrés à la cornée pourrait être examinée plus pour combattre contre les infections à HSV-1 dans les yeux.

Mots-clés : Infection à HSV-1, GF19, cornée, immunosuppression, cannabinoïdes.

Abstract

Herpes Simplex Virus serotype 1 (HSV-1) is the most common cause of infectious blindness in developed countries. Little is known about the early events in HSV-1 ocular infections since the clinical symptoms often appear a week after infection. There are two significant consequences of HSV-1 corneal infection: the viral impacts of the disease and the inflammatory impacts. In mouse corneas, after HSV-1 infection, viruses localized in the limbal area of the cornea. However, there was no/little immunohistochemical co-localization with the stem cells or transient amplifying cells. Previous work has shown that LL37, a human cathelicidin, can reduce the viral burden. GF19, a fragment of LL37 with a modification to promote permeability, reduced viral loads in vitro and in ex vivo corneas. To combat the inflammatory consequences of HSV-1 infection, a cannabinoid CB2r agonist implicated in neuroinflammation modulation, TA-A001, was tested. Mice given alkali burns to induce inflammation showed better clinical results with TA-A001 than with the drug's vehicle alone or a corticosteroid, prednisolone. In conclusion, it appears that HSV-1 quickly infects the limbus, GF19 was able to reduce viral burden, and CB2r agonists such as TA-A001 could reduce inflammation with few side effects. A combination of the anti-viral and immunosuppressant treatments could be a potential HSV-1 treatment.

Keywords: HSV-1 infection, GF19, cornea, immunosuppression, CB2r agonist.

Table of Contents

Résumé 3

Abstract 4

Table of Contents 5

List of Tables 9

List of Figures 10

List of Abbreviations and Acronyms 11

Acknowledgements 14

Chapter 1 – Introduction and Literature Review 15

1.1. The human cornea 15

1.2. HSV-1 corneal infections 16

1.2.1. Viral implications of HSV keratitis 17

1.2.2. Inflammation and immune implications of HSV keratitis 19

1.3. Treatments for HSV-1 corneal infections 23

1.3.1. Targeting HSV-1 viruses and current anti-viral drugs 23

1.3.1.1. Cathelicidins as an alternative to acyclovir 24

1.3.2. Corticosteroid treatments for HSV keratitis 26

1.3.2.1. Cannabinoid receptor agonists as an alternative to corticosteroids 27

Chapter 2 – Memoire Research Summary 29

2.1. Rationale 29

2.2. Objectives 29

2.3. Contributions 29

Chapter 3 – Methods 31

3.1. Viral stock and titration 31
3.2. *Ex vivo* HSV-1 infections 31
3.3. *Ex vivo* corneal infections for flow cytometry analysis 32
3.4. *In vivo* HSV-1 infections 32
3.5. *In vitro* efficacy assays on anti-viral peptides 33
3.6. Fabricating SiO_2 nanoparticles and CLP-LCPP hydrogels 33
3.7. *Ex vivo* antiviral efficacy of GF19 34
3.8. Bone marrow-derived dendritic cell (BMDC) culture and flow cytometric analysis 35
3.9. Corneal alkali burns in mice treated with immunosuppressants 36
3.10. Flat mount immunohistochemistry 38
3.11. Slide mounted immunohistochemistry 39
3.12. Free floating immunohistochemistry 40
3.13. Immunocytochemistry 41
3.14. Real-time quantitative PCR on whole mouse eyes 41
3.15. Cytokine multiplex assay on mouse tears 42
3.16. Statistical analyses 42
Chapter 4 – Results 46
4.1. Understanding and treating HSV-1 ocular infections 46
4.1.1. *Ex vivo* HSV-1 infection characterization 46
4.1.2. *In vivo* HSV-1 infections in mice 48
4.1.3. *In vitro* and *ex vivo* efficacy of anti-viral treatment by GF19 51
4.2. Treating ocular inflammation with a CB2r agonist 55
4.2.1. *In vitro* immune compatibility 55
4.2.2. Clinical evaluation of *in vivo* mouse corneal alkali burns 56

4.2.3. Post-mortem evaluation of *in vivo* mouse corneal alkali burns 58
Chapter 5 – Discussion 63
5.1. Understanding and treating HSV-1 ocular infections 63
5.2. Treating ocular inflammation with a CB2r agonist 66
5.3. Conclusions and future prospects 69
5.3.1. Understanding and treating HSV-1 ocular infections 69
5.3.2. Treating ocular inflammation with a CB2r agonist 69
Chapter 6 – References 71
Chapter 7 – Appendices 83
Published papers 83
Biomaterial corneal implants 84
7.1. Introduction 84
7.2. Contributions 86
7.3. Methods 86
7.3.1. Fabrication of CLP-PEG-Fibrinogen hydrogels 86
7.3.2. Fabrication of CLP-LCPP hydrogels 87
7.3.3. Application of nanoparticles 87
7.3.4. Implantation into inflamed mouse corneas 88
7.3.5. Implantation of transfecting reagents in mouse corneas 88
7.3.6. Histology and immunohistochemistry 89
7.3.7. Statistical analyses 90
7.4. Results 91
7.4.1. Early impacts of corneal implants 91
7.4.2. Comparison of CLP-based hydrogels to common corneal sealants 93

7.4.3. Efficacy of injectable CLP hydrogels for delivery through nanoparticle carriers.....96

7.5. Discussion.....98

List of Tables

Table 1. Antibodies for flow cytometry 43
Table 2. Antibodies for immunohistochemistry 44
Table 3. Oligonucleotide Sequences for qPCR 45
Table 4. Antibodies for immunohistochemistry 90

List of Figures

Figure 1. Structure and cell layout of the cornea and limbus 16
Figure 2. HSV-1 eye infection, from primary infection to latency 19
Figure 3. Immune evasion strategies of HSV-1 on the TLR pathways 22
Figure 4. Immune modulating effects of LL37 25
Figure 5. Side effects of corticosteroid use on the eye 27
Figure 6. BMDC protocol outline 36
Figure 7. Outline of alkali burned and immunosuppressant treated mice 38
Figure 8. HSV-1 infections in excised mouse and human eye bank corneas 47
Figure 9. Clinical exam progression of HSV-1 infected Swiss Webster mice 49
Figure 10. Mouse cornea immunohistochemistry at three days post HSV-1 infection 50
Figure 11. *In vitro* efficacy and immune compatibility of anti-viral GF19 52
Figure 12. *Ex vivo* efficacy of anti-viral GF19 54
Figure 13. BMDCs compatibility with CB2r agonist, TA-A001 55
Figure 14. Clinical exams of alkali burned mice treated with prednisolone, drug vehicle or TA-A001 57
Figure 15. Corneal neovascularization after two weeks on prednisolone, drug vehicle or TA-A001 treatment 59
Figure 16. Expression of extracellular vesicles and MCP-1 in prednisolone, drug vehicle or TA-A001 treated mice 60
Figure 17. Corneal nerve density and morphology after prednisolone, drug vehicle or TA-A001 treatment 62
Figure 18. Extracellular vesicles secretion and MCP-1 expression within a week after implantation in mice 93
Figure 19. Expression of extracellular vesicles and MCP-1 in implanted mice 96
Figure 20. *In vivo* transfection of mouse corneas with GFP DNA 97

List of Abbreviations and Acronyms

α-SMA: alpha smooth muscle actin

ACV: acyclovir

AMP: antimicrobial peptide

APS: ammonium persulphate

BMDC: bone marrow-derived dendritic cell

CBr: cannabinoids receptor

CD: cluster of differentiation

cGAS: cyclic GMP-AMP synthase

CLP: collagen-like peptide

DAPI: 4’,6-diamidino-2-phenylindole

DMEM: dulbecco's modified eagle medium

DMTMM: 4-(4,6-dimethoxy-1,3,5-triazin-2-yl)-4-methylmorpholinium chloride

DNA: deoxyribonucleic acid

EV: extracellular vesicles

FBS: fetal bovine serum

FIJI: FIJI is just ImageJ

GFP: green fluorescent protein

GM-CSF: granulocyte-macrophage colony-stimulating factor

H&E: hematoxylin and eosin

HCE: human corneal epithelial

HSK: herpes simplex virus keratitis

HSV: herpes simplex virus

ICP: infected cell protein

IFN: interferon

IKK: IκB kinase

IL: interleukin

IOP: intraocular pressure

LCPP: linear carboxylic phosphorylcholine co-polymer

LSCD: limbal stem cell deficiency

LPS: lipopolysaccharide

MCP-1: monocyte Chemoattractant Protein-1

MFI: median fluorescent intensity

MHC II: major histocompatibility complex II

MPC: 2-methacryloyloxyethyl phosphorylcholine

mRNA: messenger RNA

NF-κB: nuclear factor kappa B

NP: nanoparticle

PBS: phosphate buffered saline

PEG: polyethylene glycol

PFA: paraformaldehyde

qPCR: quantitative polymerase chain reaction

OCT: optical coherence tomography

RNA: ribonucleic acid

sGF19: scrambled GF19

STING: stimulator of interferon gene

TAC: transient amplifying cell

TBS: tris buffered saline

TG: trigeminal ganglion

TEMED: N,N,N’,N’-tetramethylethylenediamine

TLR: toll like receptor

TNF: tumor necrosis factor

TRAF6: tumor necrosis factor receptor-associated factor 6

Acknowledgements

I would like to thank my supervisor, Dr. May Griffith. I was first introduced to doing research through a summer internship at her lab and enjoyed it enough to continue for a Master's degree in that same lab. The skills that I have learned while there will help me immensely for the future, in particular, learning how to design experiments and trouble shooting when things go wrong.

In addition to my supervisor, I would like to thank the other people of our lab and of other labs present at the Hôpital Maisonneuve-Rosemont. Thank you to the rest of the Griffith lab, providing valuable feedback and assistance. Thank you to the Sylvie Lesage lab, in particular, Félix Lombard, Capucine Bourel, and Geneviève Chabot, for teaching me new techniques. Thank you to the Brunette lab, in particular, Marilyse Piche and Mathieu Thériault, for providing additional research opportunities. Thank you to the two clinicians I worked with, Dr. Marie-Claude Robert and Dr. Marie-Josée Aubin, for assisting in surgeries and introducing me to the clinical side of research.

Elle and Fiona also played a large role, often providing very helpful advice when I needed it and closely supervised me during my first internship. Thank you to both of them for that as well as setting as good role models. In particular, teaching me the importance of efficiency and what it means for a researcher to work efficiently, empathising the need to work smartly and to not take shortcuts at the risk of failing an experiment.

I would also like to thank the others who have assisted me outside of research. To my parents and my grandparents for always encouraging me to pursue what I enjoy and pushing me to improve my French (Merci à mes parents et grands-parents pour l'encouragement à poursuivre ce que j'aime et à mieux comprendre le français). To Sarah who would listen to me whine and provide weird stories of her own. Finally, to my Montreal friends for often being annoying and getting me to stay up late a night but also providing a fun space disconnected from work, especially to Alex and Michael, who took the fun out function and who stole shoes.

Chapter 1 – Introduction and Literature Review

1.1. The human cornea

The human cornea is the transparent front of the eye that acts as the major lens for focussing light into the eye for vision. It consists of three main cellular layers, an outmost epithelium comprising of five to six cell layers, a stroma that consists mainly of extracellular matrix around a network of keratocytes arranged in layers or lamellae, and an innermost endothelium made up of a single layer of low cuboidal-shaped cells (1). The epithelial cells are constantly replenished from progenitor cells in its basal layer as well as transiently amplifying cells. The stem cells that give rise to the transiently amplifying cells are located in the limbus, which is immediately adjacent to the cornea, situated between the cornea proper and the conjunctiva (2). Figure 1 shows the layers of the cornea and the transition of the stem cells from the limbal crypts to the basal epithelium.

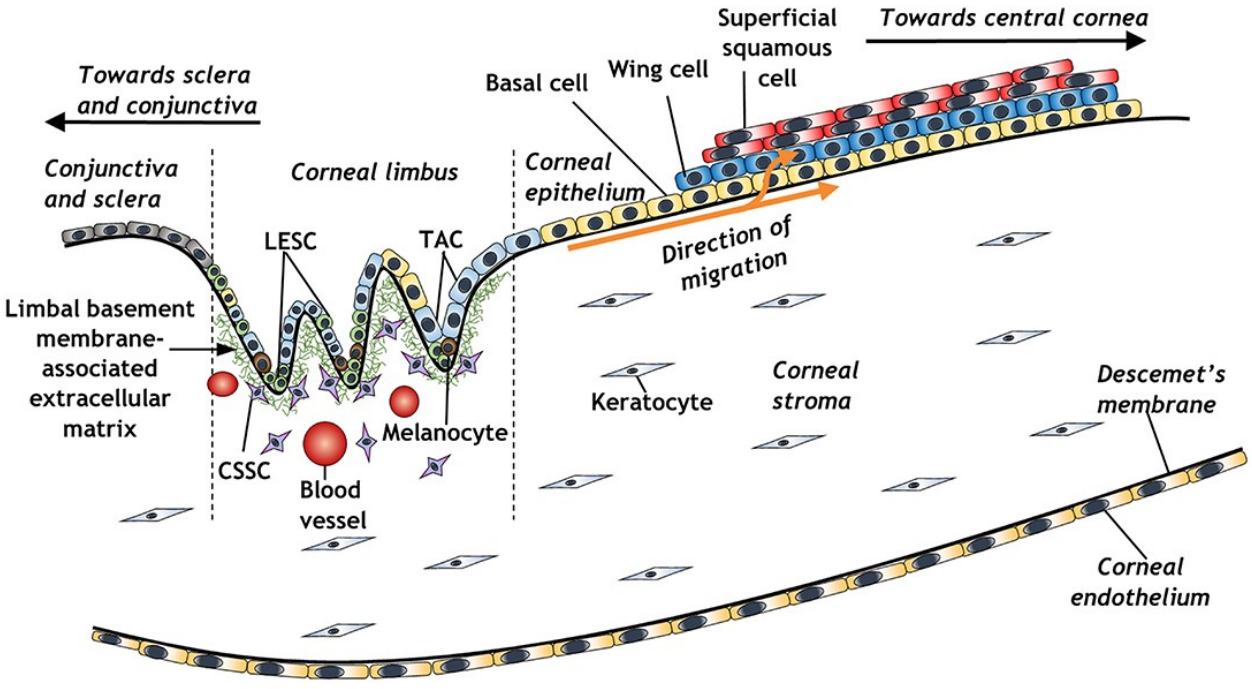

Figure 1. ***Structure and cell layout of the cornea and limbus.*** *LESC: limbal epithelial stem cell, CSSC: corneal stromal stem cell, TAC: transient amplifying cell. Reproduced from Ashworth et al. Front. Cell Dev. Biol. 2021, by a Creative Commons Attribution licence (CC-BY)* (3).

The cornea is avascular and is fully dependent upon its very dense network of nerves for trophic support. The cornea is supplied by sensory fibres that originate from the trigeminal ganglia (TG), which is also the major trophic supply (4). It also receives input from parasympathetic and sympathetic nerve fibres.

The cornea is burdened with a difficult task, to be transparent. This task is made difficult by the cornea being exposed to the environment, allowing for accidental exposure to noxious substances as well as possible infectious agents. The corneal epithelial cells are coated with a tear film that comprises several aqueous and lipids layers of protective mucus. In addition, the epithelial cells secrete innate host defence peptides such as defensins and cathelicidins that help defend the cornea against injury or infection (5).

When the tear film and epithelium are breached, for example by pathogens or injury, inflammation can occur. If the damage is severe, the inflammation may become uncontrolled, and the cornea would be unable to effectively repair the damage (6). There may be loss of transparency due to light rays scattering off scars or pockets of fluid that are formed. The loss of transparency, when irreversible, results in vision loss or blindness.

1.2. HSV-1 corneal infections

The Herpes Simplex Virus serotype 1 (HSV-1) is a double stranded DNA virus from the *Herpesviridae* family. HSV-1 can spread by direct contact of infected secretions to a vulnerable area such as the mucosal membranes or in lesions (7). HSV-1 is typically transmitted through oral-to-oral contact and can cause cold sores around the mouth (8). It can also spread by respiratory droplets and by sexual transmission (8, 9). Beyond cold sores, HSV-1 can also cause sore throats, anorexia, cervical adenopathy, and mucosal edema from oral infections (10).

HSV-1 is the main serotype responsible for corneal infections. Corneal infections can be direct or can occur through transfer from the mouth to the cornea through the nerves originating from the trigeminal ganglia (TG) which innervate both the mouth (maxillary and mandibular branches) and the cornea (ophthalmic branch) (11-13). Infections that spread to the spread into the TG and central nervous system which can lead to encephalitis, a disease with a 70% mortality rate if untreated (9).

HSV-1 is the most common infectious cause of corneal blindness, in both developed and developing countries (14, 15). Globally, there are 1.5 million new cases of HSV keratitis (HSK), corneal inflammation caused by HSV infection, with roughly 40 thousand of those cases resulting in severe vision impairment each year (11). For severe cases, human donor corneal transplants are used to restore vision. There are two main aspects that HSK can divided into: the viral implications from the infection, and the inflammation associated with HSV infections. Beyond this, there is the need for corneal transplantation to drastically improve vision.

1.2.1. Viral implications of HSV keratitis

The HSV-1 virus contains three main regions of interest, the envelope which expresses glycoproteins for viral entry into cells, the tegument which contains many proteins and nucleic acids to be released upon infection, and the nucleocapsid containing the viral genome inside. There are also two life cycles that HSV-1 can follow, a lytic and a latent cycle. During the lytic cycle, HSV-1 is actively producing more viral proteins, viral genomes and virions within the infected cells and will eventually result in cell lysis (16, 17). Additionally, HSV-1 is capable of infecting a large variety of cells, as shown with *in vitro* experiments (18-26). This is due to the variety of receptors capable of binding to the glycoproteins present on the surface of the virion (18-33). With so many cells susceptible to infection with a lytic virus, necrosis of many cells can occur resulting in necrotizing keratitis. Necrotizing keratitis is characterized by inflammation in the cornea, similar to other forms of keratitis, with the addition of a lot of active viruses in the cornea directly causing cell death (34, 35). This often occurs in the deeper regions of the cornea, the stroma, requiring higher doses of anti-viral drugs to control the infection. Due to the massive

cell death and scarring, the cornea becomes thinner and opaque, respectively. This increases the risk for corneal perforation (34).

Other forms of observed necrosis are much less understood. For example, limbal stem cell deficiencies (LSCD) are more likely to occur in people suffering with HSK (36). Cell cultures have shown that HSV-1 is capable of infecting and lysing stem cells, but it is unclear if this occurs in the host (23, 24). In humans, it has been observed that many HSK patients have a reduction of limbal stem cell populations, however it is not clear if the virus directly lysed these cells or if the infection caused a change in the environment which leads to a reduction of stem cells (37). This is highly problematic since these stem cells are needed to replenish the corneal epithelium with healthy cells (38, 39). Furthermore, flowing limbal damage, neovascularization can occur in the cornea which can further promote inflammation and increase opacity (39).

Viral latency is also problematic, making the virus difficult to fully eliminate from a patient. During latency, HSV-1 remains within a host cell but does not produce more genomes or viral proteins. Instead, it produces latency associated transcripts which keeps the virus in a latent state (40). The latent HSV-1 is capable of spontaneous reactivation and production of viable virions. Since the latently infected cells are not producing viral proteins, immune cells have difficulty identifying these cells to clear the infection. HSV-1 latency often occurs within neurons, and that the TG often harbours latently infected cells (Figure 2) (41). Interestingly, there is some debate whether HSV-1 is latent in other cells within the eye, in particular, keratocytes (42, 43). The issue with latency is that even with the acute infection controlled, the latent virus can reactivate at any time and start a new acute infection in these patients, potentially causing further damage to the cornea, while at the same time being difficult to target.

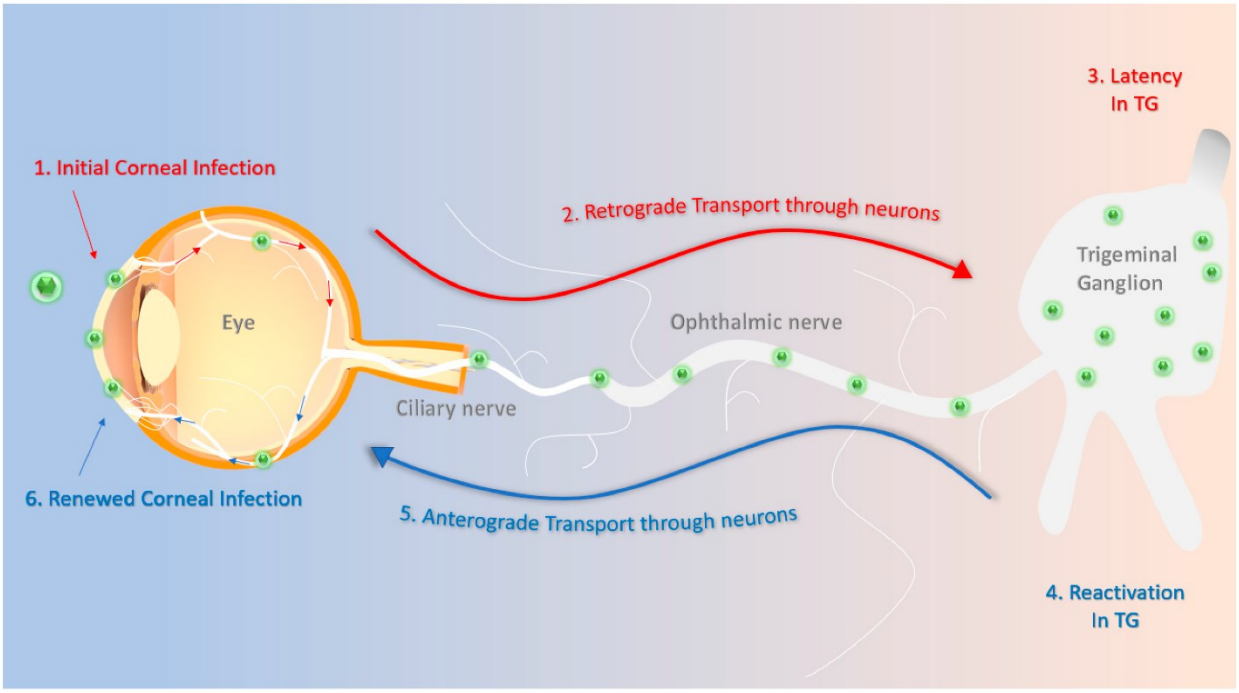

Figure 2. ***HSV-1 eye infection, from primary infection to latency.*** *HSV-1 initially infects the eye through the cornea then travels to the trigeminal ganglion (TG) where it establishes latency. Upon reactivation, virus travels back into the eye. Reproduced from Koganti et al. Microorganisms, 2019, by a Creative Commons Attribution licence (CC-BY)* (44).

1.2.2. Inflammation and immune implications of HSV keratitis

Ocular infections with HSV-1 engages the immune system which acts to reduce the viral load. However, a consequence of the ensuing inflammation is damage to the tissue. Many immune cells are capable of reducing the viral burden of the infection. For example, natural killer cells, innate lymphoid cells, dendritic cells, and macrophages all aid in reducing the viral burden (45-49). In addition to having direct effects on controlling the virus, dendritic cells and macrophages also function as antigen presenting cells and encourage the involvement of the adaptive immune system. In particular, $CD8^+$ cytotoxic T cells are essential for clearing the initial infection but are also associated with lymphangiogenesis and scarring (50, 51). Even after all viruses are cleared, the inflammatory cascade does not always cease (52, 53). In cases of prolonged inflammation, the inflammation can lead to tissue damage and scarring, cause

opacities that impair vision (54). There is conflicting evidence as to whether $CD4^+$ T cells and neutrophils help or worsen the pathogenesis of HSK. A neutrophil influx late in the acute infection is associated with the onset of severe clinical symptoms and corneal scarring, although neutrophils are beneficial early in the infection (55, 56). While $CD4^+$ T cells clear the viruses, they can secrete cytokines that promote angiogenesis or further neutrophil recruitment that can worsen the disease (52, 57, 58). There is still a lot that is not properly understood about these cells and there is also controversy with regard to their involvement as some publications claim they reduce disease severity (55, 58). Apart from immune cells, epithelial cells are also able to respond to HSV-1 through toll like receptors (TLR), with TLRs 2, 3, 4, 7 and 9 being able to strongly respond to HSV-1, as well as cyclic GMP-AMP synthase (cGAS) and stimulator of interferon gene (STING) which detects intracellular DNA (59-64).

What is important for the pathology of HSK is not the initial inflammation during the acute phase of the infection, but the prolonged inflammation afterwards. There are multiple aspects that cause prolonged inflammation in the cornea following HSV-1 infection. One major factor is that HSV-1 remains latent within the corneal nerves originating from the TG (41). The virus can reactivate and infect cells within the cornea, causing additional inflammation which can then bring in additional damage to the eyes (41, 65). Unfortunately, the mechanisms involved for reactivation are not fully understood as there have been numerous potential triggers. For example, the number of HSV-1 genomes present in a latently infected cells and the genetics of both the virus and host all have an impact on the rate of reactivation (66-69). The host's immune response also plays a role where a good interferon type 1 (IFN-1) response and certain HLAs on the major histocompatibility can reduce the rate of reactivation (70-72). Beyond genetic factors, many environmental factors have been correlated with increased rates of reactivation such as ultraviolet (UV) light, steroid drops, corneal transplantation surgery, and temperature changes (73-81). While the causes of reactivation are unclear, it is well established that recurrent HSV-1 eye infections in general results in increased inflammation, corneal damage, and opacity.

In addition to being able to reactivate, HSV-1 has multiple ways to evade or take advantage of the immune system. HSV-1 is capable of avoiding many pathogen recognition receptors. For example, infected cell protein (ICP) 0, an immediate early viral protein, uses

ubiquitin-specific peptidase 7 (USP7) to deubiquitinate tumor necrosis factor receptor-associated factor 6 (TRAF6) and IκB kinase (IKK) γ (82). Both TRAF6 and IKK γ are important for TLR signaling and their inhibition reduces the effectiveness of TLR signalling, a pathway that can respond to HSV-1 infections (59-63). Additionally, the serine-threonine protein kinase US3 that is encoded by HSV-1 and is released from the viral tegument upon infection, where it blocks the accumulation of NF-κB in the nucleus. This decreases the effectiveness of TLRs, possibly leading to a decrease of IFN-1 expression as well as other pro-inflammatory cytokines (83). ICP0 also able inhibits other pathways such as the IFNAR-JAK-STAT signaling pathway that is responsible for responding to IFN-1. ICP0 can directly bind to STAT1 which is downstream of the IFN receptors and is important for mounting a response to IFNs by producing IFN-stimulated genes (84). cGAS-STING can also be targeted by UL41, a HSV-1 tegument protein, and can diminish the expression of IFN-1 by reducing the accumulation of cGAS (64). These are some mechanisms that HSV-1 uses to evade IFN-1 (Figure 3). In addition, complement, DNA damage responses, stress granules and necrosis are other innate host defenses that can be inhibited by HSV-1 (85-88).

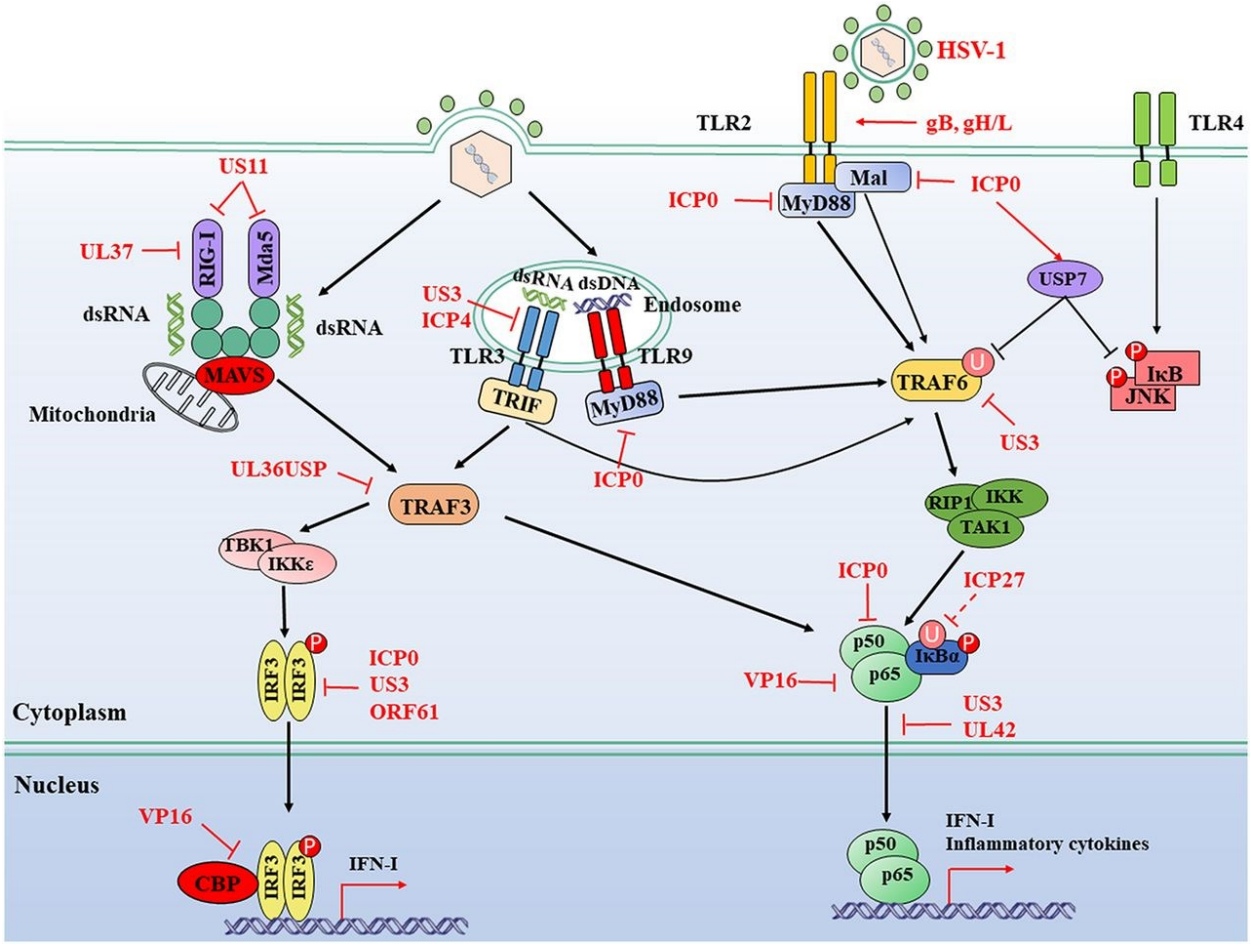

Figure 3. ***Immune evasion strategies of HSV-1 on the TLR pathways.*** *HSV-1 has multiple proteins capable of reducing the signalling from the TLR pathway. Importantly, this reduces in the amount of IFN-1 and other pro-inflammatory cytokines produced by infected cells which are crucial for an anti-viral response. For p50 and p65 to promote production of IFN-1, IRF3 or IRF7 is required (not shown). Solid lines indicate confirmed interactions between adaptors and HSV-1 proteins. Dashed lines indicate uncertain interactions or that the underlying mechanism is unknown. CBP: CREB-binding protein, P: phosphate, U: ubiquitin. Reproduced from Zhu et al. Microbiol Mol Biol Rev. 2020, by a Creative Commons Attribution licence (CC-BY)* (89).

Not only can HSV-1 interfere with many pathogen recognition receptors, either directly or downstream, but it can also interfere with immune cells. To avoid activating the adaptive immune system, HSV-1 has evolved a few mechanisms to inhibit major histocompatibility

complex II (MHC II) activity. Infected cells show a reduction in the amount of invariant chain present, which is important for the proper formation of MHC II (90). In addition to reducing the abundance of the invariant chain, glycoprotein B competes with the invariant chain to bind to HLA-DR and HLA-DM, further preventing antigen presentation (90). The direct effectiveness of immune cells can also be targeted by HSV-1, especially for dendritic cells. When infecting immature dendritic cells, many inflammatory markers such as CD1a, CD40, CD80 and CD86 are down regulated (91). Dendritic cell maturation is inhibited, leading to viral susceptibility in surrounding cells (92, 93). With such a large range of immune evasion techniques, it is very difficult for the immune system to clear the virus, often resulting in prolonged inflammation.

1.3. Treatments for HSV-1 corneal infections

1.3.1. Targeting HSV-1 viruses and current anti-viral drugs

The most common anti-viral drugs to treat HSV-1 infection are acyclovir (ACV) and its derivatives. ACV targets the thymidine kinase made by the virus (94). Once phosphorylated by the thymidine kinase, ACV and its derivatives compete with deoxyguanosine trisphosphate to be inserted into the viral genome, causing premature termination of DNA replication (95). Since these drugs require phosphorylation by a viral kinase, there is very little cytotoxicity in healthy cells. The main problem with ACV is its poor bioavailability and its water solubility. Ganciclovir, a derivative of ACV, has a similar mechanism of action but is water soluble, allowing for the use of lower concentrations of the drug (96).

While ACV and its derivatives can significantly reduce the amount of virus and reoccurrence of HSV-1 infections, prophylactic use is not efficient. For example, 23.1% patients on ACV prophylaxis were reported to have a reoccurring HSV-1 related ocular disease (97). Additionally, resistance to ACV is increasingly becoming more common in patients and is particularly an issue in immune compromised patients whose immune system may not be able to handle the virus (98, 99). Furthermore, the drugs block viral replication and does not clear latent virus. Also, the poor uptake of the drugs in the cornea necessitates the use of systemic drugs that require high concentrations to reach the cornea (100). These higher doses may lead

to undesirable side effects such as nausea, vomiting, diarrhea, blurred vision, punctuate keratitis, eye irritation, and kidney damage (101-105).

Foscarnet is often used alongside ACV. It has a different mechanism of action, interfering with the pyrophosphate binding site of DNA polymerases (106). Foscarnet has a few problems though, such as not being reliant on a viral protein to be active, and therefore, it is more cytotoxic than ACV. Additionally, herpes viruses have become resistant to foscarnet, leading to an increase in viruses being resistant to both foscarnet and ACV (107). More experimental treatments include blocking Akt signaling using BX795, DNA aptamers binding to glycoprotein D, neutralizing antibodies against glycoproteins, cleaving heparan sulfate using OGT 2115 which prevents viral release and cationic peptides (108-113).

1.3.1.1. Cathelicidins as an alternative to acyclovir

The innate immune system in humans includes the cationic host defense peptides also referred to as antimicrobial peptides (AMPs) such as cathelicidins and defensins. Cathelicidins function by inserting themselves into membranes through hydrophobic interactions causing membrane disruption. As they are highly cationic, they are more attracted to negatively charged membranes (114). Healthy host cells are protected from these cathelicidins since their outer membranes mostly consists of a neutral charge that does not attract the AMPs. The presence of cholesterol also makes it difficult for AMPs to insert themselves into the membrane (115). Humans only have one cathelicidin, LL37, which is produced by epithelial cells, including the corneal epithelial cells, and neutrophils (116, 117). Beyond having direct anti-pathogen effects, LL37 also has immunomodulatory effects. LL37 is able to promote macrophage differentiation to an M1 phenotype, which is helpful for clearing viral infections (118). Additionally, LL37 is able to enhance TLR activation, which is important for responding to viruses and producing IFN-1 (119-121). A summary of the effects of LL37 can be found in Figure 4.

When tested in cell cultures, LL37 was shown to reduce the viral activity of HSV-1 (122). Additionally, smaller bioactive fragments of LL37 have been tested on other viruses with some

success. Of interest is GF17, which has anti-viral effects against Ebola virus and Zika virus (123, 124). Cell viability studies showed that the half maximal effective concentration (EC_{50}) was greater then 50µM compared to the EC_{50} of >2µM for LL37 (123, 125). These results suggest that the smaller LL37 fragments retain their anti-viral abilities while being less cytotoxic.

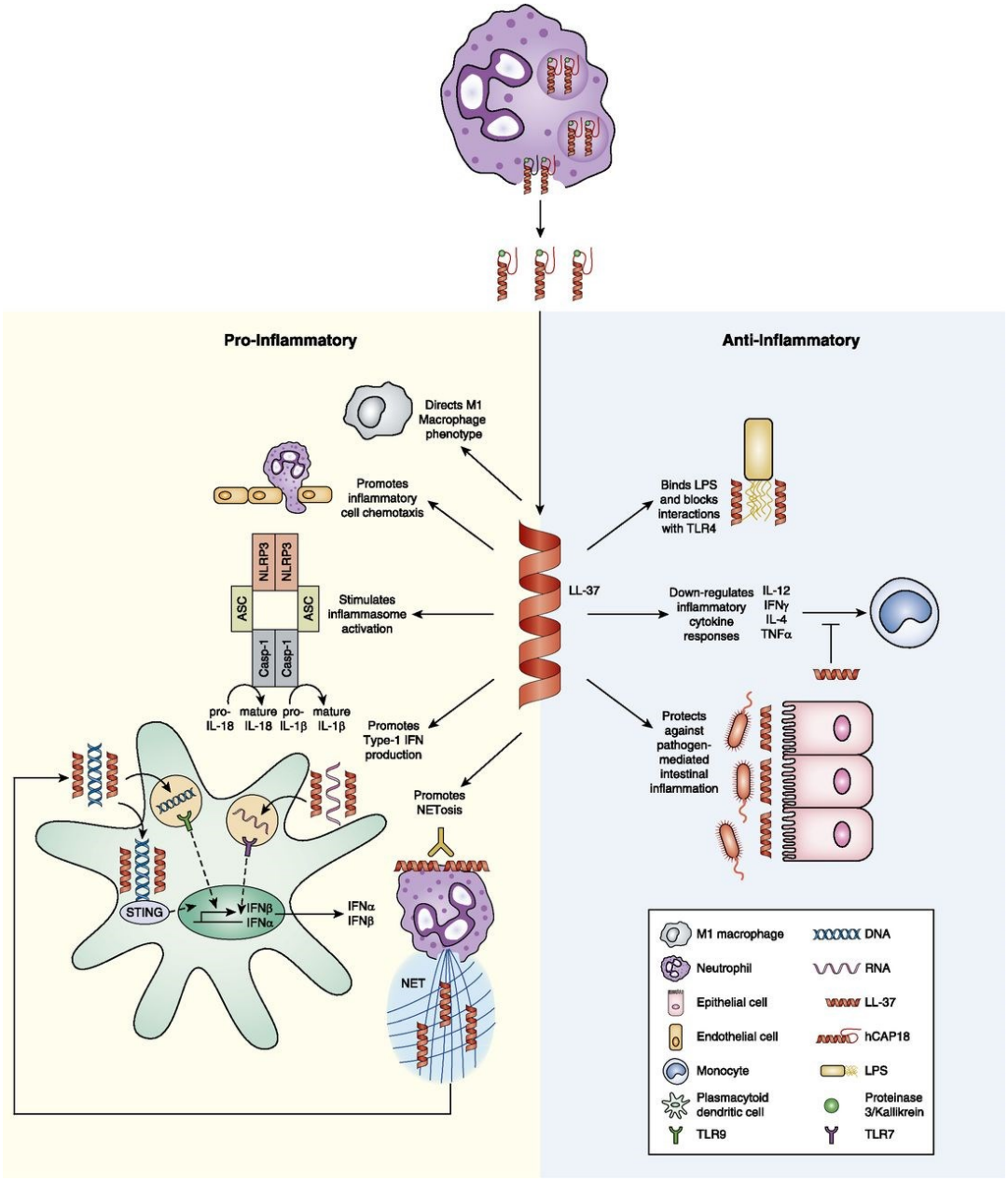

Figure 4. ***Immune modulating effects of LL37.*** *Treatment with LL37 can promote an M1 macrophage phenotype, immune cell infiltration, promote IFN-1 production, and promotes*

neutrophil NETosis. Reproduced from Kahlenberg et al. J Immunol. 2013, by a Creative Commons Attribution licence (CC-BY) (126).

1.3.2. Corticosteroid treatments for HSV keratitis

Topical corticosteroids are the main immunosuppressants used to control the inflammation from HSK (127). They are given in addition to an anti-viral treatment to minimize the severity of the disease progression (128, 129). Corticosteroids function by binding to glucocorticoid receptors that modulate over 5000 genes and exert immunosuppressant effects (130). Beyond HSK, corticosteroids are used in many ocular diseases such as uveitis, retinitis, scleritis, trauma and post-operative medication (131-135). Despite their widespread use, they have many notable side effects. The more concerning side effects are glaucoma, cataracts, and enhancement of infectious diseases (Figure 5).

In the case of glaucoma, corticosteroids can impact the trabecular meshwork by increasing the amount of extracellular material deposited that in turn blocks the aqueous outflow (136). With reduced outflow, the intraocular pressure (IOP) can build up, putting stress onto the optic nerve, resulting in damage and decreased vision.

For cataracts, it is unclear how corticosteroids affect the lens. There is speculation that steroids may bind directly to the lens and their build-up leads to decreased clarity and eventually cataracts (137, 138). Recent evidence from the lens suggests that corticosteroids cause apoptosis and prevent lens epithelial cells from differentiating fully (139, 140).

Finally, the enhancement of infectious diseases by corticosteroids can be broken into two parts, decreased wound healing and increased risk of infections. The corticosteroid treatment can delay the healing of cornea epithelial defects in rabbits (141). Furthermore, treatments can also induce the reactivation of latent HSV-1, although the mechanism is still unclear (142, 143). Interestingly, despite these disadvantages, corticosteroid treatment is still highly recommended for HSK patients seeing as the advantages outweigh the potential downsides, highlighting the need for immunosuppressants.

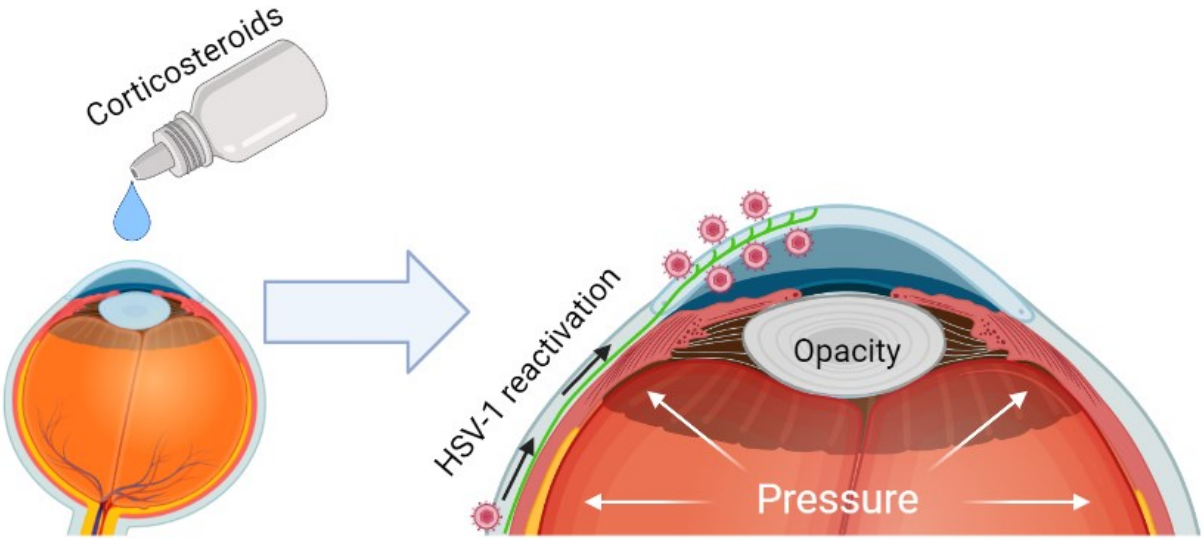

Figure 5. ***Side effects of corticosteroid use on the eye.*** *Corticosteroids are associated with increased IOP, HSV-1 reactivation, and cataracts. Created in BioRender.*

1.3.2.1. Cannabinoid receptor agonists as an alternative to corticosteroids

Interesting alternatives to corticosteroids are the agonists to cannabinoid receptors 1 and 2 (CB1r and CB2r). CB1r and CB2r are common in the human cornea, limbus, and conjunctiva and have been shown to play a role in wound healing (144, 145). In a dry eye disease model, treatment with CB1r and CB2r agonists resulted in better corneal health, with increased nerve fiber length and decreased T cell infiltration compared to the non-treated (146). In a mouse model involving a corneal wound, CB2r had higher expression after the wound and the deletion of CB2r *in vivo* resulted in slower wound healing (147). For corneal inflammation, a study performing alkali burns on the cornea to induce inflammation observed less immune cell infiltration within the stroma and less scaring compared to knockout mice lacking corneal cannabinoid receptors (148). Additionally, cannabinoids can reduce IOP by promoting the aqueous outflow, with a lower IOP reducing the risks of developing glaucoma (149). One way it does this is by upregulating enzymes that degrade extracellular matrix at the trabecular meshwork (150, 151). Additionally, there is some evidence that CD1r and CD2r agonists, in addition to 5-HT_{1A}, can reduce pain as observed in a mouse study where treated mice blinked,

squinted, and rubbed their eyes less frequently (152). Negative side effects from ocular cannabinoid treatments are not yet fully understood. In rabbit corneas, it was observed that CB1r signaling promoted corneal neovascularization, while reduced neovascularization was observed with CB1r activity was blocked (153). While neovascularization is often associated with inflammation, many studies report a reduction of inflammation with CB1r activation (144-152). Additionally, the study reporting on the neovascularization did not examine inflammatory markers beyond indicators for neovascularization (153). All together, CB1r and CB2r are very promising routes to supress inflammation, especially CB2r which plays an important role in wound healing, but further works needs to be done to fully understand what is occurring within the cornea, both positive and negative effects (144-153).

Chapter 2 – Memoire Research Summary

2.1. Rationale

Ocular HSV infections result in 40 thousand annual cases of severe vision impairment globally and are the most significant cause of corneal blindness. Current treatments available for HSV keratitis patients try to reduce the viral burden and the undesirable inflammation of the disease. However, approved anti-viral treatments have difficulty entering into the deeper regions of tissues, and there is a rise of resistant viral strains. Immunosuppressants reduce inflammation but are linked with viral reactivation as well as negative side effects such as glaucoma. Early events of HSV-1 corneal infections were examined to address these concerns and test alternatives to approved anti-virals and immunosuppressants.

2.2. Objectives

Objective 1. Identify trends in early HSV-1 eye infections and an anti-viral treatment based on naturally occurring host defence peptides for efficacy against HSV-1.

Objective 2. Reduce inflammation using TA-A001, a CB2r agonist, as an alternative treatment to corticosteroids following a corneal alkali burn.

2.3. Contributions

This memoire was written by Marc Groleau, with constructive criticism and corrections from Dr. May Griffith. All experiments and quantifications were performed by Marc Groleau unless otherwise stated.

Understanding and treating HSV-1 ocular infections

GF19 was designed by Dr. Kamal Malhotra and synthesized by Dr. Marcelo Muñoz. GF19 SiO_2 nanoparticles (NP) encapsulation was performed by Dr. Bijay Poudel and Dr. Kamal

Malhotra. Dr. Fiona Simpson and Dr. Elle Edin made the CLP-LCPP hydrogels. Félix Lombard-Vadnais assisted in BMDCs analysis.

Treating ocular inflammation with a CB2r agonist

A combination of Marc Groleau, Natalia Callai Da Silva, Dr. Naoufal Akla, and Dr. Bijay Poudel performed the alkali burns, clinical exams, and treatments on the mice. Flat mount vessel staining was performed by Dr. Naoufal Akla, imaging and quantification were performed by Marc Groleau. Fluorescein quantification was performed by Neethi Thathapudi. Félix Lombard-Vadnais and Capucine Bourel assisted in qPCR analysis.

Chapter 3 – Methods

3.1. Viral stock and titration

The HSV-1 McKrae strain was used for this study (a gift from D.J. Carr, Univ. of Oklahoma Heath Sciences Centre, Oklahoma, USA). Virus was plaque purified before usage. Virus propagation was performed in Vero cells (ATCC, CCL-81) using DMEM-Hi glucose (Sigma-Aldrich, St. Louis, MO, USA) supplemented with 10% fetal bovine serum (FBS) (Wisent, St-Bruno, QC, Canada) and penicillin-streptomycin (Gibco, Thermo Fisher Scientific, Waltham, MA, USA). Virus was collected after 3 days of infection, mixed with equal volume milk and freeze-thawed four times using dry ice. Stocks were maintained at -80°C until their usage.

Viral titers were performed by growing Vero cells in either 6 or 12 well plates with DMEM-Hi glucose supplemented with 10% FBS and penicillin-streptomycin. Once cells were 90-95% confluent, the media was removed and serum free media containing the virus at varying concentrations were added. Cells were incubated with the virus for one hour, with shaking every 15 minutes. The viral suspension was removed, and the cells were rinsed with 0.01M PBS and an overlay was applied. A liquid overlay was used, consisting of 1.2% Avicel (Sigma-Aldrich, St. Louis, MO, USA) in DMEM-Hi glucose (154). After 3 days, the liquid overlay was removed, and cells were fixed with 10% formaldehyde for 30 minutes. 0.5% crystal violet was used to stain the cells and count the plaques.

3.2. *Ex vivo* HSV-1 infections

Eyes from 30 Tg(TIE2GFP)287Sato/J mice (Aged 5 to 44 weeks) were excised. Eyeballs were rinsed with 0.01M PBS containing 3x penicillin-streptomycin and placed randomly into a 96 well plate with culture media: DMEM-Hi glucose, 10% FBS and penicillin-streptomycin. A 2mm diameter biopsy punch was used to scratch the corneas of the mice. Eyes were infected with varying amounts of HSV-1 diluted in DMEM-Hi glucose for an hour, with shaking every 15 minutes. Following the infection, the eyes were rinsed with 0.01M PBS and submerged in culture media. The eyes were cultured for 48 hours before being fixed with 4% paraformaldehyde (PFA) in 0.1M tris buffered saline (TBS) overnight at 4°C and used for flat mount staining. This was also

performed using two research-grade human corneas, which were not suitable for grafting, and were obtained from the "Banque d'yeux du Centre Universitaire d'ophtalmologie (CUO)" eye bank (CHU de Québec, QC, Canada). Eyes were cut into sixths and placed into 12 well pates. Infection and fixation procedure was the same as the mice. After fixation, the corneal wedges were put through a sucrose gradient from 5 to 20% sucrose diluted in 0.1M TBS and frozen in optimum cutting temperature using liquid nitrogen.

3.3. *Ex vivo* corneal infections for flow cytometry analysis

Eyes from 6 C57BL/6J mice (6 to 12 weeks old) were removed and rinsed with 0.01M PBS containing 3x penicillin-streptomycin. The corneas were dissected with a small surrounding scleral rim and separated from the rest of the globe. Corneas were completely submerged in DMEM-Hi glucose containing either 10^3, 10^4, 10^5 or no virus. After 1 hour in the initial infection media, eyes were rinsed in 0.01M PBS and incubated in DMEM-High glucose with 10% FBS and penicillin-streptomycin for two days. Corneas were digested in 4mg/mL collagenase from *Clostridium histolyticum* (Sigma-Aldrich, St. Louis, MO, USA) for an hour at 37°C with shaking every 10 minutes. A single cell suspension was obtained by using a plunger from a 3mL syringe and mashing the corneas against 70µm cell strainer. A live/dead stain was performed using Zombie Aqua Fixable Viability Kit (BioLegend, San Diego, CA). Samples were then fixed and permeabilized (Becton, Dickinson and Company, Franklin Lakes, NJ, USA) and stained for HSV-1 and p40 - DeltaNp63 (Table 1). A BD LSR II was used on all the samples and were analyzed using FlowJo software (Becton, Dickinson and Company, Franklin Lakes, NJ, USA). High expressing cells with HSV-1 or p40 - DeltaNp63 was observed in live, singlet cells.

3.4. *In vivo* HSV-1 infections

With ethical permission from the Animal Care and Use Committee of Maisonneuve-Rosemont Hospital, 12 Swiss Webster (CFW) mice were used to test two concentrations of HSV-1. Mice underwent clinical assessments before the infection. These tests included aesthesiometry, optical coherence tomography (OCT) and brightfield imaging in both eyes to verify that the eyes were in a healthy condition. Mice were anaesthetised with isoflurane and their right corneas were scratched using a 2mm diameter biopsy punch. A 10µL drop of either

10^4 PFU or 5×10^4 PFU diluted in 0.01M PBS was added to the right eye. Following the initial infection, mice were given Tobramycin (DIN. 02241755, Sandoz Canada, Inc., Boucherville, QC, Canada) on their infected eye twice daily for the duration of the infection. Additionally, mice were weighed and had they corneal sensitivity measured with aesthesiometry every day. After 72 hours from the initial infection, mice were sacrificed through dislocation while under anaesthesia. Eyes were excised and immediately fixed in 4% PFA in 0.1M TBS, overnight at 4°C. Globes were dissected into two halves. One half was used for flat mount staining. The other half went through a sucrose gradient from 5 to 20% sucrose in 0.1M TBS and frozen in optimum cutting temperature (Thermo Fisher Scientific, Waltham, MA, USA).

3.5. *In vitro* efficacy assays on anti-viral peptides

Human corneal epithelial (HCE) cells were cultured in 48 well plates on top of 8mm diameter cover slips in a humidified incubator at 37°C and 5% CO_2. The growth media used was KeratinoMax serum free medium with supplements (Wisent, St-Bruno, QC, Canada). Once HCE cells were 90-95% confluent, the media was removed and fresh media containing the treatment and an MOI 1 of HSV-1 was added. Treatments included the anti-viral peptides LL37, GF17, GF19 and scrambled GF19 (sGF19) at a concentration of 5, 10, 15, 25, 35 and 45µM. Controls consisted of infected, non-treated cells and non-infected, non-treated cells. Cells were incubated for an hour, rinsed with 0.01M PBS, and given fresh media containing the treatment. After 24 hours from the initial infection, the media was collected and stored at -80°C for plaque assays. Fresh media, not containing the treatment, was added to the HCE cells and after an additional 24 hours, the media was collected and stored at -80°C. Cells were fixed with 4% PFA in 0.1M TBS overnight at 4°C.

3.6. Fabricating SiO_2 nanoparticles and CLP-LCPP hydrogels

SiO_2 NPs encapsulating GF19 were produced as previously described (122). To summarize, 6mL cyclohexane was combined with 2mL Triton X-100 (both from Sigma-Aldrich, St. Louis, MO, USA). 1mL of H_2O containing GF19 was added along with adding 0.75mL tetraethylorthosilicate dropwise (Sigma-Aldrich, St. Louis, MO, USA). Solution was brought to a pH of 5.0-6.0 using ammonia hydroxide (Sigma-Aldrich, St. Louis, MO, USA) and were stirred for two days at 50°C.

Linear carboxylic phosphorylcholine co-polymer (LCPP) was prepared by adding 885mg of MPC to TRIS-HCl 0.5M pH 6.7 for a final volume of 200mL. 450mg of AC-PEG-COOH was added to the solution followed by sonication and nitrogen flushing for 30 minutes. 51.3mg of ammonium persulphate (APS) was added, then sonicated and nitrogen flushed for 5 min, followed by the addition of 33.6µL of N,N,N',N'-tetramethylethylenediamine (TEMED). Solutions were incubated at 20°C for 24 hours under positive pressure, nitrogen atmosphere, and constant stirring. Samples were dialysed in a 12-14kD molecular weight cut-off cellulose dialysis membrane. Once completed, material was freeze-dried.

Stock solutions of 15% (w/v) collagen-like peptide (CLP), 10% LCPP, and 10% DMTMM were prepared by using MOPS. 150µL of LCPP was mixed with 112.5µL of DMTMM and 337.5µL of MOPS. The solution was incubated at 65 ºC for one minute. 750µL of CLP solution was mixed with 150µL 10x GF19 encapsulated in SiO_2 and was added to the mix which was then ready to be applied to the wound.

3.7. *Ex vivo* antiviral efficacy of GF19

Eyes from 12 C57BL/6J mice (6 to 12 weeks old) were removed and rinsed with 0.01M PBS containing 3x penicillin-streptomycin. All corneas were scratched using a 2mm diameter biopsy punch and were placed randomly into a 96 well plate. Two treatments with three different conditions were tested. Free GF19 and GF19 encapsulated in SiO_2 NPs were both tested at a concentration of 45µM. The three conditions were: 1) Pre-infection, where the eyes were given media containing the treatment for an hour before the infection. 2) Immediate, where eyes were given the treatment immediately following the initial infection and fresh treatment at 24 hours. 3) Post-infection, where eyes were given the treatment after 24 hours from the initial infection. An infection only and non-infected, non-treated controls were also performed. Infections were performed by diluting the virus to 10^4 PFU in 200µL of DMEM-Hi glucose and submerging the eyes in it for 1 hour with shaking every 15 minutes. Media for all samples were collected at 24 and 48 hours for viral titering. For all eyes, after 48 hours from the initial infection, samples were fixed with 4% PFA in 0.1M TBS, overnight at 4°C. After fixation, eyes were rinsed in 0.1M TBS and used for flat mount staining.

3.8. Bone marrow-derived dendritic cell (BMDC) culture and flow cytometric analysis

A brief summary of the protocol can found in Figure 6. With ethical permission from the Animal Care and Use Committee of Maisonneuve-Rosemont Hospital, the bone marrow was obtained from the tibia and femur of male, C57BL/6J mice (6 to 12 weeks old). Bone marrow cells were divided into 10^6 cells per well in a suspension culture plate and were cultured in RPMI 1640 containing 10% (v/v) fetal bovine serum (FBS) (Wisent, ST-Bruno, QC, Canada), penicillin-streptomycin-glutamine (0.5mg/mL), 10 mM Hepes, 1 mM sodium pyruvate, 55µm of β-mercaptoethanol, and granulocyte-macrophage colony-stimulating factor (2.5ng/mL; GM-CSF) (All from Gibco, Thermo Fisher Scientific, Waltham, MA, USA). After 2 and 3 days from the initial seeding, half the media was exchanged for fresh media containing a higher concentration of GM-CSF (5.0ng/mL). On day 6, the suspended cells were collected and a Histodenz density gradient (Sigma-Aldrich, St. Louis, MO, USA) was used to isolate enlarged cells. A million cells were added to a 24-well suspension plate containing the following treatment and 2mL of media.

Cells were treated with either 45µM GF19, 45µM GF19 encapsulated in SiO_2 NPs within a CLP-LCPP hydrogel, 1µg/mL lipopolysaccharide (LPS) or were untreated. For TA-A001 testing, cells were exposed to either 45µL 0.5% CB2r agonist formulation (TA-A001), 45µL SmartCelle delivery vehicle, 45µL prednisolone, 1µg/mL LPS or no treatment by adding the components individually to the cell culture medium. After the treatment was added, the cells were cultured for an additional 24 hours. At 18 hours, GolgiStop (Becton, Dickinson and Company, Franklin Lakes, NJ, USA) was added to prevent the secretion of cytokines. Cells were stained for surface markers CD11c, CD40, CD80, and CD86 (Table 1) and Zombie Aqua Fixable Viability Kit (BioLegend, San Diego, CA). Fixation and permeabilization (Becton, Dickinson and Company, Franklin Lakes, NJ, USA) was performed to allow for intracellular staining of TNF-α (Table 1). A BD LSR II flow cytometer was used on all the samples and were analyzed using FlowJo software (Becton, Dickinson and Company, Franklin Lakes, NJ, USA). All cell suspensions were sampled for the same duration and analyzed with an LSR II. BMDCs were selected by CD11c expression and

live Zombie Aqua staining. Mean fluorescence intensity (MFI) of TNF-α, CD40, CD80, and CD86 of treated cells were compared to untreated cells to form a ratio.

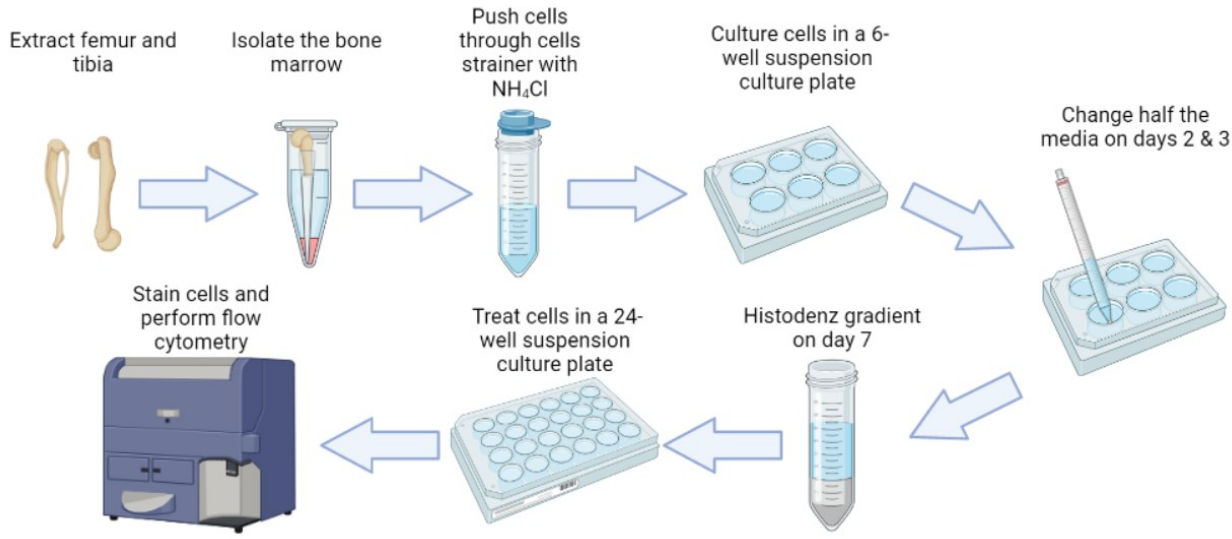

Figure 6. ***BMDC protocol outline.*** *Mouse femur and tibia were obtained and broken in half in order to centrifuge out the bone marrow. Red blood cells were lysed using NH_4Cl and a single cell suspension was obtained with a cell strainer. Cells were cultured in a 6-well suspension culture plate for seven days with a media change on days 2 and 3. A Histodenz gradient was used to isolate dendritic cells which were then cultured with the treatment for a day before being used for flow cytometry. Created in BioRender.*

3.9. Corneal alkali burns in mice treated with immunosuppressants

All experiments were performed after institutional ethics approval from the animal care committee of the Maisonneuve-Rosemont Hospital Research Centre, protocol #2021-2356. Fifty Balb/C mice, age 6 to 10 weeks, were divided into five groups of ten animals each. Under full anaesthesia, which was induced by isoflurane, each animal was given an alkali burn by soaking a 2mm diameter piece of Whatman #1 filter paper in 0.25N sodium hydroxide (NaOH) and applying it to the right cornea for 15 seconds. The eyes were then rinsed in 0.01M PBS to remove any excess NaOH. Animals in the different groups received the following treatments: Teva-Prednisolone (DIN. 00700401), as the positive control, SmartCelle delivery vehicle only as negative control and SmartCelle delivering 0.125%, 0.250% or 0.500% CB2r agonist formulation,

TA-A001. All treatments were given as 15µL eye drops 3 times daily for 2 weeks. Additionally, all mice received 4 days of Tobradex (DIN. 00778907) followed by 3 days of Tobramycin (DIN. 02241755) on their burned eye twice daily. Mice in the Prednisolone group were given 0.05 mg/kg Buprenorphine, an analgesic, on days 2, 3 and 4 post-burn.

The day before the burn and at 2 weeks post-burn, tear collection, aesthesiometry, tonometry, and OCT were performed on all the mice for both eyes. IOP measurements were measured using an iCare Tonolab (Icare Finland Oy, Vantaa, Finland) while mice had anaesthesia with isoflorane. Aesthesiometry was used to test for nerve touch sensitivity in the control and surgically operated eye by using a Cochet-Bonnet aesthesiometer (Handaya Co., Tokyo, Japan). OCT was performed to determine total corneal thickness in live animals with anaesthesia. Total corneal thickness was measured using FIJI. Additionally, sodium fluorescein staining and slit lamp examination were performed daily to determine epithelial integrity, optical clarity, and overall redness. The quantification of fluorescein was performed on all burnt mice corneas on days 0, 1, 2, 3, 7 and 13 using FIJI. The images were split to visualize only the green fluorescence which was used for the quantification. The burnt area was quantified as a percentage area within the cornea. Finally, mice were weighted every 2 days to quickly assess the overall health of the mouse.

On day 14, mice were euthanized, and the globes were collected and separated into three subgroups (Figure 7). The corneas of three mice were used for flat mount immunohistochemical staining for vessels. The corneas of a further three mice for cryo-sectioning and the rest for quantitative PCR (qPCR).

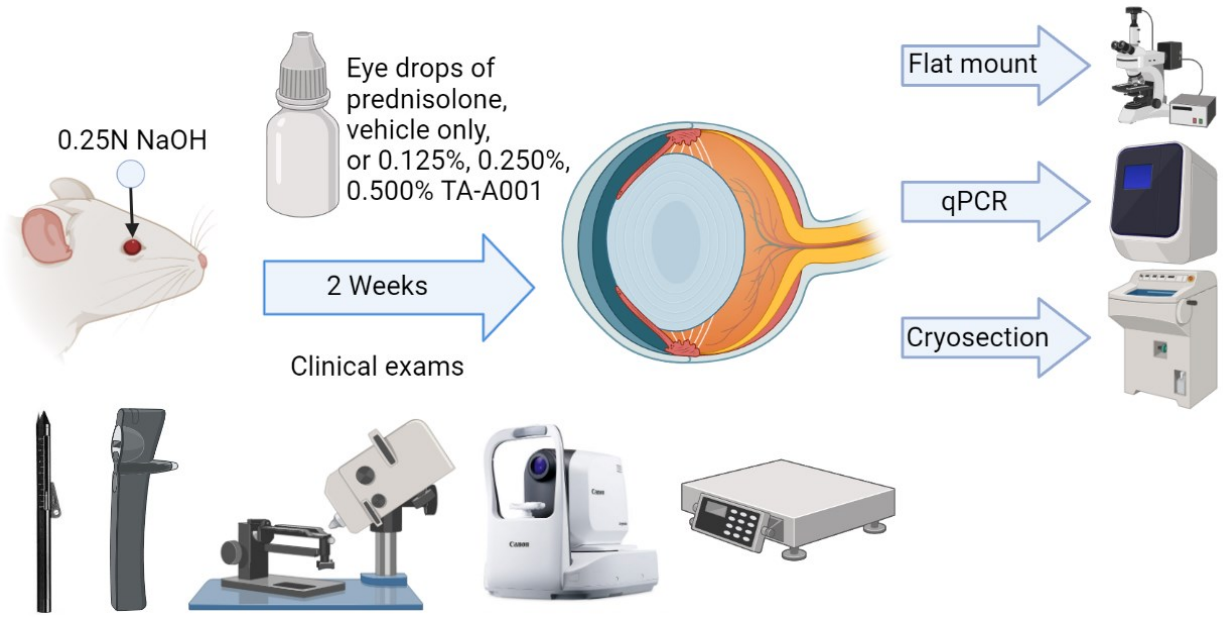

Figure 7. ***Outline of alkali burned and immunosuppressant treated mice.*** *BALB/c mice received an alkali burn on the right cornea followed by eye drops three times a day with an immunosuppressant. Clinical exams were performed on the mice for tear collection, aesthesiometry, tonometry, slit lamp, OCT, and weights. After two weeks, mice were sacrificed, and the eyes were removed. Eyes were then divided into three groups for post-mortem examination for flat mount imaging of neovascularization, qPCR, or cryosectioning. Created in BioRender.*

3.10. Flat mount immunohistochemistry

Eyes were dissected to consist of the cornea and part of the sclera encircling the cornea. Corneas were stored in 0.1M TBS at 4°C until their use. Autofluorescence quenching was performed by treating the eyes with 50mM NH_4Cl in 0.1M TBS for 30 minutes. Samples were blocked for an hour using 5% FBS and 0.3% triton x-100 diluted in 0.1M TBS. When performing mouse on mouse staining, 1:25 mouse on mouse blocking reagent (Vector Laboratories, Burlingame, CA, USA) was added to the blocking. Primary antibodies diluted in the blocking solution were added after the blocking step and were incubated overnight at 4°C (Table 2). Secondary antibodies were added after, diluted in blocking solution for four hours at room

temperature (Table 2). If conflicting secondary antibodies were being used, they would be added in separate 4-hour incubations. A nuclear counterstain was performed using 5µg/mL DAPI diluted in 0.1M TBS for 10 minutes. Corneas were mounted using Vectashield Vibrance Mounting Medium (Vector Laboratories, Burlingame, CA, USA). All flat mount samples were imaged using Zeiss Axio Imager Z2 with an AxioCam MRc color CCD camera (Carl Zeiss, Oberkochen, Germany).

To reduce non-specific autofluorescence, an unstained channel was imaged and used to subtract the fluorescence in the stained channels in FIJI. Image processing and quantifications were performed in FIJI. For quantifications, MFI was measured through the entire full flat mount (Determined by DAPI staining) based on HSV antibody fluorescence.

For flat mount staining of CD31 neovascularization, excised eyes were fixed in 2% PFA in 0.01M PBS at 4°C overnight, and then stored in 0.01M PBS until they were stained. Corneas were blocked using a solution containing 5% normal goat serum, 0.5% Triton X-100 in 0.01M PBS for two hours. Antibodies were diluted in the blocking solution, and each were incubated with the samples with washing in between the primary and secondary antibodies (Table 2). Corneas were then flattened onto a microscopy slide and immersed with Fluoroshield mounting medium containing DAPI (Sigma-Aldrich, St. Louis, MO, USA). All samples were imaged as a tilled z-stack on a Zeiss Axio Imager Z2 with an AxioCam MRc color CCD camera (Carl Zeiss, Oberkochen, Germany). Images were compressed into a maximum projection using extended depth of focus and stitched based on the vessel staining in Zen Blue. The distance between the large collecting vessels and the furthest vessel was measured in FIJI. Measurements were grouped into four categories. 0 = <300µm, 1 = 300-400µm, 2 = 401-500µm, 3 = >500µm.

3.11. Slide mounted immunohistochemistry

Excised globes were fixed in 2% PFA in 0.01M PBS for 1 hour at room temperature and then washed in 0.1M TBS. The corneas were dissected out and saturated stepwise through a gradient of 5% to 20% sucrose in 0.1M TBS as cryoprotectant to prevent cell deformation prior to embedding in Optimal Cutting Temperature compound (14-373-65, Thermo Fisher Scientific, Waltham, MA, USA) and freezing with liquid nitrogen. Samples were cut into 10µm slices on a Leica CM3050 S cryostat and mounted onto Superfrost Plus® slides.

For immunohistochemistry, sections were permeabilized in 0.3% Triton X-100 in 0.1M TBS for 15 minutes. They were then quenched for autofluorescence in 50mM ammonium chloride for 30 minutes. Following that, they were blocked for 1 hour in TBS containing 5% normal goat serum and 0.01g/mL saponin. Mouse on mouse blocking reagent was added to the blocking solution (Vector Laboratories, Burlingame, CA, USA) to reduce non-specific staining. Primary antibodies (Table 2) were diluted in the blocking solution and were added to the samples for an overnight incubation at 4°C. Sections were incubated for an hour with secondary antibodies (Table 2) which were diluted at 1:1000 in the blocking solution. Slides were quenched for autofluorescence using Vector TrueVIEW Autofluorescence Quenching Kit (Vector Laboratories, Burlingame, CA, USA). Nuclei were stained with 5µg/mL DAPI for 10 minutes and mounted in Vectashield Vibrance Mounting Medium (Vector Laboratories, Burlingame, CA, USA).

All slides were imaged on a Zeiss LSM 880 confocal microscope (Zeiss, Oberkochen, Germany). For the exosome immunolocalization, colocalization channels were built using minimum intensity thresholds of 13000 and 4500 for CD63 and TSG101, respectively. The exosome colocalization channel and Monocyte Chemoattractant Protein-1 (MCP-1) were combined the using minimum intensity thresholds of 5000 and 15000, respectively. Spot reconstruction was performed in regions of interest (ROI) for the 3 stained channels as well as the two colocalization channels using the same minimum intensity thresholds in Imaris v9.1.2 (Bitplane Inc., Concord, MA, USA). Five ROI were generated in the epithelium and five were generated in the stroma, all ROI were 750µm^3. Sum intensities and counts from the spot reconstructions were used to compare between samples.

3.12. Free floating immunohistochemistry

For cryosections, 50µm thick slices of mouse and human corneas were made and placed in 0.1M TBS at 4°C until ready for free-floating staining. Samples were stained using a free-floating protocol due to the thickness of the samples (155). Permeabilization was performed for 10 minutes in 1% Triton X-100 in 0.1M TBS. 50mM ammonium chloride was used to quench autofluorescence for 30 minutes. Samples were blocked for an hour in 0.1M TBS containing 5% FBS and 0.3% Triton X-100 in 0.1M TBS. Primary antibodies were diluted in the blocking solution

and were added to the samples for an overnight incubation at 4°C with constant rocking (Table 2). Secondary antibodies diluted in the blocking solution were incubated for 2 hours (Table 2). If conflicting secondary antibodies were being used, they would be added in separate 2 hour incubations. A nuclear counterstain was done with 5µg/mL DAPI for 10 minutes and mounted in Vectashield Vibrance Mounting Medium (Vector Laboratories, Burlingame, CA, USA). All HSV-1 stained samples were imaged using Zeiss Axio Imager Z2 with an AxioCam MRc color CCD camera (Carl Zeiss, Oberkochen, Germany). All images were processed in FIJI.

For the nerve stains, images were taken snaps were taken a Zeiss LSM 880 confocal microscope (Zeiss, Oberkochen, Germany) and processed in Imaris v9.1.2 and the quantification was performed using Zen Blue v10.0.22000. Z-stack images were converted into a maximum projection using extended depth of focus and the non-stained 488 channel was used to create a mask of the tissue. MFI of the tissue was calculated within the Zen Blue program.

3.13. Immunocytochemistry

Coverslips were transferred to a new 48 well plate for staining. Cells were permeabilized using 0.3% triton x-100 in 0.1M TBS for 15 minutes. 50mM ammonium chloride was used to quench autofluorescence for 30 minutes. Samples were blocked in 5% FBS and 0.01g/mL saponin in 0.1M TBS for an hour. Primary antibodies diluted in the blocking buffer were incubated overnight at 4°C (Table 2). Secondary antibodies diluted in blocking buffer were incubated for an hour, followed by 5µg/mL DAPI for 10 minutes to stain the nuclei (Table 2). Samples were mounted using Vectashield Vibrance Mounting Medium (Vector Laboratories, Burlingame, CA, USA) and imaged using Zeiss Axio Imager Z2 with an AxioCam MRc color CCD camera (Carl Zeiss, Oberkochen, Germany). FIJI was used to process all the images.

3.14. Real-time quantitative PCR on whole mouse eyes

Whole mouse globes were flash frozen on dry ice immediately after euthanasia and excision and were stored at -80°C until ready to be processed. RNA extraction was performed by using Direct-zol™ RNA Miniprep with TRI-Reagent (Zymo Research, Irvine, CA, USA). Tissues were placed in TRI-Reagent and sonicated for 30 seconds on and off for a total of a minute of sonication using the Branson Digital Sonifier SFX 150 (Emerson Automation Solutions, St. Louis, MO, USA).

The instructions from the Direct-ZOL™ kit were followed. Briefly, an equal amount of ethanol was added to the lysed samples, followed by an RNA wash and a 15 minute incubation with DNase I. Samples were then washed twice in pre-RNA wash, then a RNA wash and finally transferred to a new collection tube using 50µL of DNase/RNase-Free Water. For cDNA synthesis, SuperScript™ IV VILO™ was used, following the recommended procedure (Invitrogen, Thermo Fisher Scientific, Waltham, MA, USA). qPCR was performed on a 7500 Real-Time PCR System (Applied Biosystems, Thermo Fisher Scientific, Waltham, MA, USA). The cycling stage consisted of 40 cycles of 95°C for 20 seconds, 60°C for a minute, and 72°C for 30 seconds. iTaq™ Universal SYBR® Green Supermix (Bio-Rad Ltd., Mississauga, ON, Canada) was used and primers used are listed in Table 3 (Sigma-Aldrich, St. Louis, MO, USA).

3.15. Cytokine multiplex assay on mouse tears

Tears were collected by adding 1.5µL of 0.01M PBS to the mouse's eye and immediately collecting 1µL using Drummond™ Short-Length Microcaps™ Micropipets (21-170A, Thermo Fisher Scientific, Waltham, MA, USA). 9µL of assay buffer was added to the collected 1µL tear and stored at -80°C until ready for use. A cytokine multiplex assay was performed using the manufacturer's recommendations for Milliplex MAP Mouse High Sensitivity T Cell (MHSTCMAG-70K, Millipore Sigma, Oakville, ON, Canada). TNF-α, IL-1β, IL-6, IL-10 and IL-17A were tested. Briefly, plates were washed in wash buffer for 10 minutes followed by an overnight incubation at 4°C containing the samples with the magnetic beads. Samples were washed and the detection antibodies were incubated with the samples for an hour. Streptavidin-Phycoerythrin was added directly to samples and incubated for 30 minutes. Samples were washed 3 times and resuspended in MagPix Drive Fluid PLUS. Samples ran on the MagPix using Bio-Plex Manager MP Software (Luminex Crop., Austin, TX, USA). The standard curves and assay sensitivity were based on the manufacturer's instructions.

3.16. Statistical analyses

Statistical analysis for BMDCs and flow cytometry expression of HSV-1 was performed using a one-way ANOVA Tukey's multiple comparisons test with a confidence interval of 95% for each marker (GraphPad Prism 9.3.0, GraphPad Software LLC., San Diego, CA, USA). The unit of

analysis was the mouse (n = 6 per group) or the number of eyes for the *ex vivo* infections (n = 3 per group). qPCR also received the same statistical analysis as the BMDCs however the unit of analysis was n=2 for prednisolone, n=3 for vehicle and 0.250% TA-A001 and n=4 for 0.125% and 0.500% TA-A001. The ex vivo efficacy of GF19, aesthesiometry, fluorescein, OCT and weights were analysed using a two-way ANOVA Tukey's multiple comparisons test with a confidence interval of 95% for each group. Two-way ANOVA Šidák's multiple comparisons test was used to analyse tonometry, neovascularization, exosome expression and nerve expression.

Table 1. *Antibodies for flow cytometry*

Target	**Antibody**	**Dilution Factor**
p40 - DeltaNp63	Recombinant Anti-p40 - DeltaNp63 antibody [EPR17863-47], (Isotype: Rabbit IgG), (Reactivity: Mouse, Rat, Human), (Format: Unconjugated), (AP: WB, IHC, FC, ICC), (Species: Rabbit), Abcam, ab203826	1:200
Rabbit IgG	Goat anti-Rabbit IgG (H+L) Cross-Adsorbed Secondary Antibody, Alexa Fluor™ 700, Invitrogen, A-21038	1:1000
HSV-1	Herpes Simplex Virus Type 1/2 Goat anti-Virus, (Isotype: Goat IgG), (Reactivity: HSV-1, F strain), (Format: FITC), (AP: ELISA, ICC), (Species: Goat), Invitrogen, PIPA127209	1:200
CD11c	Brilliant Violet 650™ anti-mouse CD11c, (Clone: N418), (IsoType: Armenian Hamster IgG), (Reactivity: Mouse), (Format: BV650), (APP: FC), (Species: Hamster), Biolegend, 117339	1:1600
TNF-a	PerCP/Cyanine5.5 anti-mouse TNF-α, (Clone: MP6-XT22), (IstoType: Rat IgG1, κ), (Reactivity: Mouse), (Format: PerCP/Cyanine5.5), (APP: FC), (Species: Rat), Biolegend, 506321	1:800

CD40	CD40, APC, clone: 1C10, eBioscience™, 501129392	1:400
CD80	PE anti-mouse CD80, (Clone: 16-10A1), (IsoType: Armenian Hamster IgG), (Reactivity: Mouse, Cross-Reactivity: Dog (Canine)), (Format: PE), (APP: FC), (Species: Hamster), Biolegend, 104708	1:1600
CD86	FITC anti-mouse CD86, (Clone: GL-1), (IsoType: Rat IgG2a, κ), (Reactivity: Mouse), (Format: FITC), (APP: FC), (Species: Rat), Biolegend, 105006	1:50

Table 2. *Antibodies for immunohistochemistry*

Target	**Antibody**	**Dilution Factor**
HSV-1	HSV Type 1 Goat anti-Virus, Polyclonal, Invitrogen, PIPA17493	1:100
p63	Anti-p63 antibody [4A4], Abcam, ab735	1:100
α-smooth muscle actin	Anti-alpha smooth muscle Actin antibody, Abcam, ab5694	1:100
CD63	Anti-CD63 Antibody (MX-49.129.5), Santa Cruz, sc-5275	1:1000
TSG101	Recombinant Anti-TSG101 antibody [EPR7130(B)], AbCam, ab125011	1:1000
Monocyte chemoattractant protein-1	Ultra-LEAF™ Purified anti-mouse/rat/human MCP-1 Antibody, BioLegend, 505911	1:500
βIII Tubulin	Anti-beta III Tubulin antibody - Neuronal Marker, Abcam, ab18207	1:200
Substance P	Anti-Substance P Antibody, pain, clone NC1, Millipore Sigma, MAB356	1:200
CD31	Purified Rat Anti-Mouse CD31, BD Biosciences, 553370	1:100

Mouse IgG	Goat anti-Mouse IgG (H+L) Highly Cross-Adsorbed Secondary Antibody, Alexa Fluor™ Plus 647, Invitrogen, A32728	1:1000
Goat IgG	IgG (H+L) Cross-Adsorbed Donkey anti-Goat, DyLight™ 550, Invitrogen, PISA510087	1:1000
Rabbit IgG	Goat anti-Rabbit IgG (H+L) Highly Cross-Adsorbed Secondary Antibody, Alexa Fluor™ 488, Invitrogen, A11034	1:1000
Rabbit IgG	IgG (H+L) Highly Cross-Adsorbed Goat anti-Rabbit, Alexa Fluor™ 594, Invitrogen, A11037	1:1000
Armenian Hamster IgG	Goat anti-Hamster IgG (H+L) Secondary Antibody [DyLight 488] (Pre-adsorbed), Novus Biologicals, NBP1-73008	1:1000
Rat IgG	Goat anti-Rat IgG (H+L) Cross-Adsorbed Secondary Antibody, Alexa Fluor™ 594, Invitrogen, A11007	1:800
Rat IgG	Goat anti-Rat IgG (H+L) Cross-Adsorbed Secondary Antibody, Alexa Fluor™ 680, Invitrogen, A21096	1:1000

Table 3. *Oligonucleotide Sequences for qPCR*

Oligonucleotide	**Forward Oligonucleotide Sequence (5'–3')**	**Reverse Oligonucleotide Sequence (5'–3')**
MCP-1	ACTGAAGCCAGCTCTCTCTTCCTC	TTCCTTCTTGGGGTCAGCACAGAC
Tac1	CGGCCAAGGAGAGCAAAGA	ACGGCCACGAGGATTTTCAT
GAPDH	CCCAGCAAGGACACTGAGCAA	TTATGGGGGTCTGGGATGGAAA

Chapter 4 – Results

4.1. Understanding and treating HSV-1 ocular infections

4.1.1. *Ex vivo* HSV-1 infection characterization

Infections in excised eyes were used to identify trends in early HSV-1 infections. Most of the eyes, regardless of the starting virus concentration, showed many infected cells within the vicinity of the scleral rim. Starting at 10^3 PFU, virus could be seen in the limbus, colocalizing with or near p63 positive cells. p63 is a marker for stem cells and transient amplifying cells. Interestingly, at 5×10^4 PFU, the cornea was heavily infected while exposure to even higher concentrations (10^5 and 5×10^5 PFU) of virus showed fewer infected cells (Figure 8A). This observation might be due to HSV-1 lysing the cells. Flow cytometry was performed on infected eyes to verify the microscopy observations. A non-significant decrease ($p>0.05$ by one-way ANOVA Tukey's multiple comparisons test) in the number of live cells was observed in infected corneas compared to the non-infected corneas, as well as a decrease in p40-DeltaNp63 expressing cells (Figure 8B). p40-DeltaNp63 is one of six isoforms of p63 and is more specific to stem cells than p63 which stains transiently amplifying cells as well (156). Additionally, more infected cells were detected when infected with 10^3 PFU compared to the other infection concentrations (Figure 8B).

To verify the relevance of these results in humans, *ex vivo* infections with human corneas (obtained from the Héma-Québec-Vision Health Research Network biobank) were performed. Staining for p63 in the cryosectioned eyes revealed extensive colocalization of the HSV-1 infected cells with p63 and around vessels within the limbus (Figure 8C). Together, these results indicate a preference of infecting the limbus early during the infection and that stem cells or transient amplifying cells are often infected.

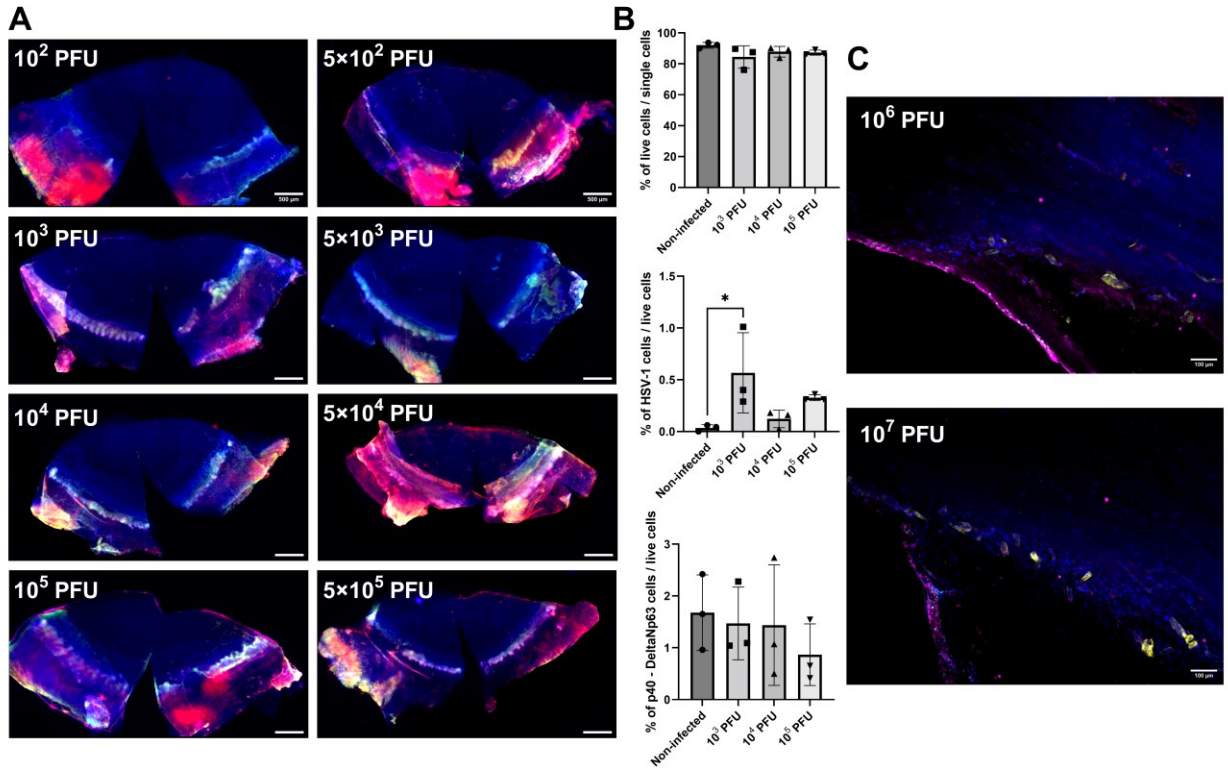

Figure 8. ***HSV-1 infections in excised mouse and human eye bank corneas.*** *(A) Eyes of Tg(TIE2GFP)287Sato/J mice were excised and infected with HSV-1 from 10^2 PFU to 5×10^5 PFU for two days in culture. Corneas were stained for HSV-1 (Red), p63 (Green), and DAPI (Blue). Scale bar: 500µm. (B) Corneas from C57BL/6J mice were infected with HSV-1 and cultured for two days. Flow cytometry was used to identify abundance of live cells, HSV-1 infected cells, and p40-DeltaNp63 expressing cells. *P ≤ 0.05 by one-way ANOVA Tukey's multiple comparisons test. (C) Ex vivo infections of human corneas with either 10^6 or 10^7 PFU. Sections were stained for HSV-1 (Magenta), p63 (Green), α-SMA (Yellow), and DAPI (Blue). Scale bar: 100µm.*

4.1.2. *In vivo* HSV-1 infections in mice

HSV-1 infections were performed by inoculating the corneas of Swiss Webster mice which are known to permit HSV-1 latency (157, 158). The mice did not show clinical signs of being distressed by the infection. There was no increased eye sensitivity (lid closure, blinking) or weight loss, and they were well-groomed with no behavioural change throughout the infection period (Figure 9). Although only the right eye was infected, virus was detected in the non-infected contralateral eye by immunohistochemistry.

Flat mount staining revealed a preferential localization of HSV-1 to the limbus and conjunctiva-sclera. Similar to the *ex vivo* infections, there was marked colocalization between p63 and HSV-1 infected cells (Figure 10). Cryosections of the corneas revealed substantial variation between the mice in terms of how strongly the viral infection had progressed. In general, for mice infected with 10^4 PFU, 75% of eyes had virus in the central corneal epithelium and 50% had virus in the corneal stroma (Figure 10). At 5×10^4 PFU, 92% and 83% of eyes had virus in the central corneal epithelium and stroma respectively.

Within the limbus, 100% of eyes infected with 5×10^4 PFU had virus present, while 83% of the eyes infected with 10^4 PFU had virus present. Furthermore, HSV-1 was often found in deeper layers of the limbal tissue and did not co-localize with p63 (Figure 10). This indicates that HSV-1 has a slight preference for infecting limbal cells over corneal cells and that the cornea has infected cells in both the epithelium and stroma before the onset of clinical symptoms.

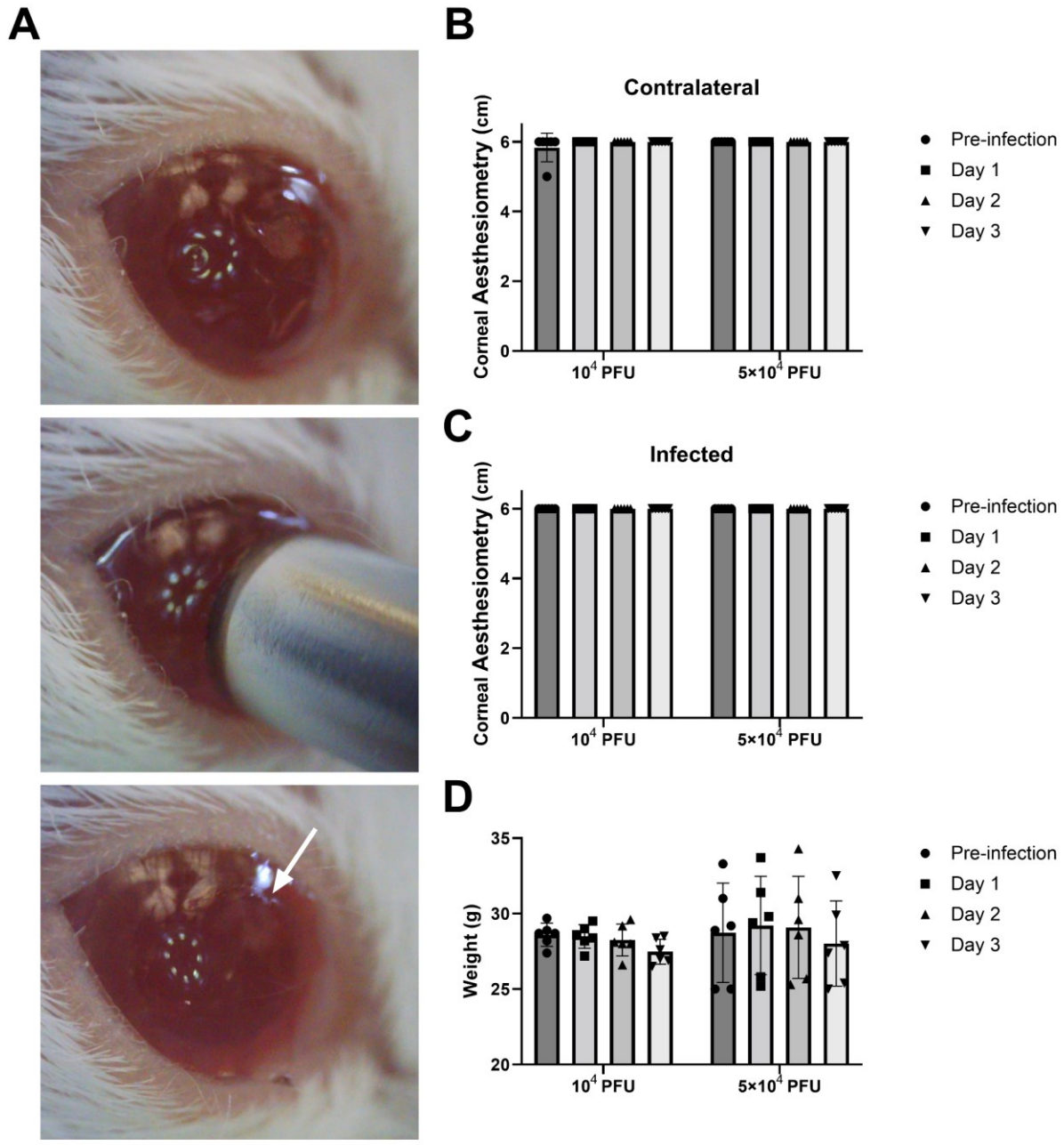

Figure 9. ***Clinical exam progression of HSV-1 infected Swiss Webster mice.*** *(A) The right corneas of Swiss Webster mice were scratched with a circular biopsy punch. Top panel was before the scratch, middle was getting scratched, and bottom was after the scratch. The white arrow indicates the top of the scratch. Corneal sensitivity was measured with an aesthesiometer of the contralateral uninfected eye (B), and the infected eye (C) showed no observable changes after HSV-1 infection. (D) The body weights of mice showed no significant post-infection changes.*

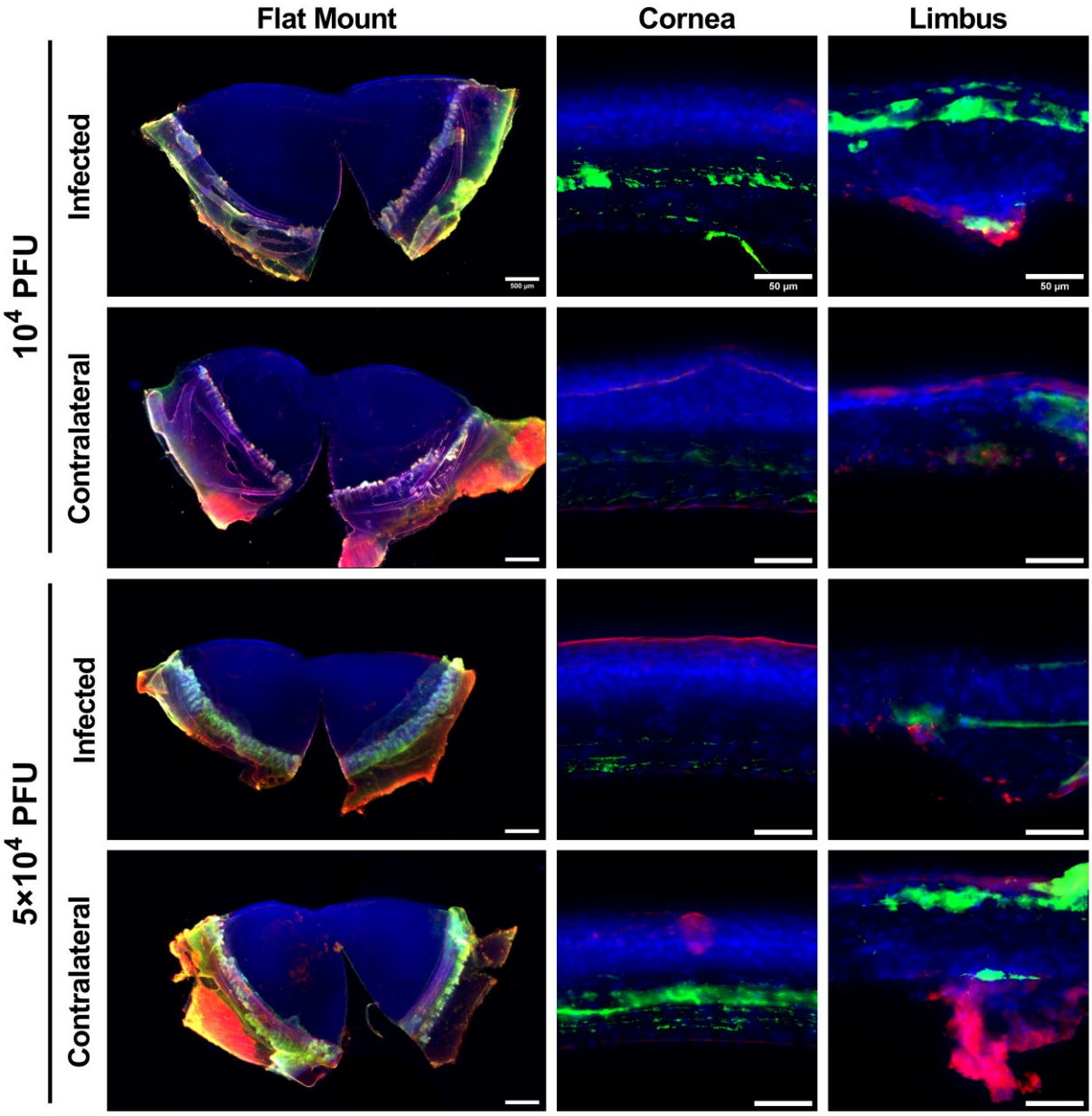

Figure 10. ***Mouse cornea immunohistochemistry at three days post HSV-1 infection.*** *Left panels show flat mounts stained for HSV-1 (Red), p63 (Green), and DAPI (Blue). Scale bar: 500µm. Center and right panels show cross-sections through the cornea and limbus, respectively. Sections were stained for HSV-1 (Red), p63 (Green), and DAPI (Blue). Scale bar: 50µm.*

4.1.3. *In vitro* and *ex vivo* efficacy of anti-viral treatment by GF19

Cell cultures with human corneal epithelial (HCE) cells were used to determine the efficacy of LL37 cathelicidin, GF17, and its modified counterpart, GF19. Starting at 5 µM, both the GF19 and LL37 cell cultures showed a decrease in the amounts of HSV-1 being released into the media compared to GF17 or the controls treated with scrambled GF19 (sGF19) peptide (Figure 11B, 24 hours) (n=3 samples). At a concentration of 15µM and higher, GF17 also showed a decreased viral release compared to sGF19. Furthermore, virus was not detected in LL37 treated cells starting at 15µM and for GF19 starting at 45µM (Figure 11B, 24 hours). After the initial 24 hours, the media was removed and fresh media not containing the peptides was given to the HCE cells. The removal of the treatment was performed to observe the presence of infected cells and the susceptibility of the remaining cells. Lack of detectable virus would indicate that the treatment either lysed infected cells, halting the production of infectious virions or was able to protect the healthy cells from infection. Interestingly, LL37 showed a notable decrease in active virus compared to the other peptides starting at 10µM (Figure 11B, 48 hours). GF19 showed very little virus present at 45µM, with two thirds of the cell cultures having no virus detected. Additionally, when looking at the DAPI staining of the cells, there was less clumping of cells and less virus detected at the higher concentrations of GF19 (Figure 11A). Together, this would suggest that GF19 at 45µM is reducing cytopathogenic effect in cells and reducing the amount of active virus being secreted, both of which appear similar to non-infected cells. BMDCs treated with hydrogels containing GF19 had lower expression of pro-inflammatory markers, indicating that the materials were immune compatible (Figure 11C). However, non-encapsulated GF19 showed comparable expressions of CD40 and CD86 to LPS treated BMDCs (Figure 11C).

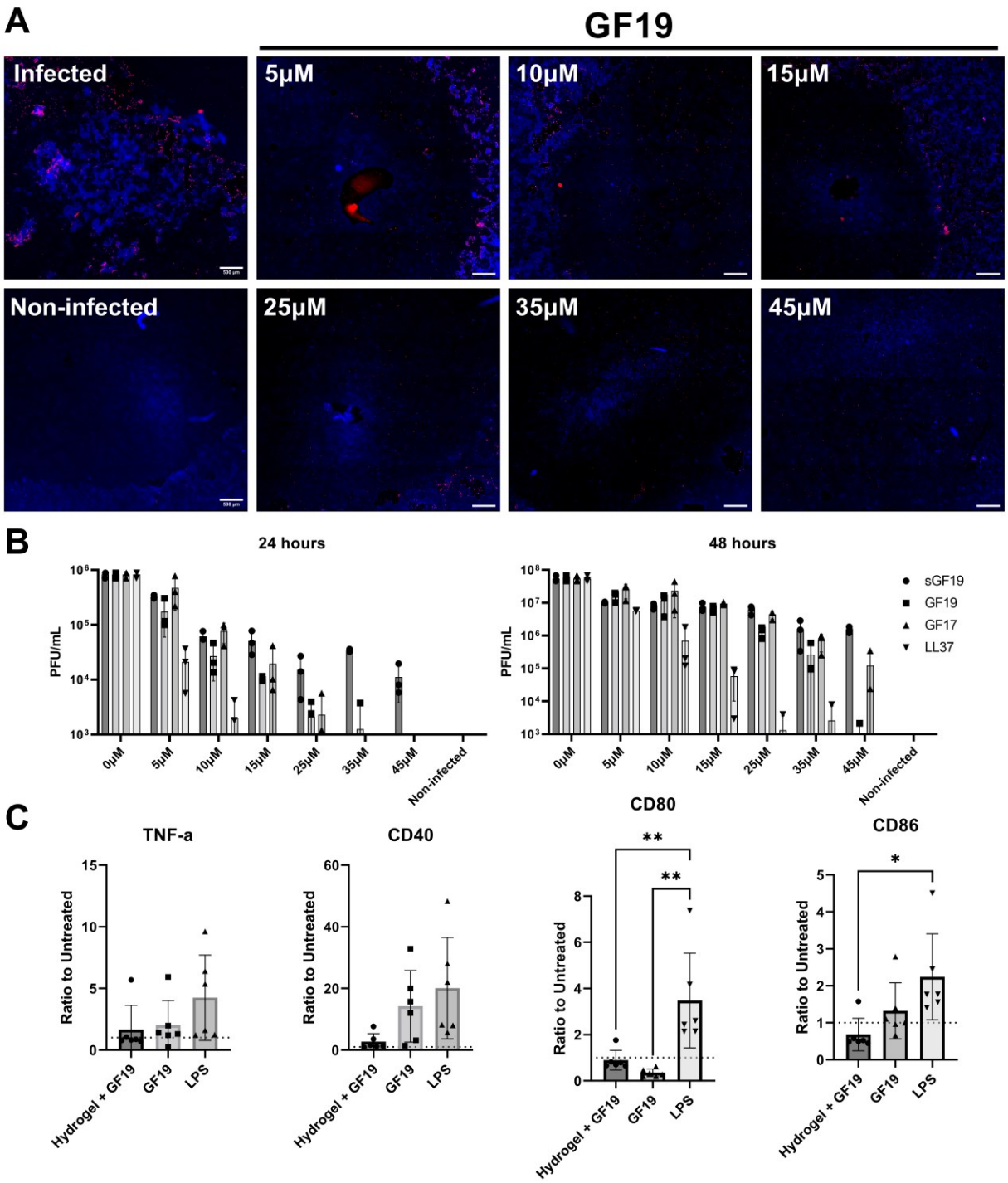

Figure 11. ***In vitro efficacy and immune compatibility of anti-viral GF19.*** *Human corneal epithelial cells were infected with HSV-1 at MOI 1 and were given anti-viral treatments of varying concentrations for the first 24 hours. Following the 24 hours, media containing the treatment was*

*removed and media not containing was added to the cells. (A) Cells were stained for HSV-1 (Red) and DAPI (Blue). Scale bar: 500µm. (B) Cell culture media was used to quantify amount of virus secreted through plaque assays. (C) BMDCs treated with LPS, 45µM GF19 or hydrogels containing 45µM GF19. Flow cytometry was used to observe expression of TNF-α, CD40, CD80, and CD86. Data was presented as a ratio of MFI of treatment over that of untreated cells. Asterisks indicate significance versus the positive control, LPS. *P ≤ 0.05 and **P ≤ 0.01 by one-way ANOVA Tukey's multiple comparisons test.*

To further test the efficacy of GF19, *ex vivo* infections were performed and given a treatment of either 45µM GF19 or 45µM GF19 encapsulated in SiO_2 NPs. Pre-treatment and immediate treatment with GF19 resulted in very little virus detected within the cornea while the delayed-treatment with GF19 had a few cells infected in the cornea but much less than that of infected corneas (Figure 12A). When GF19 was encapsulated in SiO_2 NPs, the pre-treatment was not effective at inactivating the virus and the immediate and delay treatments were not as effective as GF19 alone (Figure 12A). However, the longer-term cumulative effects of lower doses of sustained GF19 release from the NPs was not studied here. Plaque assays, performed to quantify the amount of active virus produced, had similar results to the imaging (Figure 12B). Both the *in vitro* and *ex vivo* assays show that GF19 was effective at reducing viral loads, particularly if applied prophylactically or immediately after infection.

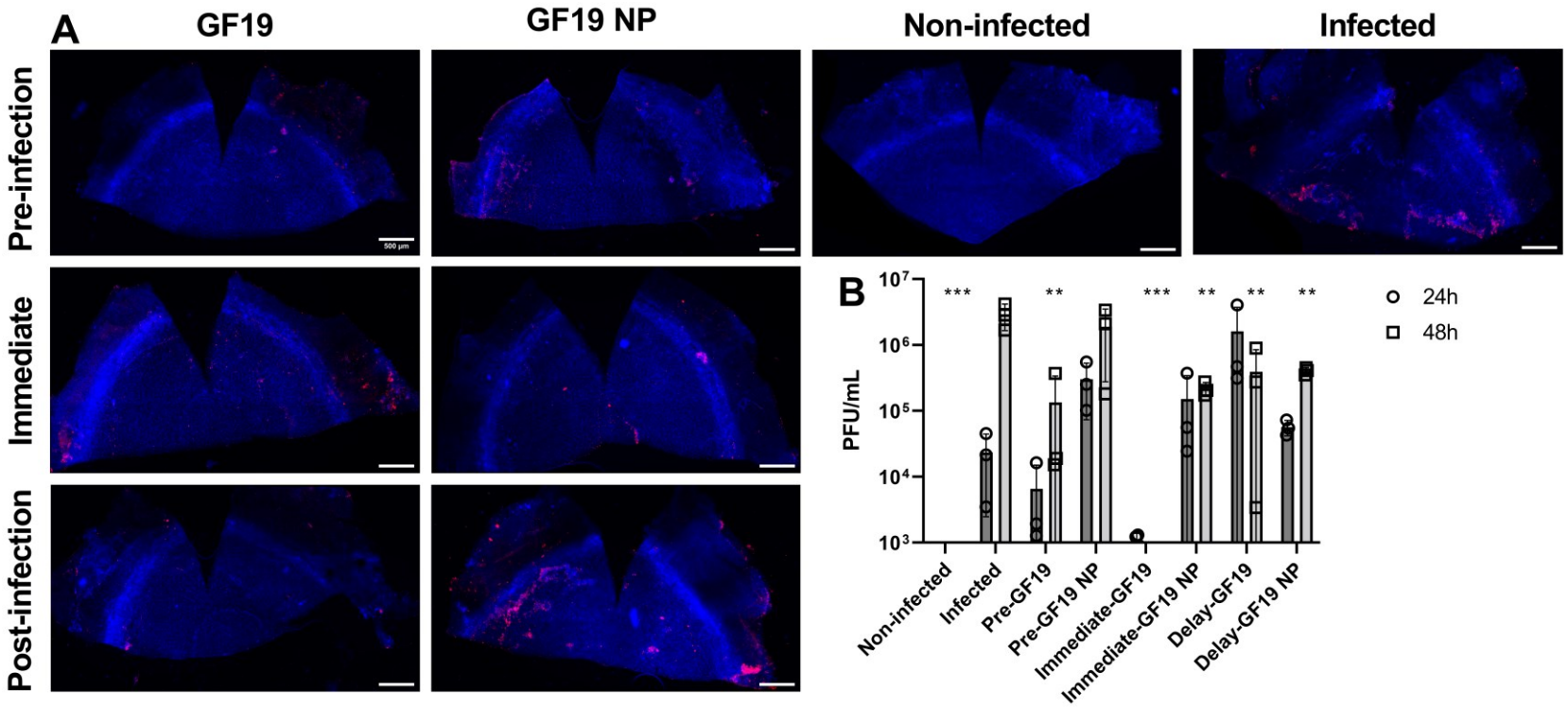

Figure 12. ***Ex vivo efficacy of anti-viral GF19.*** *Excised eyes from C57BL/6J mice were infected with 10^4 PFU for 2 days and received treatment with 45µM GF19 or 45µM GF19 encapsulated in SiO_2 NPs. Subgroups were created which separated the treatment regime into three: 1) Pre-GF19 – enucleated eyes were incubated for an hour in treatment before infection. 2) Immediate GF19 - , eyes were treated with GF19 immediately after the infection. 3) Delay GF-19 – corneas were treated with GF19 at 24 hours after the initial infection. (A) Flat mounts were stained for HSV-1 (Red) and DAPI (Blue). Scale bar: 500µm. (B) Quantifying active virus sections through plaque assays at 24 and 48 hours. Asterisks indicate significance versus the positive control, infected. *P ≤ 0.05, **P ≤ 0.01, and ***P ≤ 0.001 by two-way ANOVA Tukey's test.*

4.2. Treating ocular inflammation with a CB2r agonist

4.2.1. *In vitro* immune compatibility

BMDC cultures were used to test the immune compatibility of CB2r agonist TA-A001, making sure that TA-A001 treatment does not activate dendritic cells, cells that can promote a pro-inflammatory response in the cornea and reduce vision acuity (45-49). Expression of immune markers CD40, CD80, CD86, and TNF-α were significantly lower for cells treated with prednisolone, a high concentration of TA-A001 or the SmartCelle delivery vehicle of TA-A001 (Figure 13). Interestingly, despite starting at the same amount of BMDCs, both prednisolone and TA-A001 had a low number of live BMDCs after the treatment (Figure 13). This suggests that TA-A001 does not activate dendritic cells.

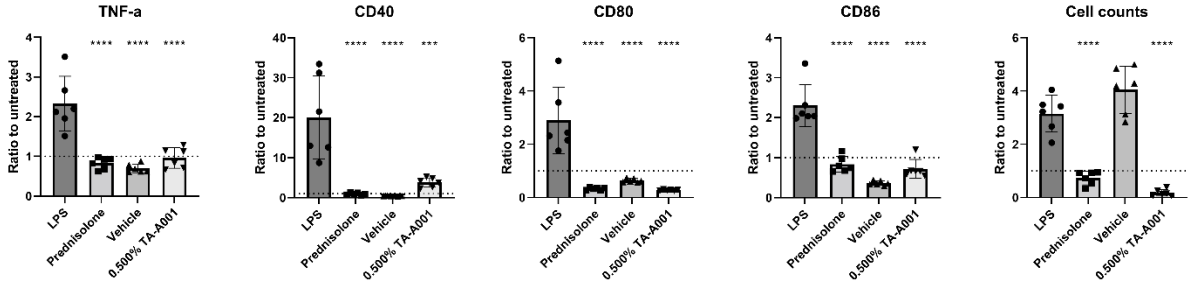

Figure 13. ***BMDCs compatibility with CB2r agonist, TA-A001.*** *BMDCs were treated with either prednisolone, SmartCelle delivery vehicle, or 0.500% TA-A001 delivered through SmartCelle. Flow cytometry was performed to measure the MFI of TNF-α, CD40, CD80, and CD86 as well as the counts of $CD11^+$ live dendritic cells. Data was presented as a ratio to the untreated cells. Asterisks indicate significance compared to the positive control, LPS. ***P ≤ 0.001 and ****P ≤ 0.0001 compared to LPS by one-way ANOVA Tukey's test.*

4.2.2. Clinical evaluation of *in vivo* mouse corneal alkali burns

Mice were given an alkali burn on the cornea and given a treatment of prednisolone, vehicle or one of three concentrations of TA-A001 for 14 days. At day 3, post-burn, two mice from the prednisolone group died. Brightfield and OCT images showed no marked morphological changes in the treated corneas except for the prednisolone group where small disruptions to the epithelium were observed (Figure 14A-B). When examining the thickness of the cornea with OCT, one cornea from the prednisolone group and one from the 0.500% TA-A001 group were very thick, and this thickness was not observed in the contralateral eyes (Figure 14E). Corneal sensitivity of prednisolone treated mice decreased at two weeks compared to before the burns (Figure 14C). The other groups as well as the contralateral eyes did not show a significant difference (Figure 14C). The IOP significantly increased after mice were treated with prednisolone but significantly decreased in mice given 0.250% or 0.500% TA-A001 (Figure 14D). Fluorescein staining of the cornea, used to detect injuries to the ocular surface, was used to determine the rate of epithelial wound closure after the alkali burn and administration of the different eye drops. By day 2 post-burn, all the groups had significantly decreased the area of the wound (Figure 14F). Between one and two weeks after wound closure and re-epithelialization, fluorescein staining of the epithelium was observed but it was diffuse as opposed to bright staining when the injury was sustained. For groups 0.250% and 0.500% TA-A001, the diffuse fluorescein took longer to appear, suggesting a more compact epithelium and a properly functioning tear film (Figure 14F). Finally, mice given prednisolone steadily lost weight through the two weeks, with a significant decrease in weight that was first observed on day 6 (Figure 14G). The clinical results show that prednisolone treatment resulted in negative side effects that were not observed in TA-A001 treated mice.

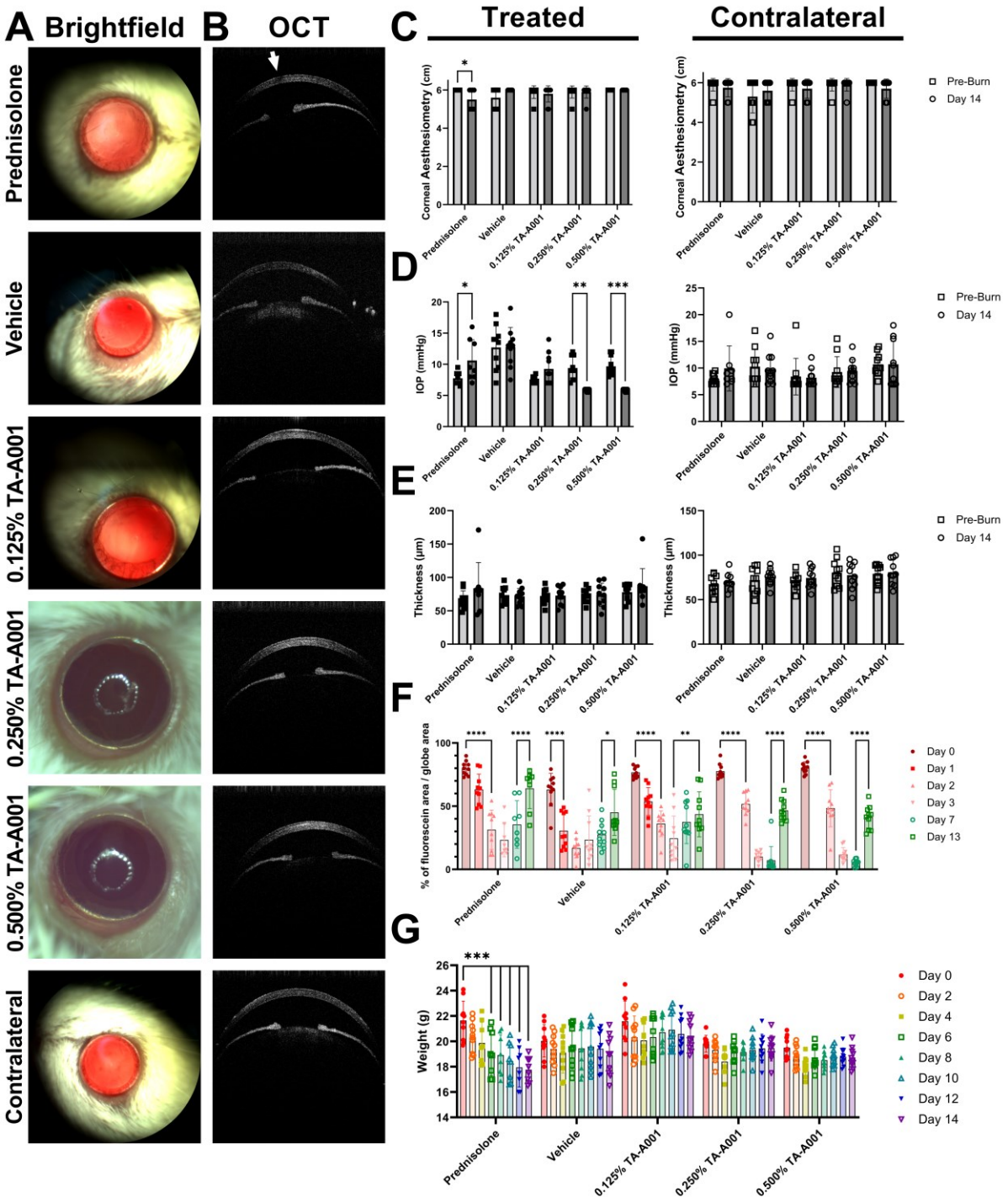

Figure 14. ***Clinical exams of alkali burned mice treated with prednisolone, drug vehicle or TA-A001.*** *Female BALB/c mice were burned with 250mM NaOH for 15 seconds, then treated with prednisolone, one of three concentrations of TA-A001 or the SmartCelle delivery vehicle alone.*

*Brightfield (A) and OCT (B) images of eyes at two weeks post-burn. The arrowhead shows a disruption of the corneal epithelial curvature. Corneal sensitivity (C), intraocular pressure (D), and corneal thickness (E) before the burn and at two weeks post-burn. (F) Fluorescein staining of the treated eyes immediately following the burn and at days 1, 2, 3, 7, and 13 post-burn. Data was presented as area of fluorescein over the full area of the mouse eye. Fluorescein staining seen on days 7 and 13 was diffuse only and is indicated by the hollow points and green colouring. (G) Weights of the mice every two days throughout the experiment. *P ≤ 0.05, **P ≤ 0.01, ***P ≤ 0.001, and ****P ≤ 0.0001 by two-way ANOVA Tukey's multiple comparisons test for all except the tonometry which used two-way ANOVA Šidák's multiple comparisons test.*

4.2.3. Post-mortem evaluation of *in vivo* mouse corneal alkali burns

Flat mount staining of $CD31^+$ vessels revealed a significant increase in corneal neovascularization in 0.500% TA-A001 treated mice (Figure 15). Despite having more neovascularization, when looking at the expression of TSG101, CD63 and MCP-1, the 0.500% TA-A001 treated mice had very little expression of all three markers, of which, CD63 and MCP-1 are markers for inflammation (Figure 16A-D). Interestingly, there was significant expression of CD63 and MCP-1 in the epithelium for 0.250% treated mice which was not observed in the other mice (Figure 16A-D). TSG101 expression did not have any significant differences. The stroma also did not have any significant differences between the samples. mRNA expression of MCP-1 had no significant differences between the samples and the 0.250% TA-A001 treated mice had the lowest expression (Figure 16E). Additionally, a cytokine multiplex assay for TNF-α, IL-1β, IL-6, IL-10 and IL-17A on individual mouse tears were below the limit of detection for the five cytokines for the vast majority of the samples, samples from both before the burn and at two weeks. These results would suggest that TA-A001 treatment promotes neovascularization and that 0.250% TA-A001 treated mice had high MCP-1 protein expression while the higher dose, 0.500% TA-A001, had no significant change in MCP-1 expression.

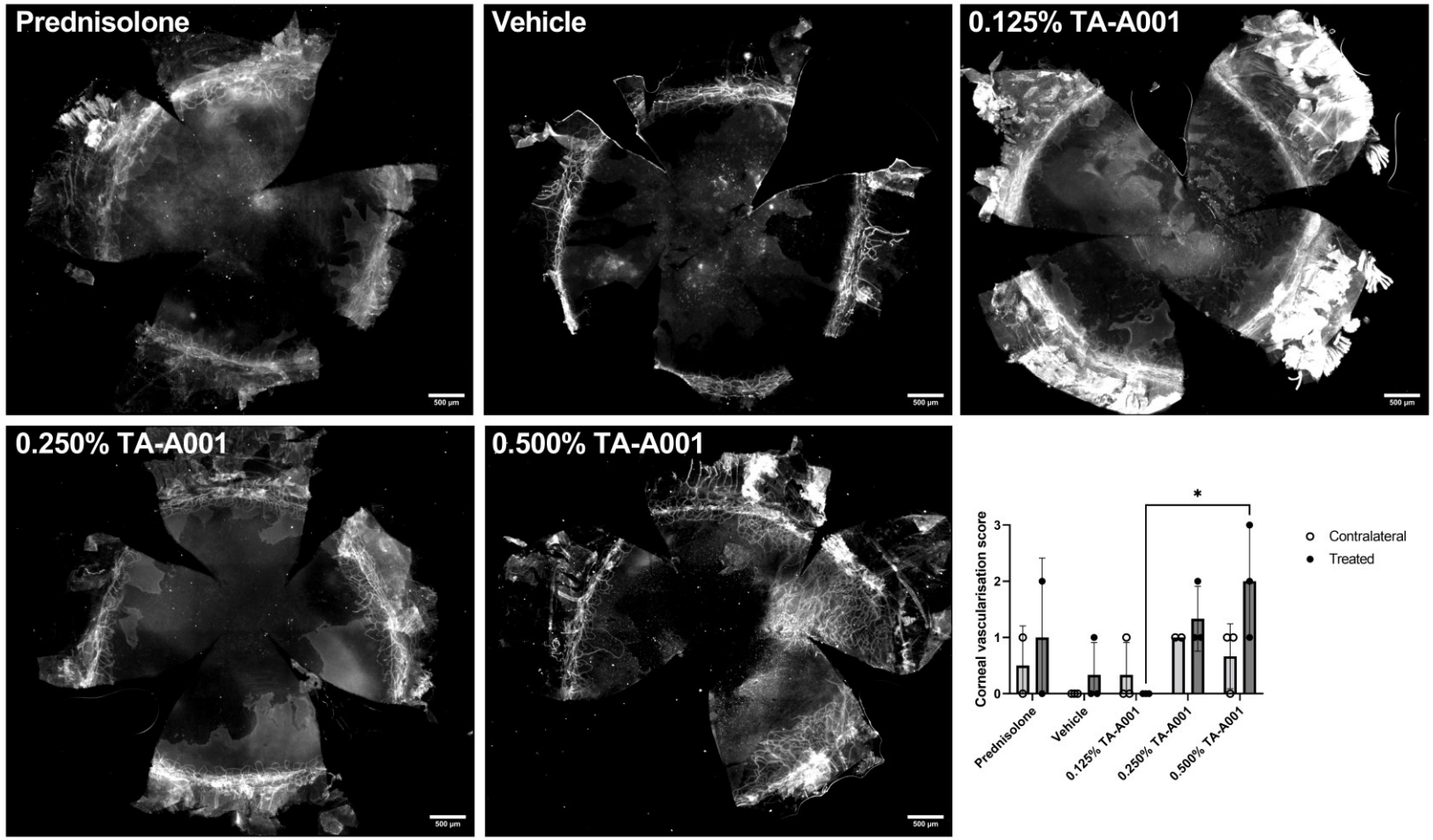

Figure 15. ***Corneal neovascularization after two weeks on prednisolone, drug vehicle or TA-A001 treatment.*** *Flat mount imaging of CD31 in the corneas. Three corneas from each group were stained except prednisolone which had two. The graph summarizes the incidence of corneal neovascularization. Scores: 0 = <300µm, 1 = 300-400µm, 2 = 401-500µm, 3 = >500µm. Scale bar: 500µm. *P ≤ 0.05 by two-way ANOVA Šidák's multiple comparisons test.*

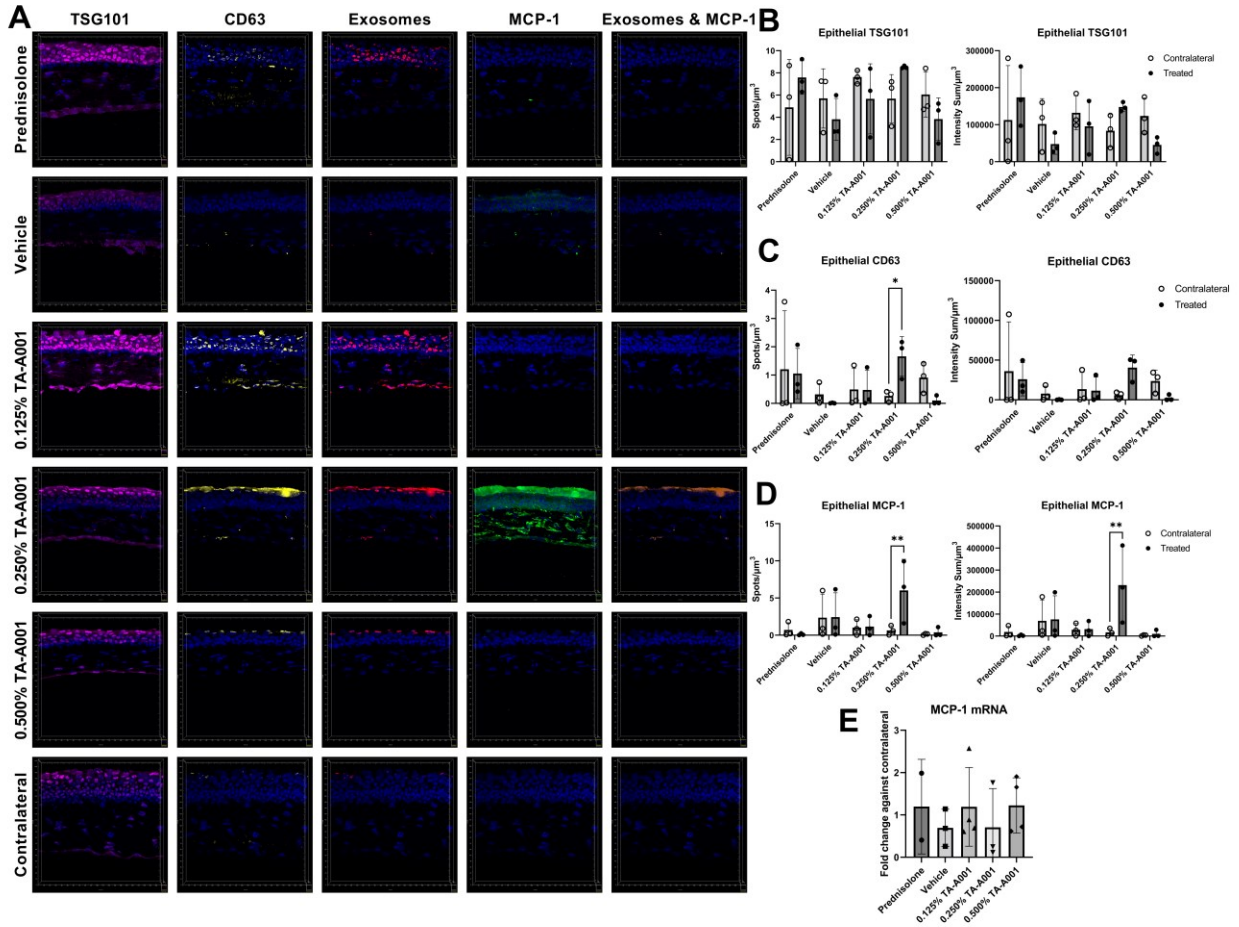

Figure 16. ***Expression of extracellular vesicles and MCP-1 in prednisolone, drug vehicle or TA-A001 treated mice.*** *(A) Cryosections of three mice per group were stained for TSG101 (Magenta), CD63 (Yellow), MCP-1 (Green), and DAPI (Blue). Colocalized channels of TSG101 and CD63 were termed exosomes (Red), colocalization of exosomes with MCP-1 was termed exosomes + MCP-1 (Brown). Quantifications of epithelial TSG101 (B), CD63 (C), and MCP-1 (D) was measured by performed spot reconstruction in Imaris v9.1.2 and measuring five random regions of interest, each of 750µm^3. (E) mRNA expression of MCP-1 in mouse eyes by qPCR. *P ≤ 0.05 and **P ≤ 0.01 by two-way ANOVA Šidák's multiple comparisons test.*

Nerve staining with antibodies against βIII tubulin and substance P (a pro-inflammatory neuropeptide), revealed slightly different expressions between the groups (n=3 per group). Substance P levels were lower in prednisolone treated mice compared to the TA-A001 treated mice, but the different was not significant ($p>0.05$) (Figure 17A-C). The mRNA expression of substance P was similar between the different groups (Figure 17D). βIII tubulin, which is a structural protein in the neuronal processes, showed similar expression amongst the different groups (Figure 17C). In the contralateral eyes, long and relatively straight nerves can be seen in the stroma and a lot of innervation in the epithelium (Figure 17A). Prednisolone treated mice did not have as much innervation and would often have a haze of βIII tubulin indicating damaged nerves (Figure 17A). Corneas treated with the lower concentrations of 0.125% and 0.250% TA-A001, showed some innervation within the epithelium. The nerves were slightly disorganised and not as uniform as in the contralateral eyes (Figure 17A). With the 0.500% TA-A001 group, the epithelial innervation and nerve organization in the stroma resembled that of the contralateral eyes (Figure 17A). This would suggest that TA-A001 treatment resulted in nerve regeneration to resemble the nerve layout of a non-burned cornea.

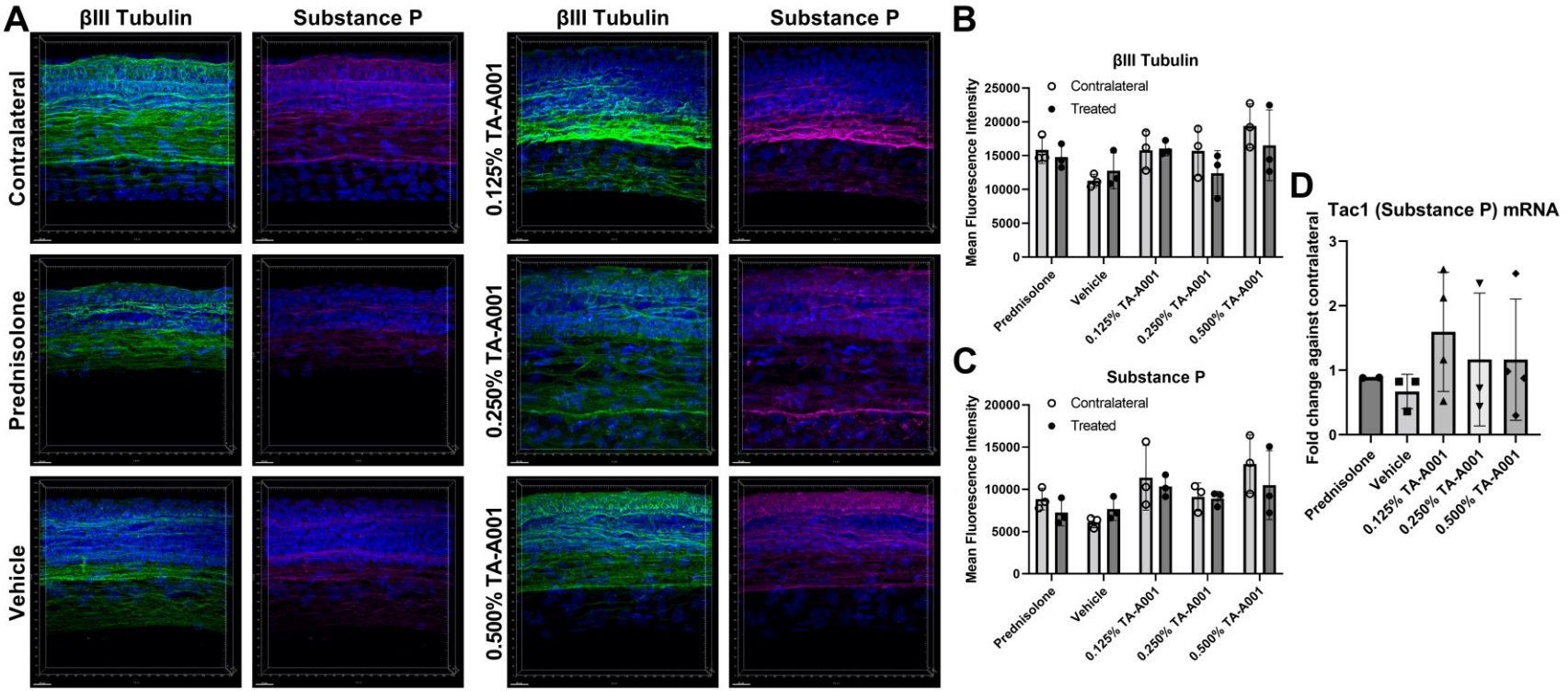

Figure 17. ***Corneal nerve density and morphology after prednisolone, drug vehicle or TA-A001 treatment.*** *(A) Thick cryosections were stained for βIII tubulin (Green), substance P (Magenta), and DAPI (Blue), n=three mice per group. Quantifications of βIII tubulin (B) and substance P (C) was measured by performing extended depth of focus in Zen Blue, creating a mask of the sample using an unstained channel, and measured the MFI. (D) mRNA expression of Tac1 of mouse eyes as determined by qPCR.*

Chapter 5 – Discussion

5.1. Understanding and treating HSV-1 ocular infections

Primary HSV-1 infections are mild and often undetected, but the viruses undergo latency after retrograde transport to the trigeminal ganglia (TG) and persistent within the body. Reactivation of the virus leads to active infection and replication in corneal cells. Reactivation often involves inflammation which is detected as HSK. If uncontrolled, HSK can lead to tissue damage and scarring. It often takes seven days for mice to develop HSK after being infected with HSV-1 (159). It is unclear how long it takes HSK to develop in infected human patients due to not knowing when the patient was infected. A case report involving a patient being infected by a donor cornea transplant took five days to develop clinical symptoms (160).

To characterise early HSV-1 eye infections, a combination of *ex vivo* and *in vivo* experiments were performed. Mouse eyes infected *ex vivo* for two days had a lot of virions present in the limbus that colocalized with p63, a stem cell and transient amplifying cell (TAC) marker (Figure 8A). Additionally, eyes that were infected had a slight, non-significant, decrease in viable cells, from having 92% live cells to 84% live cells once infected, and higher initial infection concentrations had less infected cells, from having 0.57% of cells infected at 10^3 PFU to having 0.33% cells infected at 10^5 PFU (Figure 8B). This suggests that HSV-1 begins lysing cells before HSK occurs and that cells in the limbus, in particular, stem cells and TACs, were more likely to be infected and lysed. The colocalization of infected cells with p63 was also observed in human corneas that were infected *ex vivo* for two days (Figure 8C). The increased risk of stem cells being infected and lysed coincides with HSK patients having an increased rate of limbal stem cell deficiency (LSCD) (36).

To further study the localization of the virus early in the infection, mice were infected in one eye with HSV-1 for three days. During this time, mice did not show clinical signs of HSK (Figure 9). Despite this, virus was found in both eyes for most of the mice through immunohistochemistry

and were strongly present in the limbus (Figure 10). Unlike the *ex vivo* infections, the *in vivo* infections showed little colocalization of p63 with HSV-1 (Figure 10). In humans, roughly 9.3% of HSK patients develop LSCD (135). The inconsistency of HSV-1 infections in the limbus of the infected mice might be linked with the low percentage of people who develop LSCD. It is unclear as to what caused this inconsistency, however the immune system might be playing a protective role. A difference between the *ex vivo* and the *in vivo* infections is the potential of immune responses to infiltrate into the tissue. In *ex vivo*, the eyes were limited to immune cells and defensive mechanisms present in the eye at the time of excision. For *in vivo*, immune cells or molecules have the potential to come into the site of infection. This further makes sense when observing the infection in the cornea, where most eyes had HSV-1 virions present in both the *ex vivo* and *in vivo* infections. The lack of vascularization in the cornea can make it difficult for an immune response to be mounted quickly and, as such, virus is abundant in the live infected mice. Additionally, most HSV-1 eye infections resolve themselves in one to three weeks after symptoms appear, in large part due to the immune system controlling the infection (161, 162).

HSK patients are often given ACV, or one of its derivatives, to control the viral infection. Despite their widespread use, there are multiple issues with ACV such as more than a fifth of patients still having reoccurring HSV ocular disease, the rise of ACV-resistant HSV-1, only blocking viral replication, and poor uptake into corneal tissues (97, 98, 100). Alternative anti-viral treatments are being explored, such as the use of the cationic peptide, LL37 (122). GF17, a fragment that has been effective against Zika virus and Ebola virus, has been modified with two additional amino acids, termed GF19 (123, 124). *In vitro* testing of GF19 on human corneal epithelial (HCE) cells show a reduction of HSV-1 activity during the period of treatment and after the treatment (Figure 11A-B). For the first 24 hours, while the infected cells were treated with 45µM GF19, no virus was detected in the supernatant. After the treatment was washed away, two thirds of the cell cultures treated with 45µM GF19 did not have any detected virus in the supernatant (Figure 11A-B). Additionally, there was a decrease in virions present with 25µM and 35µM GF19 treatment compared to the scrambled GF19 (sGF19). Since LL37 is capable of modulating the immune response and promote an IFN-1 response, it is likely that the post-treatment effects of GF19 are due to it also modulating the immune response (119). The anti-

viral properties observed by LL37 in the HCE cell cultures may also be due to the toxicity of LL37 which previous studies indicate high toxicity starting at 2µM in HCE cells (125).

To assess the inflammatory capacity of GF19, 45µM GF19 was given to BMDCs for 24 hours. Expression of CD40 and CD86 on treated BMDCs were like LPS treated BMDCs (Figure 11C). CD40 and CD86 are both costimulatory molecules which promote naïve T cell differentiation (163). Furthermore, CD40 can also promote a $CD8^+$ T cell response as well as promoting natural killer cell proliferation, both cells important in responding to ocular HSV-1 infections (48, 50, 58, 164, 165). This suggests that the use of GF19 could promote immune cell responses that are beneficial in responding against HSK. Interestingly, the expression of CD40 and CD86 are decreased when GF19 was delivered through SiO_2 NPs in a CLP-LCPP hydrogel (Figure 11C). Seeing as GF19 was causing the upregulation of desirable costimulatory molecules, it might not be beneficial to deliver the treatment through a hydrogel as it is reducing the inflammatory effects of GF19 and might lead to a less potent anti-viral response.

The efficacy of GF19 was also tested in an *ex vivo* setting using multiple treatment conditions, such as treating before the infection, immediately after the infection and after 24 hours form the initial infection. Treatment with GF19 in all three conditions resulted in a reduction of virus secreted into the media (Figure 12). Interestingly, the pre-treatment with GF19 was able to reduce the number of virions secreted despite being washed out before the infection. Since LL37 is able to promote an IFN-1 response in treated cells and that IFN-1 plays a large role in combating HSV-1 infections, the protective effects of GF19 could be due to promoting an IFN-1 expression (70, 71, 83, 84, 119-121). When the GF19 was delivered through SiO_2 NPs, the pre-treatment was not effective at reducing the viral burden, but the other conditions were able to reduce the amount of virus secreted. The pre-treatment was most likely ineffective because in one hour, very little GF19 would have been released from the SiO_2 NPs designed for sustained release, and not in sufficient quantity to have had a strong effect.

5.2. Treating ocular inflammation with a CB2r agonist

Corticosteroids are often prescribed to patients suffering from keratitis, including HSK. While effective at reducing inflammation, they also come with notable side effects, in particular, elevated IOP and glaucoma (136). Agonists to cannabinoids receptors (CBr) are a potential alternative treatment, with publications showcasing the improved wound healing and decreased IOP with CBr agonist treatment (136, 146-149). CB2r agonist TA-A001 delivered through SmartCelle vehicle, the vehicle alone, and prednisolone were given to BMDCs. The expression of inflammatory markers TNF-α, CD86, and CD86 were similar between TA-A001 treated cells and those treated with prednisolone (Figure 13). CD40 was slightly more expressed in TA-A001 treated cells but were still significantly lower than the cells treated with the positive control, LPS. Since the CD40 expression was still very low compared to the LPS activated cells, the CD40 may not be playing a pro-inflammatory role. Low levels of CD40 on dendritic cells can promote regulatory T cells generation (166). Additionally, BMDC counts were very low in TA-A001 treated cultures which coincides with previous studies claiming that CBrs can promote NF-κB-dependent apoptosis (167). The combination of causing apoptosis and low expression of CD40 in BMDCs may play a role in reducing inflammation in a live model.

Alkali burns were used to induce corneal inflammation in mice, which were then treated with one of three concentrations of TA-A001, the vehicle alone, or prednisolone. Mice treated with prednisolone had eyes that were less touch-sensitive, had more diffuse fluorescein staining at two weeks, and had a higher IOP than before the treatment (Figure 14C). The prednisolone treated mice also lost weight over the 2-week study that indicated an adverse effect on overall health of the animals, which was not observed in the other groups (Figure 14G). On the contrary, mice treated either 0.250% TA-A001 or 0.500% TA-A001 had no weight loss and showed a decrease in IOP (Figure 14). Importantly, lowering the IOP reduces the risk of developing glaucoma (168). The mice treated with higher concentrations of TA-A001 performed much better in the clinical examinations compared to the prednisolone treated mice.

Post-mortem immunohistochemical examinations of sectioned corneas were performed to obtain a more complete understanding of what is occurring in these mice. Neovascularization

was measured in the mice by staining for CD31, a marker that can stain blood vessels in the cornea (169). The mice treated with 0.500% TA-A001 had a significantly more vasculature expression in the cornea (Figure 15). This coincides with a previous cannabinoid study where a CB1r blockade reduced neovascularization in the cornea (153). Neovascularization in the cornea often causes a decrease in vision and optical clarity, as well as being associated with inflammation suggesting that care is needed when determining the optimal dosage of TA-A001 (170, 171).

To better understand the inflammation in the cornea, exosomes markers TSG101 and CD63, which are involved in cell-cell communication were stained in addition to MCP-1, a marker for inflammation, a potent chemoattractant for monocytes/macrophages, and can be transported by exosomes (172-175). In the epithelium, there was a significant increase of CD63 and MCP-1 expression for mice treated with 0.250% TA-A001 but the other treatments did not have a significant difference (Figure 16).

Cells secreting $CD63^{+}$ exosomes as well as MCP-1 expression can promote corneal neovascularization which may be one of the contributors to the vascularization observed in TA-A001 treated corneas (173, 176). Upregulation of MCP-1 by 0.250% TA-A001 but not the other doses suggests pro-inflammatory activity. Interestingly, CD63 and MCP-1 had very low expression in the 0.500% treated mice despite these mice having more corneal neovascularization. The lack of expression in these corneas may be indicative of a lack of prolonged inflammation despite the vascularization. What may be happening is that TA-A001 treatment may cause a temporary increase in expression of MCP-1 in corneas and that the time for when MCP-1 is expressed is dose dependent, with higher concentrations of TA-A001 resulting in an earlier MCP-1 expression. This could explain why the 0.500% TA-A001 treated mice had a significant increase in neovascularization with low MCP-1 expression, since the temporary MCP-1 expression occurred before day 14 and could have promoted the neovascularization observed at day 14. Unfortunately, MCP-1 expression was only examined at day 14, requiring additional timepoints to study if the time of high MCP-1 expression was dose dependent. Additionally, no significant differences in mRNA expression were observed for MCP-1 for any of the treatment groups suggesting a lack of inflammation (Figure 16E). Interestingly, for 0.250% TA-A001 treated mice, they had a significant protein increase of MCP-1 in the epithelium but had the lowest MCP-1

mRNA expression. This might be due to the lack of specificity from the qPCR assay which looked at the MCP-1 mRNA within the eye instead of focusing on the corneal epithelium which was observed for protein expression. To examine other potential sources of neovascularization, other inflammatory markers were examined.

Another way to assess inflammation is the secretion of cytokines into the tear film. During inflammatory conditions, low concentrations of cytokines could be detected in the tear film of mice (177-180). When trying to observe TNF-α, IL-1β, IL-6, IL-10 and IL-17A expression in the tear films, the cytokine concentrations were below the limit of detection for the vast majority of samples after the two weeks of treatment. Of note, IL-1β plays a large role in corneal neovascularization and the lack of it could suggest a greater importance of MCP-1 or other factors as the cause of the neovascularization observed (176). As such, it is unlikely that these pro-inflammatory cytokines contributed to the neovascularization observed in 0.500% TA-A001 treated mice.

Finally, another marker for inflammation is the release of substance P from neurons. Substance P is stored within neurons in the cornea and upon stress, will release the neuropeptide promoting inflammation through stimulating macrophages and promoting vascularization (181-184). Staining for βIII tubulin, a nerve marker, and substance P showed a non-significant increase in substance P expression with TA-A001 treatment (Figure 17). Interestingly, in the images, substance P was highly colocalized with βIII tubulin, suggesting that substance P was not released and remained within the nerves. This is further supported with the insignificant difference in Tac1 mRNA expression within the eye. Under inflammatory conditions, increased expression of Tac1 mRNA can be found in the cornea, so the lack of Tac1 expression seen in TA-A001 treated mice suggests that lack of producing and releasing substance P (183). Since substance P remained in the nerves and that Tac1 expression did not significantly differ, it is unlikely that substance P contributed to the neovascularization seen in the 0.500% TA-A001 treated mice. Additionally, when observing βIII tubulin staining, the innervation of the epithelium appears slightly different between the treatments (Figure 17). The epithelial innervation of 0.500% TA-A001 treated mice were similar to the non-burned contralateral eyes, while prednisolone treated mice had hazier and more diffuse βIII tubulin staining. This suggests that TA-A001 treatment was able to help

sensory neuron regrowth following the alkali burn and is probably why only the prednisolone treated mice saw a decrease in corneal sensitivity.

5.3. Conclusions and future prospects

5.3.1. Understanding and treating HSV-1 ocular infections

To summarize, early after HSV-1 eye infections occur, a lot of virions were present in the limbus, some of which co-localizes with stem cells and TACs. It would be interesting to see if the host's immune system plays a big role in stem cell infections and if so, what the factors for stem cell infections would be. Another portion that could be studied is what are the other cells being infected. Many of the corneas had infected cells and it could be beneficial to understand which cells in particular are harbouring the virus. If HSV-1 is actively lysing these cells, a potential treatment could be to supplement the function of the lysed cells. For example, if myofibroblasts, cells capable of producing large amount of collagen and extracellular matrix, were being lysed, a treatment to help maintain a proper extracellular matrix could reduce the disease severity.

Additionally, efficacy tests with GF19 shows that the anti-viral peptide was able to reduce viral burden even when washed out of the cells and produced some activation of BMDCs. It is likely that GF19 is exerting immune modulating effects on the cells however more work would need to be done to properly identify what is occurring. Despite not fully understanding the mechanisms of viral protection that GF19 uses, it has clearly shown anti-viral properties and should be pushed further into testing. It would be important to see if GF19 can effectively reduce the viral burden of an HSV-1 eye infection, both as a preventative treatment and as a therapeutic treatment.

5.3.2. Treating ocular inflammation with a CB2r agonist

The CB2r agonist, TA-A001, showed a reduction in inflammation that was comparable to the widely used corticosteroid, prednisolone, but with less side effects such as increased intraocular pressure or disruption of the epithelium. In addition to being better tolerated, high concentrations of TA-A001 had a comparable level of inflammation as prednisolone treated mice

except, TA-A001 treated corneas had more vascularization and had more epithelial innervation. More work should be done to better understand the vascularization seen and if it is connected with the elevated expression of MCP-1 seen in the 0.250% TA-A001 treated mice. Other then the neovascularization, 0.500% TA-A001 appears to reduce inflammation to a similar extent as prednisolone while minimizing negative consequences and promoting innervation.

Another area that would be interesting to further explore is the use of TA-A001 with HSV-1 infections. Since corticosteroids have the potential of reactivating latent HSV-1, along with the other negative side effects, a CB2r agonist may provide immune suppression without HSV-1 reactivation. A potential concern with the use of TA-A001 is the increased MCP-1 expression since MCP-1 expression in HSK can promote $CD4^+$ T cell infiltration which promotes disease severity (185). Since the MCP-1 was not highly expressed with the highest concentration of TA-A001, it is unclear how MCP-1 was expressed due to TA-A001 and if it would have a negative impact in HSK.

Beyond the use of these treatments individually, future endeavours could look at combining the anti-viral GF19 and the immunosuppressant TA-A001. Controlling HSK is both a viral problem but also an inflammatory problem, requiring both types of treatments. Combining GF19 treatments with TA-A001, if successful, could result in a combinational treatment that has less side effects than the conventionally used treatments.

Chapter 6 – References

1. Sridhar MS. Anatomy of cornea and ocular surface. Indian J Ophthalmol. 2018;66(2):190-4.
2. Ebrahimi M, Taghi-Abadi E, Baharvand H. Limbal stem cells in review. J Ophthalmic Vis Res. 2009;4(1):40-58.
3. Ashworth S, Harrington J, Hammond GM, Bains KK, Koudouna E, Hayes AJ, et al. Chondroitin Sulfate as a Potential Modulator of the Stem Cell Niche in Cornea. Front Cell Dev Biol. 2020;8:567358.
4. Yang AY, Chow J, Liu J. Corneal Innervation and Sensation: The Eye and Beyond. Yale J Biol Med. 2018;91(1):13-21.
5. McDermott AM. The role of antimicrobial peptides at the ocular surface. Ophthalmic Res. 2009;41(2):60-75.
6. Vaidyanathan U, Hopping GC, Liu HY, Somani AN, Ronquillo YC, Hoopes PC, et al. Persistent Corneal Epithelial Defects: A Review Article. Med Hypothesis Discov Innov Ophthalmol. 2019;8(3):163-76.
7. Saleh D, Yarrarapu SNS, Sharma S. Herpes Simplex Type 1. StatPearls. Treasure Island (FL): StatPearls Publishing. Copyright © 2022, StatPearls Publishing LLC.; 2022.
8. Whitley RJ. Herpesviruses. Medical Microbiology 4th edition. 1996:Chapter 68.
9. Whitley RJ. Herpes simplex encephalitis: adolescents and adults. Antiviral Res. 2006;71(2-3):141-8.
10. Miller GG, Dummer JS. Herpes simplex and varicella zoster viruses: forgotten but not gone. Am J Transplant. 2007;7(4):741-7.
11. Farooq AV, Shukla D. Herpes simplex epithelial and stromal keratitis: an epidemiologic update. Surv Ophthalmol. 2012;57(5):448-62.
12. Theil D, Derfuss T, Paripovic I, Herberger S, Meinl E, Schueler O, et al. Latent herpesvirus infection in human trigeminal ganglia causes chronic immune response. Am J Pathol. 2003;163(6):2179-84.
13. Hüfner K, Horn A, Derfuss T, Glon C, Sinicina I, Arbusow V, et al. Fewer latent herpes simplex virus type 1 and cytotoxic T cells occur in the ophthalmic division than in the maxillary and mandibular divisions of the human trigeminal ganglion and nerve. J Virol. 2009;83(8):3696-703.
14. Liesegang TJ. Herpes simplex virus epidemiology and ocular importance. Cornea. 2001;20(1):1-13.
15. World Health Organization. Basics of HSV (Herpes Simplex Virus) Keratitis.
16. Hardy WR, Sandri-Goldin RM. Herpes simplex virus inhibits host cell splicing, and regulatory protein ICP27 is required for this effect. J Virol. 1994;68(12):7790-9.
17. Jenkins HL, Spencer CA. RNA polymerase II holoenzyme modifications accompany transcription reprogramming in herpes simplex virus type 1-infected cells. J Virol. 2001;75(20):9872-84.
18. Akhtar J, Tiwari V, Oh MJ, Kovacs M, Jani A, Kovacs SK, et al. HVEM and nectin-1 are the major mediators of herpes simplex virus 1 (HSV-1) entry into human conjunctival epithelium. Invest Ophthalmol Vis Sci. 2008;49(9):4026-35.

19. Guzman G, Oh S, Shukla D, Engelhard HH, Valyi-Nagy T. Expression of entry receptor nectin-1 of herpes simplex virus 1 and/or herpes simplex virus 2 in normal and neoplastic human nervous system tissues. Acta Virol. 2006;50(1):59-66.
20. Prandovszky E, Horváth S, Gellért L, Kovács SK, Janka Z, Toldi J, et al. Nectin-1 (HveC) is expressed at high levels in neural subtypes that regulate radial migration of cortical and cerebellar neurons of the developing human and murine brain. J Neurovirol. 2008;14(2):164-72.
21. Tiwari V, Oh MJ, Kovacs M, Shukla SY, Valyi-Nagy T, Shukla D. Role for nectin-1 in herpes simplex virus 1 entry and spread in human retinal pigment epithelial cells. Febs j. 2008;275(21):5272-85.
22. Shah A, Farooq AV, Tiwari V, Kim MJ, Shukla D. HSV-1 infection of human corneal epithelial cells: receptor-mediated entry and trends of re-infection. Mol Vis. 2010;16:2476-86.
23. Choudhary S, Marquez M, Alencastro F, Spors F, Zhao Y, Tiwari V. Herpes simplex virus type-1 (HSV-1) entry into human mesenchymal stem cells is heavily dependent on heparan sulfate. J Biomed Biotechnol. 2011;2011:264350.
24. Orosz L, Gallyas E, Kemény L, Mándi Y, Facskó A, Megyeri K. Involvement of p63 in the herpes simplex virus-1-induced demise of corneal cells. J Biomed Sci. 2010;17(1):47.
25. Tiwari V, Clement C, Xu D, Valyi-Nagy T, Yue BY, Liu J, et al. Role for 3-O-sulfated heparan sulfate as the receptor for herpes simplex virus type 1 entry into primary human corneal fibroblasts. J Virol. 2006;80(18):8970-80.
26. Tiwari V, Clement C, Scanlan PM, Kowlessur D, Yue BY, Shukla D. A role for herpesvirus entry mediator as the receptor for herpes simplex virus 1 entry into primary human trabecular meshwork cells. J Virol. 2005;79(20):13173-9.
27. Karasneh GA, Shukla D. Herpes simplex virus infects most cell types in vitro: clues to its success. Virol J. 2011;8:481.
28. Gianni T, Salvioli S, Chesnokova LS, Hutt-Fletcher LM, Campadelli-Fiume G. αvβ6- and αvβ8-integrins serve as interchangeable receptors for HSV gH/gL to promote endocytosis and activation of membrane fusion. PLoS Pathog. 2013;9(12):e1003806.
29. Campadelli-Fiume G, Cocchi F, Menotti L, Lopez M. The novel receptors that mediate the entry of herpes simplex viruses and animal alphaherpesviruses into cells. Rev Med Virol. 2000;10(5):305-19.
30. Montgomery RI, Warner MS, Lum BJ, Spear PG. Herpes simplex virus-1 entry into cells mediated by a novel member of the TNF/NGF receptor family. Cell. 1996;87(3):427-36.
31. Satoh T, Arii J, Suenaga T, Wang J, Kogure A, Uehori J, et al. PILRalpha is a herpes simplex virus-1 entry coreceptor that associates with glycoprotein B. Cell. 2008;132(6):935-44.
32. Arii J, Kawaguchi Y. The Role of HSV Glycoproteins in Mediating Cell Entry. Adv Exp Med Biol. 2018;1045:3-21.
33. Shukla D, Liu J, Blaiklock P, Shworak NW, Bai X, Esko JD, et al. A novel role for 3-O-sulfated heparan sulfate in herpes simplex virus 1 entry. Cell. 1999;99(1):13-22.
34. Reddy JC, Rapuano CJ. Current Concepts in the Management of Herpes Simplex Anterior Segment Eye Disease. Current Ophthalmology Reports. 2013;1(4):194-203.
35. Toriyama K, Inoue T, Suzuki T, Kobayashi T, Ohashi Y. Necrotizing keratitis caused by acyclovir-resistant herpes simplex virus. Case Rep Ophthalmol. 2014;5(3):325-8.
36. Carreno-Galeano JT, Dohlman TH, Yin J, Dana R. Limbal Stem Cell Deficiency Associated With Herpes Keratitis. Cornea. 2021;40(8):967-71.

37. Liu X, Xu S, Wang Y, Jin X, Shi Y, Zhang H. Bilateral Limbal Stem Cell Alterations in Patients With Unilateral Herpes Simplex Keratitis and Herpes Zoster Ophthalmicus as Shown by In Vivo Confocal Microscopy. Invest Ophthalmol Vis Sci. 2021;62(6):12.
38. Altshuler A, Amitai-Lange A, Tarazi N, Dey S, Strinkovsky L, Hadad-Porat S, et al. Discrete limbal epithelial stem cell populations mediate corneal homeostasis and wound healing. Cell Stem Cell. 2021;28(7):1248-61.e8.
39. Sangwan VS. Limbal stem cells in health and disease. Biosci Rep. 2001;21(4):385-405.
40. Steiner I, Spivack JG, O'Boyle DR, 2nd, Lavi E, Fraser NW. Latent herpes simplex virus type 1 transcription in human trigeminal ganglia. J Virol. 1988;62(9):3493-6.
41. Roizman B, Whitley RJ. An inquiry into the molecular basis of HSV latency and reactivation. Annu Rev Microbiol. 2013;67:355-74.
42. Kennedy DP, Clement C, Arceneaux RL, Bhattacharjee PS, Huq TS, Hill JM. Ocular herpes simplex virus type 1: is the cornea a reservoir for viral latency or a fast pit stop? Cornea. 2011;30(3):251-9.
43. Perng GC, Zwaagstra JC, Ghiasi H, Kaiwar R, Brown DJ, Nesburn AB, et al. Similarities in regulation of the HSV-1 LAT promoter in corneal and neuronal cells. Invest Ophthalmol Vis Sci. 1994;35(7):2981-9.
44. Koganti R, Yadavalli T, Shukla D. Current and Emerging Therapies for Ocular Herpes Simplex Virus Type-1 Infections. Microorganisms. 2019;7(10).
45. Kanangat S, Thomas J, Gangappa S, Babu JS, Rouse BT. Herpes simplex virus type 1-mediated up-regulation of IL-12 (p40) mRNA expression. Implications in immunopathogenesis and protection. J Immunol. 1996;156(3):1110-6.
46. Hirose S, Wang S, Tormanen K, Wang Y, Tang J, Akbari O, et al. Roles of Type 1, 2, and 3 Innate Lymphoid Cells in Herpes Simplex Virus 1 Infection In Vitro and In Vivo. J Virol. 2019;93(13).
47. Donaghy H, Bosnjak L, Harman AN, Marsden V, Tyring SK, Meng TC, et al. Role for plasmacytoid dendritic cells in the immune control of recurrent human herpes simplex virus infection. J Virol. 2009;83(4):1952-61.
48. Carr DJ, Wuest T, Ash J. An increase in herpes simplex virus type 1 in the anterior segment of the eye is linked to a deficiency in NK cell infiltration in mice deficient in CXCR3. J Interferon Cytokine Res. 2008;28(4):245-51.
49. Frank GM, Buela KA, Maker DM, Harvey SA, Hendricks RL. Early responding dendritic cells direct the local NK response to control herpes simplex virus 1 infection within the cornea. J Immunol. 2012;188(3):1350-9.
50. Banerjee K, Biswas PS, Kumaraguru U, Schoenberger SP, Rouse BT. Protective and pathological roles of virus-specific and bystander CD8+ T cells in herpetic stromal keratitis. J Immunol. 2004;173(12):7575-83.
51. Conrady CD, Zheng M, Stone DU, Carr DJ. CD8+ T cells suppress viral replication in the cornea but contribute to VEGF-C-induced lymphatic vessel genesis. J Immunol. 2012;189(1):425-32.
52. Suryawanshi A, Veiga-Parga T, Rajasagi NK, Reddy PB, Sehrawat S, Sharma S, et al. Role of IL-17 and Th17 cells in herpes simplex virus-induced corneal immunopathology. J Immunol. 2011;187(4):1919-30.
53. Yun H, Lathrop KL, Hendricks RL. A Central Role for Sympathetic Nerves in Herpes Stromal Keratitis in Mice. Invest Ophthalmol Vis Sci. 2016;57(4):1749-56.

54. Deshpande S, Banerjee K, Biswas PS, Rouse BT. Herpetic eye disease: immunopathogenesis and therapeutic measures. Expert Rev Mol Med. 2004;6(8):1-14.
55. Daheshia M, Kanangat S, Rouse BT. Production of key molecules by ocular neutrophils early after herpetic infection of the cornea. Exp Eye Res. 1998;67(6):619-24.
56. Osorio Y, Wechsler SL, Nesburn AB, Ghiasi H. Reduced severity of HSV-1-induced corneal scarring in IL-12-deficient mice. Virus Res. 2002;90(1-2):317-26.
57. Hendricks RL, Tumpey TM, Finnegan A. IFN-gamma and IL-2 are protective in the skin but pathologic in the corneas of HSV-1-infected mice. J Immunol. 1992;149(9):3023-8.
58. Ghiasi H, Cai S, Perng GC, Nesburn AB, Wechsler SL. Both CD4+ and CD8+ T cells are involved in protection against HSV-1 induced corneal scarring. Br J Ophthalmol. 2000;84(4):408-12.
59. Lundberg P, Welander P, Han X, Cantin E. Herpes simplex virus type 1 DNA is immunostimulatory in vitro and in vivo. J Virol. 2003;77(20):11158-69.
60. Liu Z, Guan Y, Sun X, Shi L, Liang R, Lv X, et al. HSV-1 activates NF-kappaB in mouse astrocytes and increases TNF-alpha and IL-6 expression via Toll-like receptor 3. Neurol Res. 2013;35(7):755-62.
61. Li H, Zhang J, Kumar A, Zheng M, Atherton SS, Yu FS. Herpes simplex virus 1 infection induces the expression of proinflammatory cytokines, interferons and TLR7 in human corneal epithelial cells. Immunology. 2006;117(2):167-76.
62. Sørensen LN, Reinert LS, Malmgaard L, Bartholdy C, Thomsen AR, Paludan SR. TLR2 and TLR9 synergistically control herpes simplex virus infection in the brain. J Immunol. 2008;181(12):8604-12.
63. Villalba M, Hott M, Martin C, Aguila B, Valdivia S, Quezada C, et al. Herpes simplex virus type 1 induces simultaneous activation of Toll-like receptors 2 and 4 and expression of the endogenous ligand serum amyloid A in astrocytes. Med Microbiol Immunol. 2012;201(3):371-9.
64. Su C, Zheng C. Herpes Simplex Virus 1 Abrogates the cGAS/STING-Mediated Cytosolic DNA-Sensing Pathway via Its Virion Host Shutoff Protein, UL41. J Virol. 2017;91(6).
65. Tullo A. Pathogenesis and management of herpes simplex virus keratitis. Eye (Lond). 2003;17(8):919-22.
66. Sawtell NM. Comprehensive quantification of herpes simplex virus latency at the single-cell level. J Virol. 1997;71(7):5423-31.
67. Centifanto-Fitzgerald YM, Yamaguchi T, Kaufman HE, Tognon M, Roizman B. Ocular disease pattern induced by herpes simplex virus is genetically determined by a specific region of viral DNA. J Exp Med. 1982;155(2):475-89.
68. Caspary L, Schindling B, Dundarov S, Falke D. Infections of susceptible and resistant mouse strains with herpes simplex virus type 1 and 2. Arch Virol. 1980;65(3-4):219-27.
69. Stulting RD, Kindle JC, Nahmias AJ. Patterns of herpes simplex keratitis in inbred mice. Invest Ophthalmol Vis Sci. 1985;26(10):1360-7.
70. Jouanguy E, Zhang SY, Chapgier A, Sancho-Shimizu V, Puel A, Picard C, et al. Human primary immunodeficiencies of type I interferons. Biochimie. 2007;89(6-7):878-83.
71. Menachery VD, Pasieka TJ, Leib DA. Interferon regulatory factor 3-dependent pathways are critical for control of herpes simplex virus type 1 central nervous system infection. J Virol. 2010;84(19):9685-94.

72. Lekstrom-Himes JA, Hohman P, Warren T, Wald A, Nam JM, Simonis T, et al. Association of major histocompatibility complex determinants with the development of symptomatic and asymptomatic genital herpes simplex virus type 2 infections. J Infect Dis. 1999;179(5):1077-85.
73. Group HEDS. Psychological stress and other potential triggers for recurrences of herpes simplex virus eye infections. Herpetic Eye Disease Study Group. Arch Ophthalmol. 2000;118(12):1617-25.
74. Toma HS, Murina AT, Areaux RG, Jr., Neumann DM, Bhattacharjee PS, Foster TP, et al. Ocular HSV-1 latency, reactivation and recurrent disease. Semin Ophthalmol. 2008;23(4):249-73.
75. Itzhaki RF, Wozniak MA. Herpes simplex virus type 1, apolipoprotein E, and cholesterol: a dangerous liaison in Alzheimer's disease and other disorders. Prog Lipid Res. 2006;45(1):73-90.
76. Gallar J, Tervo TM, Neira W, Holopainen JM, Lamberg ME, Miñana F, et al. Selective changes in human corneal sensation associated with herpes simplex virus keratitis. Invest Ophthalmol Vis Sci. 2010;51(9):4516-22.
77. Perng GC, Osorio N, Jiang X, Geertsema R, Hsiang C, Brown D, et al. Large Amounts of Reactivated Virus in Tears Precedes Recurrent Herpes Stromal Keratitis in Stressed Rabbits Latently Infected with Herpes Simplex Virus. Curr Eye Res. 2016;41(3):284-91.
78. Spruance SL, Kriesel JD, Evans TG, McKeough MB. Susceptibility to herpes labialis following multiple experimental exposures to ultraviolet radiation. Antiviral Res. 1995;28(1):57-67.
79. Arshad S, Petsoglou C, Lee T, Al-Tamimi A, Carnt NA. 20 years since the Herpetic Eye Disease Study: Lessons, developments and applications to clinical practice. Clin Exp Optom. 2021;104(3):396-405.
80. Kriesel JD. The roles of inflammation, STAT transcription factors, and nerve growth factor in viral reactivation and herpes keratitis. DNA Cell Biol. 2002;21(5-6):475-81.
81. White ML. Herpes Simplex Virus Keratitis: A Treatment Guideline - 2014. American Academy of Ophthalmology.
82. Daubeuf S, Singh D, Tan Y, Liu H, Federoff HJ, Bowers WJ, et al. HSV ICP0 recruits USP7 to modulate TLR-mediated innate response. Blood. 2009;113(14):3264-75.
83. Sen J, Liu X, Roller R, Knipe DM. Herpes simplex virus US3 tegument protein inhibits Toll-like receptor 2 signaling at or before TRAF6 ubiquitination. Virology. 2013;439(2):65-73.
84. Halford WP, Weisend C, Grace J, Soboleski M, Carr DJ, Balliet JW, et al. ICP0 antagonizes Stat 1-dependent repression of herpes simplex virus: implications for the regulation of viral latency. Virol J. 2006;3:44.
85. Burgess HM, Mohr I. Defining the Role of Stress Granules in Innate Immune Suppression by the Herpes Simplex Virus 1 Endoribonuclease VHS. J Virol. 2018;92(15).
86. Parkinson J, Lees-Miller SP, Everett RD. Herpes simplex virus type 1 immediate-early protein vmw110 induces the proteasome-dependent degradation of the catalytic subunit of DNA-dependent protein kinase. J Virol. 1999;73(1):650-7.
87. Orvedahl A, Alexander D, Tallóczy Z, Sun Q, Wei Y, Zhang W, et al. HSV-1 ICP34.5 confers neurovirulence by targeting the Beclin 1 autophagy protein. Cell Host Microbe. 2007;1(1):23-35.
88. Guo H, Omoto S, Harris PA, Finger JN, Bertin J, Gough PJ, et al. Herpes simplex virus suppresses necroptosis in human cells. Cell Host Microbe. 2015;17(2):243-51.
89. Zhu H, Zheng C. The Race between Host Antiviral Innate Immunity and the Immune Evasion Strategies of Herpes Simplex Virus 1. Microbiol Mol Biol Rev. 2020;84(4).

90. Neumann J, Eis-Hübinger AM, Koch N. Herpes simplex virus type 1 targets the MHC class II processing pathway for immune evasion. J Immunol. 2003;171(6):3075-83.
91. Mikloska Z, Bosnjak L, Cunningham AL. Immature monocyte-derived dendritic cells are productively infected with herpes simplex virus type 1. J Virol. 2001;75(13):5958-64.
92. Heilingloh CS, Kummer M, Mühl-Zürbes P, Drassner C, Daniel C, Klewer M, et al. L Particles Transmit Viral Proteins from Herpes Simplex Virus 1-Infected Mature Dendritic Cells to Uninfected Bystander Cells, Inducing CD83 Downmodulation. J Virol. 2015;89(21):11046-55.
93. Ma Y, Chen M, Jin H, Prabhakar BS, Valyi-Nagy T, He B. An Engineered Herpesvirus Activates Dendritic Cells and Induces Protective Immunity. Sci Rep. 2017;7:41461.
94. Gnann JW, Jr., Barton NH, Whitley RJ. Acyclovir: mechanism of action, pharmacokinetics, safety and clinical applications. Pharmacotherapy. 1983;3(5):275-83.
95. Whitley RJ, Gnann JW, Jr. Acyclovir: a decade later. N Engl J Med. 1992;327(11):782-9.
96. Chou TY, Hong BY. Ganciclovir ophthalmic gel 0.15% for the treatment of acute herpetic keratitis: background, effectiveness, tolerability, safety, and future applications. Ther Clin Risk Manag. 2014;10:665-81.
97. Miserocchi E, Modorati G, Galli L, Rama P. Efficacy of valacyclovir vs acyclovir for the prevention of recurrent herpes simplex virus eye disease: a pilot study. Am J Ophthalmol. 2007;144(4):547-51.
98. Duan R, de Vries RD, van Dun JM, van Loenen FB, Osterhaus AD, Remeijer L, et al. Acyclovir susceptibility and genetic characteristics of sequential herpes simplex virus type 1 corneal isolates from patients with recurrent herpetic keratitis. J Infect Dis. 2009;200(9):1402-14.
99. Rousseau A, Pharm SB, Gueudry J, Deback C, Haigh O, Schweitzer C, et al. Acyclovir-Resistant Herpes Simplex Virus 1 Keratitis: A Concerning and Emerging Clinical Challenge. Am J Ophthalmol. 2022;238:110-9.
100. Majumdar S, Gunda S, Mitra A. Functional expression of a sodium dependent nucleoside transporter on rabbit cornea: Role in corneal permeation of acyclovir and idoxuridine. Curr Eye Res. 2003;26(3-4):175-83.
101. Yildiz C, Ozsurekci Y, Gucer S, Cengiz AB, Topaloglu R. Acute kidney injury due to acyclovir. CEN Case Rep. 2013;2(1):38-40.
102. Perry CM, Faulds D. Valaciclovir. A review of its antiviral activity, pharmacokinetic properties and therapeutic efficacy in herpesvirus infections. Drugs. 1996;52(5):754-72.
103. Zhang Y, Cong Y, Teng Y. Acute renal injury induced by valacyclovir hydrochloride: A case report. Exp Ther Med. 2016;12(6):4025-8.
104. Kaufman HE, Haw WH. Ganciclovir ophthalmic gel 0.15%: safety and efficacy of a new treatment for herpes simplex keratitis. Curr Eye Res. 2012;37(7):654-60.
105. Colin J, Hoh HB, Easty DL, Herbort CP, Resnikoff S, Rigal D, et al. Ganciclovir ophthalmic gel (Virgan; 0.15%) in the treatment of herpes simplex keratitis. Cornea. 1997;16(4):393-9.
106. Meyer PR, Rutvisuttinunt W, Matsuura SE, So AG, Scott WA. Stable complexes formed by HIV-1 reverse transcriptase at distinct positions on the primer-template controlled by binding deoxynucleoside triphosphates or foscarnet. J Mol Biol. 2007;369(1):41-54.
107. Bonnafous P, Naesens L, Petrella S, Gautheret-Dejean A, Boutolleau D, Sougakoff W, et al. Different mutations in the HHV-6 DNA polymerase gene accounting for resistance to foscarnet. Antivir Ther. 2007;12(6):877-88.

108. Hadigal SR, Agelidis AM, Karasneh GA, Antoine TE, Yakoub AM, Ramani VC, et al. Heparanase is a host enzyme required for herpes simplex virus-1 release from cells. Nat Commun. 2015;6:6985.
109. Tiwari V, Liu J, Valyi-Nagy T, Shukla D. Anti-heparan sulfate peptides that block herpes simplex virus infection in vivo. J Biol Chem. 2011;286(28):25406-15.
110. Bultmann H, Busse JS, Brandt CR. Modified FGF4 signal peptide inhibits entry of herpes simplex virus type 1. J Virol. 2001;75(6):2634-45.
111. Yadavalli T, Agelidis A, Jaishankar D, Mangano K, Thakkar N, Penmetcha K, et al. Targeting Herpes Simplex Virus-1 gD by a DNA Aptamer Can Be an Effective New Strategy to Curb Viral Infection. Mol Ther Nucleic Acids. 2017;9:365-78.
112. Chuluunbaatar U, Roller R, Feldman ME, Brown S, Shokat KM, Mohr I. Constitutive mTORC1 activation by a herpesvirus Akt surrogate stimulates mRNA translation and viral replication. Genes Dev. 2010;24(23):2627-39.
113. Clark K, Plater L, Peggie M, Cohen P. Use of the pharmacological inhibitor BX795 to study the regulation and physiological roles of TBK1 and IkappaB kinase epsilon: a distinct upstream kinase mediates Ser-172 phosphorylation and activation. J Biol Chem. 2009;284(21):14136-46.
114. Henzler-Wildman KA, Martinez GV, Brown MF, Ramamoorthy A. Perturbation of the hydrophobic core of lipid bilayers by the human antimicrobial peptide LL-37. Biochemistry. 2004;43(26):8459-69.
115. Skerlavaj B, Gennaro R, Bagella L, Merluzzi L, Risso A, Zanetti M. Biological characterization of two novel cathelicidin-derived peptides and identification of structural requirements for their antimicrobial and cell lytic activities. J Biol Chem. 1996;271(45):28375-81.
116. Gordon YJ, Huang LC, Romanowski EG, Yates KA, Proske RJ, McDermott AM. Human cathelicidin (LL-37), a multifunctional peptide, is expressed by ocular surface epithelia and has potent antibacterial and antiviral activity. Curr Eye Res. 2005;30(5):385-94.
117. Sørensen OE, Follin P, Johnsen AH, Calafat J, Tjabringa GS, Hiemstra PS, et al. Human cathelicidin, hCAP-18, is processed to the antimicrobial peptide LL-37 by extracellular cleavage with proteinase 3. Blood. 2001;97(12):3951-9.
118. van der Does AM, Beekhuizen H, Ravensbergen B, Vos T, Ottenhoff TH, van Dissel JT, et al. LL-37 directs macrophage differentiation toward macrophages with a proinflammatory signature. J Immunol. 2010;185(3):1442-9.
119. Chamilos G, Gregorio J, Meller S, Lande R, Kontoyiannis DP, Modlin RL, et al. Cytosolic sensing of extracellular self-DNA transported into monocytes by the antimicrobial peptide LL37. Blood. 2012;120(18):3699-707.
120. Scott MG, Davidson DJ, Gold MR, Bowdish D, Hancock RE. The human antimicrobial peptide LL-37 is a multifunctional modulator of innate immune responses. J Immunol. 2002;169(7):3883-91.
121. Lai Y, Adhikarakunnathu S, Bhardwaj K, Ranjith-Kumar CT, Wen Y, Jordan JL, et al. LL37 and cationic peptides enhance TLR3 signaling by viral double-stranded RNAs. PLoS One. 2011;6(10):e26632.
122. Lee CJ, Buznyk O, Kuffova L, Rajendran V, Forrester JV, Phopase J, et al. Cathelicidin LL-37 and HSV-1 Corneal Infection: Peptide Versus Gene Therapy. Transl Vis Sci Technol. 2014;3(3):4.

123. He M, Zhang H, Li Y, Wang G, Tang B, Zhao J, et al. Cathelicidin-Derived Antimicrobial Peptides Inhibit Zika Virus Through Direct Inactivation and Interferon Pathway. Front Immunol. 2018;9:722.
124. Yu Y, Cooper CL, Wang G, Morwitzer MJ, Kota K, Tran JP, et al. Engineered Human Cathelicidin Antimicrobial Peptides Inhibit Ebola Virus Infection. iScience. 2020;23(4):100999.
125. Huang LC, Petkova TD, Reins RY, Proske RJ, McDermott AM. Multifunctional roles of human cathelicidin (LL-37) at the ocular surface. Invest Ophthalmol Vis Sci. 2006;47(6):2369-80.
126. Kahlenberg JM, Kaplan MJ. Little peptide, big effects: the role of LL-37 in inflammation and autoimmune disease. J Immunol. 2013;191(10):4895-901.
127. Wilhelmus KR, Gee L, Hauck WW, Kurinij N, Dawson CR, Jones DB, et al. Herpetic Eye Disease Study. A controlled trial of topical corticosteroids for herpes simplex stromal keratitis. Ophthalmology. 1994;101(12):1883-95; discussion 95-6.
128. Power WJ, Hillery MP, Benedict-Smith A, Collum LM. Acyclovir ointment plus topical betamethasone or placebo in first episode disciform keratitis. Br J Ophthalmol. 1992;76(12):711-3.
129. Collum LM, Logan P, Ravenscroft T. Acyclovir (Zovirax) in herpetic disciform keratitis. Br J Ophthalmol. 1983;67(2):115-8.
130. Comstock TL, Decory HH. Advances in corticosteroid therapy for ocular inflammation: loteprednol etabonate. Int J Inflam. 2012;2012:789623.
131. Valdes LM, Sobrin L. Uveitis Therapy: The Corticosteroid Options. Drugs. 2020;80(8):765-73.
132. Zur D, Iglicki M, Loewenstein A. The Role of Steroids in the Management of Diabetic Macular Edema. Ophthalmic Res. 2019;62(4):231-6.
133. Saxena R, Singh D, Menon V. Controversies in neuro-ophthalmology: steroid therapy for traumatic optic neuropathy. Indian J Ophthalmol. 2014;62(10):1028-30.
134. Salinger CL, Gaynes BI, Rajpal RK. Innovations in topical ocular corticosteroid therapy for the management of postoperative ocular inflammation and pain. Am J Manag Care. 2019;25(12 Suppl):S215-s26.
135. Beardsley RM, Suhler EB, Rosenbaum JT, Lin P. Pharmacotherapy of scleritis: current paradigms and future directions. Expert Opin Pharmacother. 2013;14(4):411-24.
136. Kersey JP, Broadway DC. Corticosteroid-induced glaucoma: a review of the literature. Eye (Lond). 2006;20(4):407-16.
137. Manabe S, Bucala R, Cerami A. Nonenzymatic addition of glucocorticoids to lens proteins in steroid-induced cataracts. J Clin Invest. 1984;74(5):1803-10.
138. Dickerson JE, Jr., Dotzel E, Clark AF. Steroid-induced cataract: new perspective from in vitro and lens culture studies. Exp Eye Res. 1997;65(4):507-16.
139. Jobling AI, Augusteyn RC. What causes steroid cataracts? A review of steroid-induced posterior subcapsular cataracts. Clin Exp Optom. 2002;85(2):61-75.
140. Petersen A, Carlsson T, Karlsson JO, Jonhede S, Zetterberg M. Effects of dexamethasone on human lens epithelial cells in culture. Mol Vis. 2008;14:1344-52.
141. Sarchahi AA, Meimandi Parizi A, Eghtedari M, Keshavarz S. Effect of different treatment regimen with dexamethasone and acetylcysteine on corneal wound healing in rabbits. Iran J Med Sci. 2011;36(3):188-95.

142. Gulkilik G, Demirci G, Ozdamar AM, Muftuoglu GI. A case of herpetic keratitis after intravitreal triamcinolone injection. Cornea. 2007;26(8):1000-1.
143. Jusufbegovic D, Schaal S. Quiescent Herpes Simplex Keratitis Reactivation After Intravitreal Injection of Dexamethasone Implant. Retin Cases Brief Rep. 2017;11(4):296-7.
144. Iribarne M, Torbidoni V, Julián K, Prestifilippo JP, Sinha D, Rettori V, et al. Cannabinoid receptors in conjunctival epithelium: identification and functional properties. Invest Ophthalmol Vis Sci. 2008;49(10):4535-44.
145. Straiker AJ, Maguire G, Mackie K, Lindsey J. Localization of cannabinoid CB1 receptors in the human anterior eye and retina. Invest Ophthalmol Vis Sci. 1999;40(10):2442-8.
146. Steven P, Heß D, Jens H, Dautzenberg FM, Stern ME, Gehlsen U. Application of a Cannabinoid-Receptor Agonist in a Mouse Model of Desiccating Stress. Investigative Ophthalmology & Visual Science. 2019;60(9):273-.
147. Murataeva N, Miller S, Dhopeshwarkar A, Leishman E, Daily L, Taylor X, et al. Cannabinoid CB2R receptors are upregulated with corneal injury and regulate the course of corneal wound healing. Exp Eye Res. 2019;182:74-84.
148. Yang Y, Yang H, Wang Z, Varadaraj K, Kumari SS, Mergler S, et al. Cannabinoid receptor 1 suppresses transient receptor potential vanilloid 1-induced inflammatory responses to corneal injury. Cell Signal. 2013;25(2):501-11.
149. Cairns EA, Baldridge WH, Kelly ME. The Endocannabinoid System as a Therapeutic Target in Glaucoma. Neural Plast. 2016;2016:9364091.
150. Panahi Y, Manayi A, Nikan M, Vazirian M. The arguments for and against cannabinoids application in glaucomatous retinopathy. Biomed Pharmacother. 2017;86:620-7.
151. Weinreb RN, Robinson MR, Dibas M, Stamer WD. Matrix Metalloproteinases and Glaucoma Treatment. J Ocul Pharmacol Ther. 2020;36(4):208-28.
152. Thapa D, Cairns EA, Szczesniak AM, Toguri JT, Caldwell MD, Kelly MEM. The Cannabinoids Δ(8)THC, CBD, and HU-308 Act via Distinct Receptors to Reduce Corneal Pain and Inflammation. Cannabis Cannabinoid Res. 2018;3(1):11-20.
153. Pisanti S, Picardi P, Prota L, Proto MC, Laezza C, McGuire PG, et al. Genetic and pharmacologic inactivation of cannabinoid CB1 receptor inhibits angiogenesis. Blood. 2011;117(20):5541-50.
154. Baer A, Kehn-Hall K. Viral concentration determination through plaque assays: using traditional and novel overlay systems. J Vis Exp. 2014(93):e52065.
155. Abcam. Immunohistochemistry (IHC): the complete guide.
156. Joe AW, Yeung SN. Concise review: identifying limbal stem cells: classical concepts and new challenges. Stem Cells Transl Med. 2014;3(3):318-22.
157. Sawtell NM, Thompson RL. Rapid in vivo reactivation of herpes simplex virus in latently infected murine ganglionic neurons after transient hyperthermia. J Virol. 1992;66(4):2150-6.
158. Perng GC, Slanina SM, Ghiasi H, Nesburn AB, Wechsler SL. The effect of latency-associated transcript on the herpes simplex virus type 1 latency-reactivation phenotype is mouse strain-dependent. J Gen Virol. 2001;82(Pt 5):1117-22.
159. Tian X, Wang T, Zhang S, Wang Q, Hu X, Ge C, et al. PEDF Reduces the Severity of Herpetic Simplex Keratitis in Mice. Invest Ophthalmol Vis Sci. 2018;59(7):2923-31.

160. Thuret G, Acquart S, Gain P, Thuret G, Dumollard JM, Manissolle C, et al. Ultrastructural demonstration of replicative herpes simplex virus type 1 transmission through corneal graft. Transplantation. 2004;77(2):325-6.
161. Shimeld C, Hill TJ, Blyth WA, Easty DL. Passive immunization protects the mouse eye from damage after herpes simplex virus infection by limiting spread of virus in the nervous system. J Gen Virol. 1990;71 (Pt 3):681-7.
162. Thygeson P. Historical observations on herpetic keratitis. Surv Ophthalmol. 1976;21(2):82-90.
163. Carenza C, Calcaterra F, Oriolo F, Di Vito C, Ubezio M, Della Porta MG, et al. Costimulatory Molecules and Immune Checkpoints Are Differentially Expressed on Different Subsets of Dendritic Cells. Front Immunol. 2019;10:1325.
164. Amakata Y, Fujiyama Y, Andoh A, Hodohara K, Bamba T. Mechanism of NK cell activation induced by coculture with dendritic cells derived from peripheral blood monocytes. Clin Exp Immunol. 2001;124(2):214-22.
165. Bennett SR, Carbone FR, Karamalis F, Flavell RA, Miller JF, Heath WR. Help for cytotoxic-T-cell responses is mediated by CD40 signalling. Nature. 1998;393(6684):478-80.
166. Martin S, Agarwal R, Murugaiyan G, Saha B. CD40 expression levels modulate regulatory T cells in Leishmania donovani infection. J Immunol. 2010;185(1):551-9.
167. Do Y, McKallip RJ, Nagarkatti M, Nagarkatti PS. Activation through cannabinoid receptors 1 and 2 on dendritic cells triggers NF-kappaB-dependent apoptosis: novel role for endogenous and exogenous cannabinoids in immunoregulation. J Immunol. 2004;173(4):2373-82.
168. Jayaram H. Intraocular pressure reduction in glaucoma: Does every mmHg count? Taiwan J Ophthalmol. 2020;10(4):255-8.
169. Le VNH, Schneider AC, Scholz R, Bock F, Cursiefen C. Fine Needle-Diathermy Regresses Pathological Corneal (Lymph)Angiogenesis and Promotes High-Risk Corneal Transplant Survival. Sci Rep. 2018;8(1):5707.
170. Sharif Z, Sharif W. Corneal neovascularization: updates on pathophysiology, investigations & management. Rom J Ophthalmol. 2019;63(1):15-22.
171. Clements JL, Dana R. Inflammatory corneal neovascularization: etiopathogenesis. Semin Ophthalmol. 2011;26(4-5):235-45.
172. Ahmed I, Akram Z, Iqbal HMN, Munn AL. The regulation of Endosomal Sorting Complex Required for Transport and accessory proteins in multivesicular body sorting and enveloped viral budding - An overview. Int J Biol Macromol. 2019;127:1-11.
173. Han KY, Tran JA, Chang JH, Azar DT, Zieske JD. Potential role of corneal epithelial cell-derived exosomes in corneal wound healing and neovascularization. Sci Rep. 2017;7:40548.
174. Spandau UH, Toksoy A, Verhaart S, Gillitzer R, Kruse FE. High expression of chemokines Gro-alpha (CXCL-1), IL-8 (CXCL-8), and MCP-1 (CCL-2) in inflamed human corneas in vivo. Arch Ophthalmol. 2003;121(6):825-31.
175. Théry C, Witwer KW, Aikawa E, Alcaraz MJ, Anderson JD, Andriantsitohaina R, et al. Minimal information for studies of extracellular vesicles 2018 (MISEV2018): a position statement of the International Society for Extracellular Vesicles and update of the MISEV2014 guidelines. J Extracell Vesicles. 2018;7(1):1535750.

176. Yoshida S, Yoshida A, Matsui H, Takada Y, Ishibashi T. Involvement of macrophage chemotactic protein-1 and interleukin-1beta during inflammatory but not basic fibroblast growth factor-dependent neovascularization in the mouse cornea. Lab Invest. 2003;83(7):927-38.
177. Siemasko KF, Gao J, Calder VL, Hanna R, Calonge M, Pflugfelder SC, et al. In vitro expanded CD4+CD25+Foxp3+ regulatory T cells maintain a normal phenotype and suppress immune-mediated ocular surface inflammation. Invest Ophthalmol Vis Sci. 2008;49(12):5434-40.
178. Schaumburg CS, Siemasko KF, De Paiva CS, Wheeler LA, Niederkorn JY, Pflugfelder SC, et al. Ocular surface APCs are necessary for autoreactive T cell-mediated experimental autoimmune lacrimal keratoconjunctivitis. J Immunol. 2011;187(7):3653-62.
179. Corrales RM, Villarreal A, Farley W, Stern ME, Li DQ, Pflugfelder SC. Strain-related cytokine profiles on the murine ocular surface in response to desiccating stress. Cornea. 2007;26(5):579-84.
180. Narayanan S, Corrales RM, Farley W, McDermott AM, Pflugfelder SC. Interleukin-1 receptor-1-deficient mice show attenuated production of ocular surface inflammatory cytokines in experimental dry eye. Cornea. 2008;27(7):811-7.
181. Hoyer D, Bartfai T. Neuropeptides and neuropeptide receptors: drug targets, and peptide and non-peptide ligands: a tribute to Prof. Dieter Seebach. Chem Biodivers. 2012;9(11):2367-87.
182. Bignami F, Rama P, Ferrari G. Substance P and its Inhibition in Ocular Inflammation. Curr Drug Targets. 2016;17(11):1265-74.
183. Byun YS, Mok JW, Chung SH, Kim HS, Joo CK. Ocular surface inflammation induces de novo expression of substance P in the trigeminal primary afferents with large cell bodies. Sci Rep. 2020;10(1):15210.
184. Liu L, Dana R, Yin J. Sensory neurons directly promote angiogenesis in response to inflammation via substance P signaling. Faseb j. 2020;34(5):6229-43.
185. Lee SK, Choi BK, Kang WJ, Kim YH, Park HY, Kim KH, et al. MCP-1 derived from stromal keratocyte induces corneal infiltration of CD4+ T cells in herpetic stromal keratitis. Mol Cells. 2008;26(1):67-73.
186. Oliva MS, Schottman T, Gulati M. Turning the tide of corneal blindness. Indian J Ophthalmol. 2012;60(5):423-7.
187. Gain P, Jullienne R, He Z, Aldossary M, Acquart S, Cognasse F, et al. Global Survey of Corneal Transplantation and Eye Banking. JAMA Ophthalmol. 2016;134(2):167-73.
188. Remeijer L, Maertzdorf J, Doornenbal P, Verjans GM, Osterhaus AD. Herpes simplex virus 1 transmission through corneal transplantation. Lancet. 2001;357(9254):442.
189. Williams KA, Keane MC, Galettis RA, Mills RA, Jones VJ, Coster DJ. The Australian Corneal Graft Registry: 2018 Report: Australian Corneal Graft Registry; 2018.
190. Jhanji V, Young AL, Mehta JS, Sharma N, Agarwal T, Vajpayee RB. Management of corneal perforation. Surv Ophthalmol. 2011;56(6):522-38.
191. Vote BJ, Elder MJ. Cyanoacrylate glue for corneal perforations: a description of a surgical technique and a review of the literature. Clin Exp Ophthalmol. 2000;28(6):437-42.
192. McTiernan CD, Simpson FC, Haagdorens M, Samarawickrama C, Hunter D, Buznyk O, et al. LiQD Cornea: Pro-regeneration collagen mimetics as patches and alternatives to corneal transplantation. Sci Adv. 2020;6(25).
193. Sharma A, Kaur R, Kumar S, Gupta P, Pandav S, Patnaik B, et al. Fibrin glue versus N-butyl-2-cyanoacrylate in corneal perforations. Ophthalmology. 2003;110(2):291-8.

194. Jangamreddy JR, Haagdorens MKC, Mirazul Islam M, Lewis P, Samanta A, Fagerholm P, et al. Short peptide analogs as alternatives to collagen in pro-regenerative corneal implants. Acta Biomater. 2018;69:120-30.
195. Simpson FC, McTiernan CD, Islam MM, Buznyk O, Lewis PN, Meek KM, et al. Collagen analogs with phosphorylcholine are inflammation-suppressing scaffolds for corneal regeneration from alkali burns in mini-pigs. Commun Biol. 2021;4(1):608.
196. Khatoon Z, Guzmán-Soto I, McTiernan CD, Lazurko C, Simpson F, Zhang L, et al. Nanoengineering the surface of corneal implants: towards functional anti-microbial and biofilm materials. RSC Adv. 2020;10(40):23675-81.
197. Alarcon EI, Vulesevic B, Argawal A, Ross A, Bejjani P, Podrebarac J, et al. Coloured cornea replacements with anti-infective properties: expanding the safe use of silver nanoparticles in regenerative medicine. Nanoscale. 2016;8(12):6484-9.
198. Buznyk O, Azharuddin M, Islam MM, Fagerholm P, Pasyechnikova N, Patra HK. Collagen-based scaffolds with infused anti-VEGF release system as potential cornea substitute for high-risk keratoplasty: A preliminary in vitro evaluation. Heliyon. 2020;6(10):e05105.
199. Sharma M, Liu W, Perincheri S, Gunasekaran M, Mohanakumar T. Exosomes expressing the self-antigens myosin and vimentin play an important role in syngeneic cardiac transplant rejection induced by antibodies to cardiac myosin. Am J Transplant. 2018;18(7):1626-35.
200. Zhang Y, Guan DL, Xia CQ, Han ZY, Xu JJ, Gao JZ, et al. Relationship between the expression levels of CD61, CD63, and PAC-1 on platelet surface in peripheral blood and the transplanted kidney function. Transplant Proc. 2003;35(4):1360-3.
201. Liu Q, Rojas-Canales DM, Divito SJ, Shufesky WJ, Stolz DB, Erdos G, et al. Donor dendritic cell-derived exosomes promote allograft-targeting immune response. J Clin Invest. 2016;126(8):2805-20.
202. Yamaguchi T, Higa K, Tsubota K, Shimazaki J. Elevation of preoperative recipient aqueous cytokine levels in eyes with primary graft failure after corneal transplantation. Mol Vis. 2018;24:613-20.
203. Yamagami S, Miyazaki D, Ono SJ, Dana MR. Differential chemokine gene expression in corneal transplant rejection. Invest Ophthalmol Vis Sci. 1999;40(12):2892-7.

Chapter 7 – Appendices

These appendices contain work that was done for several projects that are not directly part of my thesis work. However, I am a contributor or co-author on these projects.

Published papers

- Simpson FC, Islam MM, Buznyk O, Edin E, **Groleau M**, Kozak-Ljunggren M, Magrelli FM, AbuSamra DB, Argüeso P, Chodosh J, Liszka A, Fagerholm P, Griffith M (2022) Electron-Beam Irradiated Recombinant Human Collagen-Phosphorylcholine Corneal Implants Retain Pro-Regeneration Capacity. Front Bioeng Biotechnol. 10: 883977. doi: 10.3389/fbioe.2022.883977
- Juarez A, Djallali M, Piché M, Thériault M, **Groleau M**, Beroual S, McTiernan CD, Lin G, Hélie P, Carrier M, Griffith M, Brunette I (2021) A Liquid Hydrogel to Restore Long Term Corneal Integrity After Perforating and Non-Perforating Trauma in Feline Eyes. Frontiers Bioeng Biotechnol. https://doi.org/10.3389/fbioe.2021.773294
- Haagdorens M, Edin E, Fingerholm P, **Groleau M**, Shtein Z, Ulčinas A, Yaari A, Samanta A, Cepla A, Liszka A, Tassignon M-J, Simpson F, Shoseyov O, Valiokas R, Isabel Pintelon, Ljunggren MK, Griffith M (2021) Plant Recombinant human collagen type I hydrogels for corneal regeneration. Regen Eng Transl Med. https://doi.org/10.1007/s40883-021-00220-3
- McTiernan CD, Simpson FC, Haagdorens M, Samarawickrama C, Hunter D, Buznyk O, Fagerholm P, Ljunggren MK, Lewis P, Pintelon I, Olsen D, Edin E, **Groleau M**, Allan BD, Griffith M (2020) LiQD Cornea: Pro-regeneration collagen mimetics as patches and alternatives to corneal transplantation. Sci Adv. 6(25): eaba2187. doi: 10.1126/sciadv.aba2187 (*Auteurs correspondants)

Biomaterial corneal implants

7.1. Introduction

The cornea is crucial for vision and irreversible damage can result in blindness. Globally, an estimated 23 million people have unilateral corneal blindness while 4.9 million are bilaterally corneal blind (186). The only commonly accepted treatment to restore a patient's vision is through transplantation with human donor corneas. However, there is a severe global shortage of donor corneas resulting in only one cornea being available for approximately 70 patients (187). With such a lack of donors, patients can remain on a waiting list for long periods of time. Unfortunately, patients suffering from perforations do not have the luxury of time and require immediate treatment to save the eye. In addition to the donor cornea shortfall, although rare, corneal transplants can transmit pathogens (160, 188). A decrease in corneal graft survival rates from 84% in non-infected patients to 52% in has been noted in donor transmitted HSV patients after four years (189).

Alternatives to donor corneal transplants are being explored, in particular cell-free biomaterial implants that promote *in situ* tissue regeneration corneal tissue. Currently, cyanoacrylate glue is used for emergency purposes, such as for corneal perforations which need to be sealed as quickly as possible to save the globe (190, 191). Unfortunately, cyanoacrylate glue has poor biocompatibility, with particular concern of damaging endothelial cells and promoting inflammation. Furthermore, if the glue is not fully polymerized, toxic cyanoacrylate monomers can hydrolysis into formaldehyde, which promotes scarring and neovascularization (190-193). Fibrin glue has also been used for wound closure in human corneas and have shown better biocompatibility than cyanoacrylate (193). However, fibrin glue takes longer to polymerize and is not as readily available as cyanoacrylate glue (191, 193). Both fibrin glue and cyanoacrylate glue are intended for short term treatments. Patients still require a corneal transplant to restore vision, creating the need for non-donor alternatives to function long term.

Both solid and injectable liquid cell-free implants made from a wide range of biomaterials from fully synthetic polymers to decellularized extracellular matrices have been developed as alternatives to donor corneal transplantation. One in particular comprising a fully synthetic

collagen analogue made of collagen-like peptides (CLP) conjugated to polyethylene glycol (PEG), has been tested both as solid corneal implants and an injectable liquid formulation. These CLP-PEG-based biomaterials were designed to recreate the collagenous extracellular matrix of the human cornea, and to stimulate regeneration of corneal tissues. Solid CLP-PEG implants are able to regenerate the tissues and nerves in mini-pig corneas (194). The incorporation of a synthetic phosphorylcholine lipid, 2-methacryloyloxyethyl phosphorylcholine (MPC) that is known to suppress inflammation into solid CLP-PEG implants were able to block inflammation and allow corneal tissues and nerves regeneration in mini-pig corneas (195). Circumventing inflammation resulted in decreased haze or neovascularization, compared to CLP-PEG implants without MPC (195). While effective, solid implants are limited by the need for an operating team since the implantation procedure is similar to that of a donor corneal transplant.

Corneal perforations are considered emergencies and require urgent care. Liquid glue-filler formulations have been developed by several groups that can be injected into the perforation, sealing the wound. CLP-PEG-Fibrinogen, a liquid formulation of the CLP-PEG implants developed by the Griffith Lab were in mini-pig corneas, and showed similar regeneration stimulating capacity as the solid implants, and regenerated neo-corneas were similar to syngeneic transplant in the corneas (192, 194). However, MPC was not included in these implants, nor were they tested under conditions of inflammation. A new CLP formulation that included MPC was developed and was composed of CLP with a linear carboxylic phosphorylcholine copolymer (CLP-LCPP) and was tested in corneal perforations with light alkali burns to simulate inflammation.

An additional benefit for synthetic implants is the ability to make further modifications to them such as delivering treatments through the hydrogels. Nanoparticles (NPs) mixed in with the hydrogel scaffold are able to have additional functions beyond mimicking a healthy cornea. Silver NPs have been incorporated into hydrogels and implanted into mice subcutaneously have shown anti-microbial proprieties against *Pseudomonas aeruginosa*, *Staphylococcus aureus*, and *Staphylococcus epidermidis* (196). Furthermore, NPs can be loaded with a treatment. LL37 packed into silver NPs mixed into a hydrogel intended for corneal implants showed anti-microbial effects *in vitro* with minimal release of NPs from the collagen hydrogels (197). Other potential

treatments include gold NPs delivering anti-neovascularization antibodies in a collagen hydrogel (198).

In this study, we sought to determine the possibility of using the secretion of extracellular vesicles (EVs), particularly exosomes, to distinguish between biomaterials that promoted seamless regeneration versus those that cause adverse events. We discovered that exosomes were produced in all mini-pig corneas that had regenerated (192). We compared the two formulations containing collagen-like peptides (CLPs) with biomaterials known to produce inflammation or cytotoxic reactions to search for EV-exosome indicators of graft integration or failure. Finally, the use of NPs were examined for their compatibility in the implants and their effectiveness at delivering treatments.

7.2. Contributions

Injectable materials were tested on mice by surgeon Dr. Marie-Claude Robert. Materials were made by Drs. Fiona Simpson, Elle Edin, and Bijay Poudel. Quantification of exosome expression was performed by Dr. Santiago Costantino. Everything else was performed by Marc Groleau.

7.3. Methods

7.3.1. Fabrication of CLP-PEG-Fibrinogen hydrogels

Production of CLP-PEG-Fibrinogen used the same method as previously described (192). To make the CLP-PEG, 20mL of H_2O was degassed using nitrogen for 20 minutes. 770mg of eight-arm PEG-maleimide was added to the 20mL of degassed H_2O, followed by 625mg CLP, and stirred for 20 minutes. 2M NaOH was used to raise the pH to 4.5 while adding 30mL of degassed H_2O. The solution would then be stirred for five days, monitoring the pH, and adjusting it to 4.5 when needed. Finally, 50mL of H_2O was added to the solution to then be filtered through 0.45µm syringe filter and dialysed daily for seven days at a pH of 4.5 (molecular weight cut-off: 14kD). Once completed, material was freeze-dried.

CLP-PEG and fibrinogen (Tisseel, Baxter International, Deerfield, IL, USA) were added together and mixed in with H_2O give a final dilution of 10 and 1% (w/w), respectively. Reconstitution would take two to three weeks and once resuspended, the solution would be heated above 37°C to melt it and centrifuged at 3000rpm for 10 minutes. This would be repeated until there were no more bubbles present.

CLP-PEG-Fibrinogen hydrogels were made by heating the CLP-PEG/fibrinogen mixture to 50°C and were transferred to a heated T-piece mixing system. 4-(4,6-dimethoxy-1,3,5-triazin-2-yl)-4-methylmorpholinium chloride (DMTMM), a crosslinker, was added for a final concentration of 2% into the T-piece and mixed until homogeneous. To apply into the cornea, a solution of 250U/mL of thrombin was first applied to the wound followed by the application of the T-piece mixture.

7.3.2. Fabrication of CLP-LCPP hydrogels

LCPP was prepared by adding 885mg of MPC to TRIS-HCl 0.5M pH 6.7 for a final volume of 200mL. 450mg of AC-PEG-COOH was added to the solution followed by sonication and nitrogen flushing for 30 minutes. 51.3mg of APS was added, then sonicated and nitrogen flushed for 5 min, followed by the addition of 33.6µL of TEMED. Solutions were incubated at 20°C for 24 hours under positive pressure, nitrogen atmosphere, and constant stirring. Samples were dialysed in a 12-14kD molecular weight cut-off cellulose dialysis membrane. Once completed, material was freeze-dried.

Stock solutions of 15% CLP, 10% LCPP, and 10% DMTMM were prepared by using MOPS. 150µL of LCPP was mixed with 112.5µL of DMTMM and 337.5µL of MOPS. The solution was incubated at 65 ºC and a minute. 750µL of CLP solution and 150µL of MOPS was added to the mix which was then ready to be applied to the wound.

7.3.3. Application of nanoparticles

SiO_2 NPs were produced as previously described. To summarize, 6mL cyclohexane was combined with 2mL Triton X-100 (Both from Sigma-Aldrich, St. Louis, MO, USA). 0.75mL tetraethylorthosilicate was added dropwise (Sigma-Aldrich, St. Louis, MO, USA) and the solution was brought to a pH of 5.0-6.0 using ammonia hydroxide (Sigma-Aldrich, St. Louis, MO, USA) and

were stirred for two days at 50°C. Both SiO_2 NPs and lipid NPs were then mixed with the hydrogel solution before the addition of a cross linker for the CLP-PEG-Fibrinogen implants or mixed in with the CLP solution for CLP-LCPP implants.

7.3.4. Implantation into inflamed mouse corneas

With ethics approval from the animal care committee of the Maisonneuve-Rosemont Hospital Research Centre, protocol #2021-2356. Forty-two Balb/C mice, age 6 to 10 weeks, were divided into multiple groups of 3 animals each. Before the surgeries, mice were given an analgesic, 0.05 mg/kg buprenorphine. Under full anaesthesia, which was induced by ketamine and xylazine (50/5 mg/kg), each animal was given an alkali burn by soaking a 2mm diameter piece of Whatman #1 filter paper in 0.125N sodium hydroxide (NaOH) and applying it to the right cornea for 15 seconds. A 1mm full perforation was performed in the burned eye and it was filled with one of the treatments. The treatments include CLP-Peg-Fibrinogen with and without SiO_2 NPs, CLP-LCPP with either SiO_2 NPs, mesoporous SiO_2 NPs or no NPs, cyanoacrylate glue, fibrin glue or gelatin. As a control for the implant, mice received the burn but did not receive a full perforation or implant afterwards. Additionally, all mice received buprenorphine for 2 days, twice daily and Tobradex eye drops (DIN. 00778907) for 7 days, twice a day. Mice were sacrificed on days 1, 3, 7, and 14. Eyes were removed and fixed in 0.1M phosphate buffer with 0.18M sucrose and 4% PFA, overnight at 4°C.

7.3.5. Implantation of transfecting reagents in mouse corneas

The experiment was performed after institutional ethics approval from the animal care committee of the Maisonneuve-Rosemont Hospital Research Centre, protocol #2021-2356. Twelve Balb/C mice, age 6 to 10 weeks, were divided into groups of 3 animals each. Mice underwent slip lamp examination and OCT to verify the health of the cornea before starting the experiment. Before the surgeries, mice were given buprenorphine (0.05 mg/kg), an analgesic. Ketamine and xylazine (50/5 mg/kg) were used for anaesthesia during the operations, a 1mm full perforation was performed in the left eye and it was filled with one of the treatments. The treatments were all CLP-LCPP with lipid NPs either containing nothing or one of the two transfection formulations tested, both supposed to cause the production of green fluorescent protein (GFP). Before the operation and on days 3, 7, 10 and 14 post-operation, a blue light was

used to excite any GFP present. OCT was performed on day 14 to assess corneal healing. Additionally, all mice received buprenorphine for 2 days, twice daily and eye drops of Tobradex (DIN. 00778907) for 4 days, followed by 3 days of Tobramycin (DIN. 02241755), both eye drops were given twice a day. Mice were euthanized on day 14 and their eyes were dissected and fixed in 4% PFA in 0.1M TBS, overnight at 4°C.

7.3.6. Histology and immunohistochemistry

The fixed eyes were passed through a sucrose gradient from 5% to 20% in 0.1M TBS and globes were frozen in optimum cutting temperature (14-373-65, Thermo Fisher Scientific, Waltham, MA, USA).

For hematoxylin and eosin H&E staining, the sections were rinsed in distilled water and stained with Harris hematoxylin (HHS32-1L, Sigma-Aldrich, St. Louis, MO, USA) for 8 minutes. Slides were washed and placed into a 1% acid alcohol solution and Scott's tap water. Dehydration with 95% ethanol was done before staining with eosin-phloxine solution (HT110316-500ML, Sigma-Aldrich, St. Louis, MO, USA). All samples were cleared in xylene and mounted with Permount Mounting Medium (SP15-100, Thermo Fisher Scientific, Waltham, MA, USA) and imaged using Zeiss Axio Imager Z2 with an AxioCam MRc color CCD camera (Carl Zeiss, Oberkochen, Germany).

For immunohistochemistry, sections were permeabilized in 0.3% Triton X-100 in 0.1M TBS for 15 minutes and quenched in 50mM ammonium chloride for 30 minutes. Following that, they were blocked for 1 hour in TBS containing 5% normal goat serum and 0.01g/mL saponin. For stains that had a mouse primary antibody, mouse on mouse blocking reagent was added to the blocking (Vector Laboratories, Burlingame, CA, USA). Primary antibodies were diluted in the blocking solution and were added to the samples for an overnight incubation at 4°C (Table 6). Sections were incubated for an hour with secondary antibodies which were diluted at 1:1000 in the blocking solution (Table 6). For the exosome stain consisting of CD63, TSG101 and MCP-1, slides were quenched for autofluorescence using Vector TrueVIEW Autofluorescence Quenching Kit (Vector Laboratories, Burlingame, CA, USA). Nuclei were stained with 5µg/mL DAPI for 10 minutes and mounted in Vectashield Vibrance Mounting Medium (Vector Laboratories,

Burlingame, CA, USA). All slides were imaged on a Zeiss LSM 880 confocal microscope (Zeiss, Oberkochen, Germany). Exosome quantification was performed by compressing the images into a maximum projection and measure the MFI of the sample. Snaps of the samples were performed using Imaris v9.1.2 (Bitplane Inc., Concord, MA, USA).

7.3.7. Statistical analyses

A one-way ANOVA Tukey's multiple comparison was used to analyse the BMDCs (n = 3). MFI of CD63, TSG101 and MCP-1 was measured, and the treated eyes were divided by the contralateral, non-treated eye of the same mouse. A two-way ANOVA Tukey's multiple comparisons test with a confidence interval of 95% for each marker (GraphPad Prism 9.3.0, GraphPad Software LLC., San Diego, CA, USA) was used. The unit of analysis was the mouse (n = 3 per group, except CLP-Peg-Fibrinogen for day 3 which had an n = 2).

Table 4. *Antibodies for immunohistochemistry*

Target	**Antibody**	**Dilution Factor**
GFP	Anti-GFP from mouse IgG1κ (clones 7.1 and 13.1), Sigma-Aldrich, 11814460001	1:200
CD63	Anti-CD63 Antibody (MX-49.129.5), Santa Cruz, sc-5275	1:1000
TSG101	Recombinant Anti-TSG101 antibody [EPR7130(B)], AbCam, ab125011	1:1000
Monocyte chemoattractant protein-1	Ultra-LEAF™ Purified anti-mouse/rat/human MCP-1 Antibody, BioLegend, 505911	1:500
Mouse IgG	Goat anti-Mouse IgG (H+L) Highly Cross-Adsorbed Secondary Antibody, Alexa Fluor™ Plus 647, Invitrogen, A32728	1:1000

Rabbit IgG	IgG (H+L) Highly Cross-Adsorbed Goat anti-Rabbit, Alexa Fluor™ 594, Invitrogen, A11037	1:1000
Armenian Hamster IgG	Goat anti-Hamster IgG (H+L) Secondary Antibody [DyLight 488] (Pre-adsorbed), Novus Biologicals, NBP1-73008	1:1000

7.4. Results

7.4.1. Early impacts of corneal implants

To gain a better understanding of early events in biomaterial-corneal cell interactions within an inflamed eye, a corneal alkali burn model of inflammation in mice was developed. One cornea of each mouse received an alkali burn followed by a full-thickness perforation. Control animals received an alkali burn only. The perforations were filled an injectable hydrogel comprising CLP-PEG-Fibrinogen. H&E showed that cells were infiltrating the implant in the stroma within the first day and that by day 3, the corneas had re-epithelialized (Figure 18A). Both patched corneas and corneas that received burns only showed a similar morphology in H&E sections.

The burned corneas expressed exosome markers TSG101 and CD63, as well as MCP-1 throughout the 7-day observation period (Fig. 18B-E). In the burned and patched corneas, the regenerating neo-corneas showed increased expression of TSG101 and CD63, although these increases were not significant ($p>0.05$ by a two-way ANOVA Tukey's multiple comparisons test). The increase in MCP-1 observed on day 3, however, was significant ($p\leq0.05$) (Figure 18E). MCP-1 expression decreased by day 7. In the burned eyes, an increase in MCP-1 expression was observed on day 7 but was not significant (Figure 18E). All three markers were predominantly in the stroma, mostly deeper into the tissue (Figure 18B).

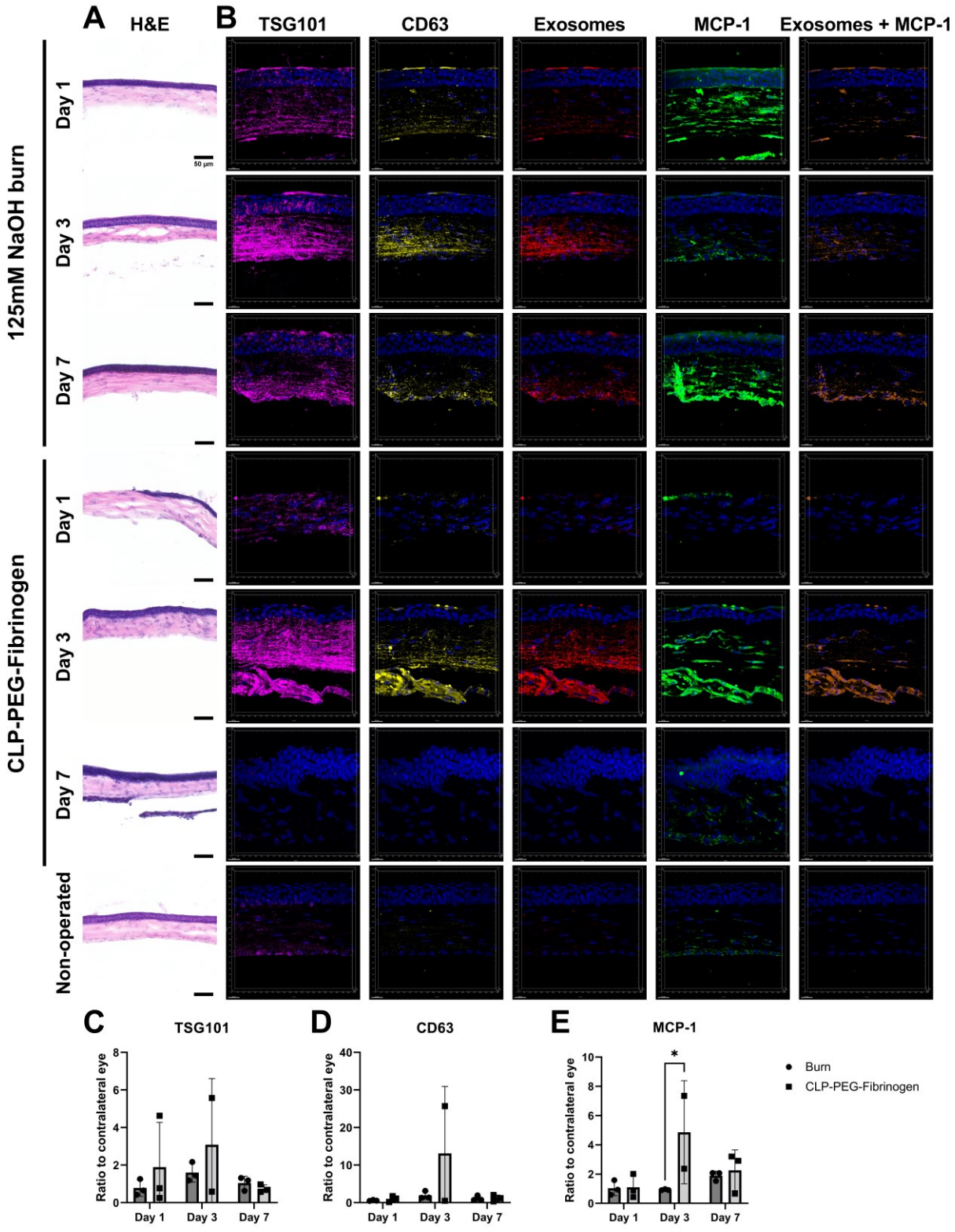
A
H&E
B
TSG101
CD63
Exosomes
MCP-1
Exosomes + MCP-1
125mM NaOH burn
CLP-PEG-Fibrinogen
Day 1
Day 3
Day 7
Non-operated
50 µm
C
TSG101
D
CD63
E
MCP-1
Ratio to contralateral eye
Day 1
Day 3
Day 7
*
Burn
CLP-PEG-Fibrinogen

Figure 18. ***Extracellular vesicles secretion and MCP-1 expression within a week after implantation in mice.*** *All 18 mice were given an alkali burn and half of the mice received a full thickness perforation and CLP-PEG-Fibrinogen implant in addition to the alkali burn. Mice were sacrificed at days 1, 3, and 7 with three mice per group. (A) Corneas received H&E staining to observe cell infiltration and re-epithelialization. Scale bar: 50µm. (B) Corneal sections were also stained for TSG101 (Magenta), CD63 (Yellow), MCP-1 (Green), and DAPI (Blue). Colocalization of TSG101 and CD63 was shown in the exosome channel (Red) and the colocalization of the exosomes and MCP-1 was shown in the exosomes + MCP-1 channel (Brown). Quantification of the TSG101 (C), CD63 (D), and MCP-1 (E) was performed on the tissue and the data was presented as a ration between the implanted eye and the contralateral eye. *P ≤ 0.05 by two-way ANOVA Tukey's multiple comparisons test.*

7.4.2. Comparison of CLP-based hydrogels to common corneal sealants

Histopathological examination of H&E stained sections revealed a disorganized and distended cornea after treatment with cyanoacrylate glue and fibrin glue, both of which are approved for human use (Figure 19A). Mouse corneas that received gelatin implants had epithelial defects as well as a disorganized stroma (Figure 19A). CLP-PEG-Fibrinogen and CLP-LCPP implants, with and without NPs, showed morphologically similar epithelial and stromal cell compartments to non-operated corneas at 14 days post-operation (Figure 19A).

All groups showed staining for CD63, a marker for extracellular vesicles (EVs) that are more abundant during inflammation, TSG101, another EV marker but is less associated with inflammation, as well as MCP-1, a marker for inflammation and promotes macrophage infiltration (172-175, 199-203). There was high expression of CD63 and MCP-1 for cyanoacrylate glue, fibrin glue, and gelatin implants, suggesting that these eyes were inflamed (Figure 19B-E). CLP-PEG-Fibrinogen implants had high expression of TSG101 while CLP-LCPP implants had the lowest expression of all three markers compared to the other implants (Figure 19B-E). Interestingly, when SiO_2 NPs were delivered through a CLP-LCPP implant, there was an increase in both of the EVs markers but when SiO_2 NPs were delivered through CLP-PEG-Fibrinogen, there

was a decrease in expression. Additionally, for all the implants, the EV markers were localized predominantly within the epithelium except for the fibrin glue implants, which were mostly in the stroma (Figure 19B). The colocalization channels for exosomes, TSG101 colocalizing with CD63, and exosomes with MCP-1 had a similar expression pattern as the CD63 (Figure 19B).

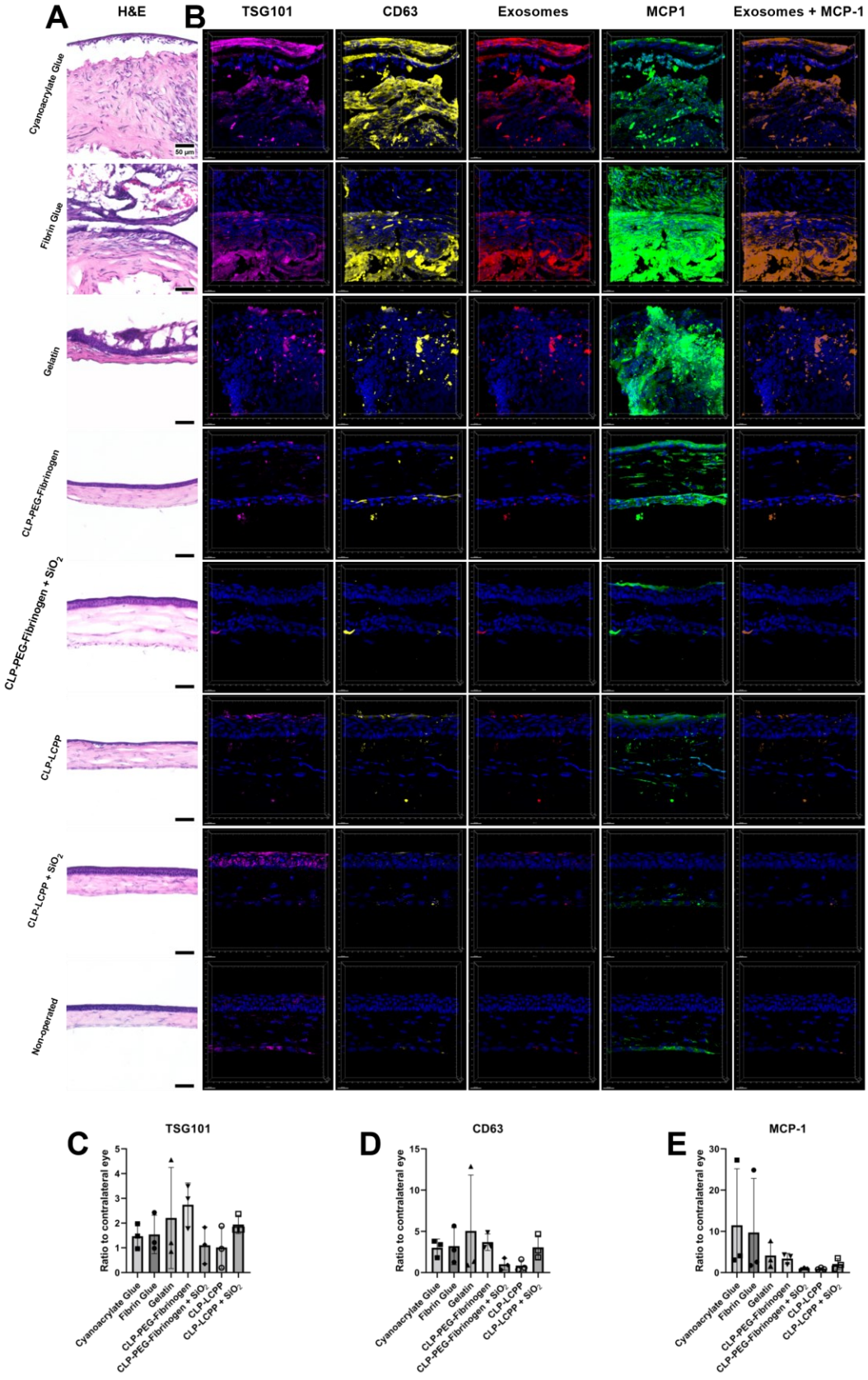
A
H&E
B
TSG101
CD63
Exosomes
MCP1
Exosomes + MCP-1
Cyanoacrylate Glue
Fibrin Glue
Gelatin
CLP-PEG-Fibrinogen
CLP-PEG-Fibrinogen + SiO2
CLP-LCPP
CLP-LCPP + SiO2
Non-operated
50 μm
C
TSG101
D
CD63
E
MCP-1
Ratio to contralateral eye
Cyanoacrylate Glue
Fibrin Glue
Gelatin
CLP-PEG-Fibrinogen
CLP-PEG-Fibrinogen + SiO2
CLP-LCPP
CLP-LCPP + SiO2

Figure 19. Expression of extracellular vesicles and MCP-1 in implanted mice. Corneal implants were given to 3 female BALB/c mice per material after they received an alkali burn and full thickness perforation. (A) Corneas were stained for H&E. Scale bar: 50μm. (B) Two weeks after the implants, samples were stained for TSG101 (Magenta), CD63 (Yellow), MCP-1 (Green), and DAPI (Blue). An exosomes channel (Red) was created based on the colocalization of CD63 and TSG101 as well as an exosomes + MCP-1 channel (Brown) based on the colocalization of exosomes with MCP-1. Quantification of the TSG101 (C), CD63 (D), and MCP-1 (E) was performed on the imaged tissue. Data was presented as a ratio of the implanted eye by the contralateral eye. **P ≤ 0.05 by two-way ANOVA Tukey's multiple comparisons test.*

7.4.3. Efficacy of injectable CLP hydrogels for delivery through nanoparticle carriers

Injectable CLP based hydrogels were tested for their utility for the potential delivery of drugs or other bioactives through the incorporation of nanoparticles. Lipid NPs loaded with an *in vivo* transfection reagent carrying DNA for Green Fluorescent Protein (GFP) was incorporated into CLP-LCPP. Initial testing showed uptake of the DNA and faint green fluorescence while, subsequent testing did not reveal GFP uptake (Figure 20A-C). Brightfield and OCT imaging showed that some of the implants were glued to the lens but were otherwise similar to the non-operated eye (Figure 20D-E). Corneas transfected *in vivo* with GFP showed no GFP expression in the implants except for in the initial test (Figure 20F). However, it was noted that the collagen-citrate glue needed to retain CLP-LCPP filled most of the cornea so the amounts of GFP-containing liposomes within the CLP-LCPP reaching the corneal cells was questionable, and therefore the results were inconclusive.

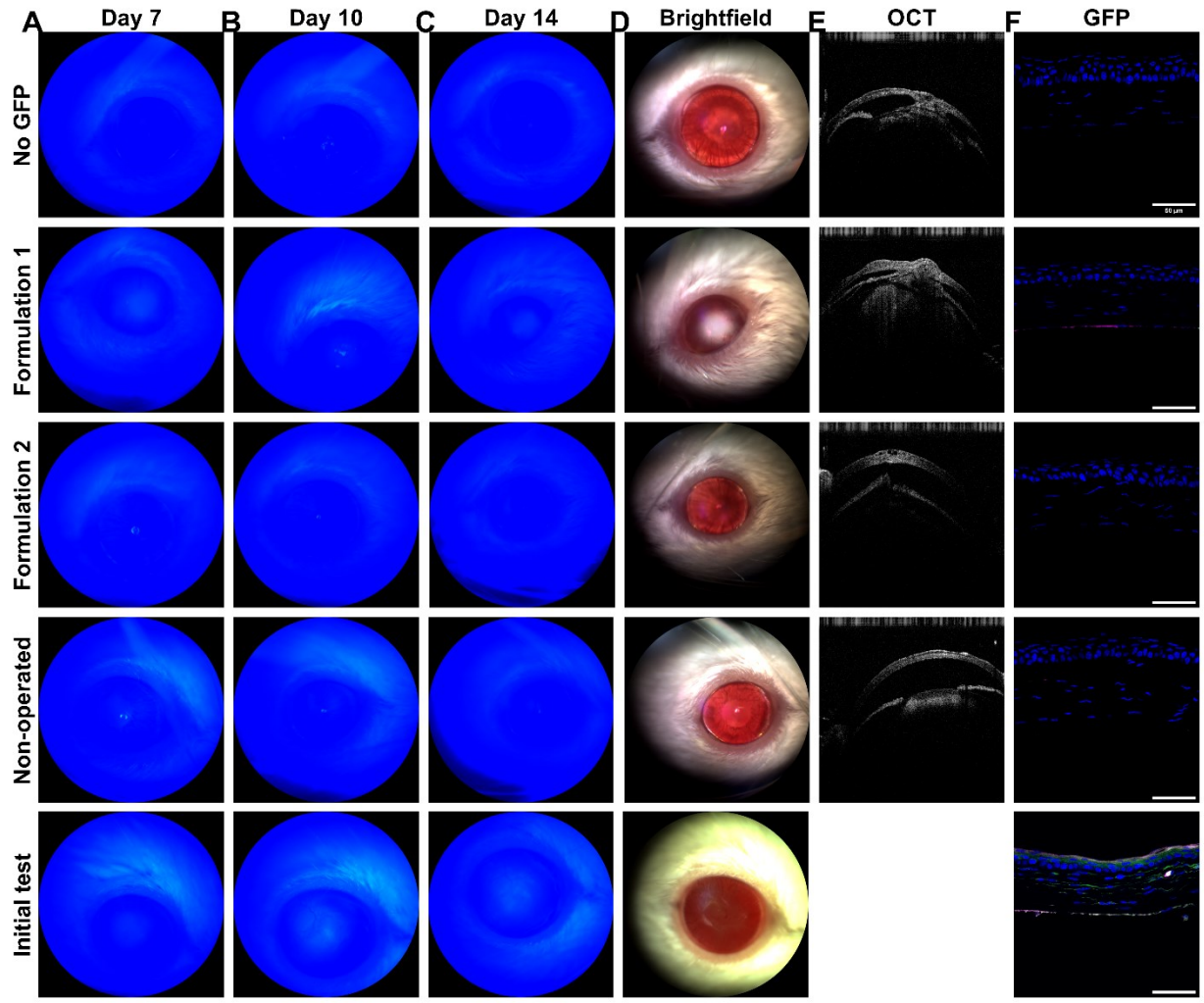

Figure 20. ***In vivo transfection of mouse corneas with GFP DNA.*** *Female BALB/c mice were given a full thickness perforation and a CLP-LCPP implant containing lipid NPs. Formulation 1 and 2 both contain a transfecting reagent capable of causing cells to produce GFP. The initial test of one mouse was of formulation 2, the other groups were 3 mice each. Blue light was used to excite the GFP in a live mouse on days 7 (A), 10 (B), and 14 (C). Brightfield (D) and OCT (E) imaging of the cornea was also taken on day 14. (F) Corneal sections were imaged for GFP (Green), stained GFP (Magenta), and DAPI (Blue). Scale Bar: 50µm.*

7.5. Discussion

To address the shortage of human donor corneas, biomaterials that gel spontaneously in the body have been developed. In order to gain a greater understanding of the early events after a corneal implant, CLP-PEG-Fibrinogen implanted mice were compared to alkali burn only mice. H&E staining showed that the initially cell-free biomaterials were rapidly repopulated by overgrowth of epithelium and ingrowth of stromal cells starting at day 3 (Figure 18A). Exosomes are recognised as products of cell-cell interaction. In this case, they were produced as a result of cell-biomaterial interactions and were examined for their utility to predict graft integration or failure using exosome markers and MCP-1. MCP-1 is strongly associated with corneal graft failure, with overexpression of MCP-1 associated with increased likely of graft failure and even the high expression of MCP-1 before an implant is also associated with increased graft failure (202, 203). CD63 is associated with graft failures for cardiac and renal transplantation, although not much work has looked into CD63 expression in corneal graft failures (199-201). CD63 is often used as an exosome marker. Staining for CD63, TSG101, and MCP-1 revealed that there was a large increase in MCP-1 expression at three days post corneal implant (Figure 18B-E). While the high expression of MCP-1 is concerning since it might indicate a greater risk of graft failure, the MCP-1 dropped to much lower levels by day 7, making it unclear if the MCP-1 expression will contribute towards graft failure. Since long-term 12 month studies in mini-pigs have used the same material, CLP-PEG-Fibrinogen, and have shown stably integrated and fully regenerated neo-corneas, it is unlikely that a transient increase in MCP-1 expression is correlated to graft failure (192). It is more likely that sustained high levels of MCP-1 expression would be more predictive of serious grafting consequences.

As previously observed, the addition of MPC to CLP-PEG solid implants resulted in less haze and vascularization compared to CLP-PEG implants without MPC (195). In an effort to improve the liquid formulation implants, LCPP, a polymer of MPC, was used for implantation and compared to CLP-PEG-Fibrinogen. Mice were given alkali burns to induce inflammation followed by a full thickness perforation and implant for two weeks. H&E staining shows that both cyanoacrylate glue and fibrin glue implants resulted in a very thick stroma with a high amount of cell infiltration (Figure 19A). On the other hand, corneal perforations treated with CLP based

materials (CLP-PEG-Fibrinogen and CLP-LCPP), healed and regenerated neo-corneas that were comparable with non-operated eyes.

Comparing the different materials, samples were stained for CD63, TSG101, and MCP-1 to assess inflammation and the early risks of graft failure. The materials currently approved for human use, cyanoacrylate glue and fibrin glue, had a lot of CD63 and MCP-1 expression in the cornea in comparison to the CLP based materials and the non-operated eyes (Figure 19B-E). This would suggest that the CLP based materials would have better long-term graft survival compared to cyanoacrylate glue and fibrin glue. Additionally, CLP-LCPP implants had slightly lower expression of all three markers than CLP-PEG-Fibrinogen implants (Figure 19B-E). This would suggest that these implants would function better in the long term, similar to what was observed when MPC was added to solid CLP-PEG implants (195).

As for the additional modifications to the implants, SiO_2 NPs were added to the CLP materials which were implanted into mouse corneas. Interestingly, their impact on MCP-1 expression varied slightly depending on the material. CLP-PEG-Fibrinogen implants supplemented with SiO_2 NPs had a non-significantly lower MCP-1 expression compared to the implant without SiO_2 NPs while the opposite effect was observed for CLP-LCPP (Figure 19B-E). As such, it seems that the addition of NPs only had a minor effect on the cornea and could potentially be used to deliver a treatment.

Beyond SiO_2 NPs, lipid NPs were tested for their efficacy at delivering their treatment to cells through a CLP-LCPP implant. The lipid NPs that were given to the mice contained a transfecting reagent that would cause the cells to express GFP. The initial test with these lipid NPs showed a bit of GFP expression in the cornea when excited with a blue light and stained for GFP in cryosections (Figure 20). While this was an encouraging result, the repeated attempt produced very little or no GFP expression. This was most likely due to the difficulty in filling minute corneal perforations in mice with a glue followed by hydrogel, strongly suggesting the need for a simpler application method.

In conclusion, biomaterials were tested to see their suitability for corneal implantation. Early observations of the cornea following implantation shows a temporary high expression of

MCP-1 which dissipates within a week. The CLP-PEG-Fibrinogen and CLP-LCPP materials were associated with regeneration of neo-corneas that resembled healthy untreated corneas. They showed lower expression of CD63 and MCP-1 than cyanoacrylate glue and fibrin glue which resulted in distended and disorganized corneas. This supports the contention that exosomes may have utility for predicting biomaterials implantation outcomes. However, more work is needed for confirmation.